



**Removal of Wastewater Contaminants by Adsorption Using
Iron on Carbon Foam.**

By

Khumalo Siphesihle Praise-God, B.Sc. Eng., M.Sc.

A thesis submitted in the Discipline of Chemical Engineering
University of KwaZulu-Natal

In fulfilment of the requirements for the degree
of Doctor of Philosophy in Engineering, Chemical Engineering

December 2022

Supervisor: Professor David Lokhat

DECLARATION 1 - PLAGIARISM

I, ...Siphesihle...Praise-God...Khumalo....., declare that

1. The research reported in this thesis, except where otherwise indicated, is my original research.
2. This thesis has not been submitted for any degree or examination at any other university.
3. This thesis does not contain other persons' data, pictures, graphs, or other information, unless specifically acknowledged as being sourced from other persons.
4. This thesis does not contain other persons' writing, unless specifically acknowledged as being sourced from other researchers. Where other written sources have been quoted, then:
 - a. Their words have been re-written, but the general information attributed to them has been referenced
 - b. Where their exact words have been used, then their writing has been placed in italics and inside quotation marks and referenced.
5. This thesis does not contain text, graphics or tables copied and pasted from the Internet, unless specifically acknowledged, and the source being detailed in the thesis and in the References sections.

Signed

.....

Date: 18/12/2022

As the candidate's Supervisor I agree to the submission of this thesis.

.....

Professor David Lokhat

Date: 15/12/2022

DECLARATION 2 - PUBLICATIONS

This section presents the articles that form part and/or include the research presented in this thesis. The following articles have been published or are under review:

ISI/SCOPUS/ DoHET Accredited Journals

Khumalo, Siphesihle, Praise-God, Lokhat, David, Sewpersad, Ajay, Seevrain Aleshya. (2022). Preparation and Structural Properties of Carbon Foam Derived from Natural Grain and Waste Pyrolytic Char. *Scientific Reports*. (Submitted and under review)

Khumalo, Siphesihle, Praise-God, Lokhat, David, Chetty, K. Chetty Latisha. Synthesis of novel carbon-supported iron oxide sorbents for adsorption of dye from aqueous solutions: equilibrium and flow-through studies. *Scientific Reports* **12**, 20009 (2022). <https://doi.org/10.1038/s41598-022-24257-8>

Khumalo, Siphesihle, Praise-God, Lokhat, David, Jasmine-Tré Anwar, Reddy, Huvin.a (2022). Synthesis of Iron on Carbon Foam for Use in the Removal of Phenol from Aqueous Solutions. *Molecules* **2023**, *28*, 1272. <https://doi.org/10.3390/molecules28031272>

Khumalo, Siphesihle, Praise-God, Lokhat, David, Sewpersad, Ajay. (2022). Preparation and Use of Iron on Carbon Foam for Removal of Organic Dye from Water – Batch Studies. (Submitted and under review)

DEDICATION

Dedicated to my late mother and father, Mrs Thandi Khumalo and Mr Selby Khumalo, for their faith, love, and belief in me.

ACKNOWLEDGEMENTS

First and foremost, I would like to thank the creator of the heavens and earth, the Lord God Almighty, Jesus Christ.

I would like to express my deepest gratitude to my supervisor, Prof. David Lokhat, for his undivided assistance, guidance, and support throughout the duration of this research. I would like to offer my deepest gratitude to my wife, Nompumelelo Khumalo, and my kids, Siphesihle, Siphosethu, and Asimbonge, for their love, support, and inspiration. To my family at large and friends, your constant support and encouragement did not go unnoticed. My sincere gratitude also goes to Kimbelin Chetty, Latisha Chetty, Ajay Sewpersad, Huvin Reddy, Anwar Chante J., and Aleshya Seevnrain, who were involved in data collection during the study. I would like to acknowledge financial support from the National Research Foundation.

"There is time for everything under the sun."

Table of Contents

DECLARATION 1 - PLAGIARISM.....	ii
DECLARATION 2 - PUBLICATIONS	iv
DEDICATION	v
ACKNOWLEDGEMENTS	vi
Abstract	xv
Chapter One	1
Introduction and Background of Study	1
Introduction	2
1.1 Background study.....	2
1.2 Research motivation.....	3
1.3 Statement of research problem	3
1.4 Aims and Objectives of Research	4
1.5 Thesis Overview.....	5
References	5
Chapter Two.....	7
Literature Review.....	7
2.....	Literature review
.....	8
2.1 Introduction.....	8
2.2 Conventional waste management methods	8
2.2.1 Coagulation and Flocculation.....	9
2.2.2 Froth floatation.....	9
2.2.3 Chemical oxidation	9
2.2.4 Chemical precipitation	9
2.2.5 Ion exchange	9
2.2.6 Membrane separation techniques	10
2.2.7 Electrochemical method.....	10
2.3 Adsorption.....	10
2.4 Types of Adsorptions	11
2.5 Adsorption Isotherms	12
2.5.1 Langmuir adsorption isotherm	12
2.5.2 Freundlich adsorption isotherm.....	12
2.5.3 Temkin adsorption isotherm.....	13
2.6 Adsorption kinetics	13
2.6.1 Pseudo-first order and pseudo-second order	13
2.6.2 Intraparticle diffusion.....	14

2.7	Activated carbon	15
2.8	Metal oxides	15
2.9	Naturally derived carbon foam as a support.....	15
2.10	Metal loadings	16
2.11	Column adsorption	17
2.12	Flow through apparatus for wastewater treatment	17
2.13	Breakthrough curve and saturation point	18
2.14	Methylene Blue	18
	References	19
3.....	Chapter Three	23
	Abstract	24
	Introduction	25
	Materials and methods	25
	Materials and Chemicals	25
	Methods.....	25
	Carbon foam Preparation	25
	Laboratory tube furnace setup.....	27
	Results and Discussion	27
	Open Flame Test	27
	3.1.1 Ethanol-soaked Burn Test	29
	3.1.2 Strength Test	29
	3.1.3 Characterisation.....	31
	Conclusion	31
	References	32
Chapter Four.....	34
	Abstract	34
	Introduction	35
	Materials and Methods	36
	Materials and chemicals	36
	Sorbent preparation	36
	Spectrophotometric analysis	36
	Calibration of the Spectrophotometer	37
	Batch Tests.....	37
	Flow-through Tests	38
	Results and Discussion	38
	Preparation of sorbent	38

Discussion	39
Advantages and disadvantages.....	39
Characterisation of an adsorbent.....	39
Effect of Iron content	40
Effect of sorbent dosage.....	42
Effect of contact time	43
Adsorption kinetics	45
Pseudo-first and pseudo-second order equations	45
Intraparticle diffusion.....	46
Equilibrium Adsorption.....	47
Adsorption mechanism.....	49
Flow-through apparatus.....	49
Effect of Flowrate.....	50
Effect of bed height.....	51
Industrial application of flow-through apparatus	53
Thermodynamic Analysis	54
Conclusion.....	54
References	55
Chapter Five.....	61
Abstract.....	62
Introduction	63
Materials and Methods	64
Materials and chemicals	64
Preparation of Carbon Foam	64
Results and discussion.....	64
Characterization of carbon foam	64
Effect of Initial Concentration.....	66
Effect of time on adsorption.....	67
Mechanism	68
Kinetic modelling.....	68
Intraparticle diffusion.....	70
Equilibrium adsorption.....	70
Conclusion.....	72
References	72
Chapter Six.....	78
Abstract.....	79

Introduction	80
Materials and Methods	81
Equipment and materials used.....	81
Sample Preparation	81
Aqueous Solution Preparation.....	81
Results and discussion	82
Sorbent preparation	82
Characterisation.....	82
Effect of time.....	83
Effect of sorbent dosage nanoparticles.....	83
Effect of initial concentration.....	84
Effect of temperature.....	85
Equilibrium Adsorption.....	87
Thermodynamic Analysis	88
Adsorption Kinetics.....	88
Conclusion	90
Chapter Seven	92
Concluding Remarks and Future Research Scope	92
Conclusion	93
Significance and Impact of the Research	94
Future Research Scope.....	94
Appendices	95
Appendix A Calibration.....	96
Appendix B	98
Chapter 4 Raw data.....	98
Chapter 5 Raw data.....	103
Chapter 6 Raw data.....	106
Appendix C Calculations.....	108
Appendix D Results.....	110
Appendix E Pictures.....	118

Lists of Figures

Chapter	Figure	Title	Page
2	1	Adsorption in wastewater treatment	12
	2	Plot of the intraparticle diffusion model for methylene blue adsorption	15
	3	Pore blockage on carbon support	17
	4	Characteristics of the breakthrough curve in the fixed bed column1	19
	5	Structural formula of Methylene blue	20
3	1	Scheme of carbon foam preparation	27
	2	Fabrication of carbon foam derived from bread	28
	3	Scheme of tube furnace carbonisation	28
	4	Results of open flame test and ethanol-soaked burnt test	30
	5	Photograph of char samples, soon after removal from the tube furnace	31
	6	Mass fraction versus the maximum weight the samples can Withstand	32
	7	Figure 1 MET image conducted on a Jeol 2100 HRTEM operating at 200 KV carbon foam based on natural grain and pyrolytic char	33
4	1	Flow-through apparatus setup	41
	2	Figure 2 MET image conducted on a Jeol 2100 HRTEM operating at 200KV a. carbon foam with 0% wt iron b. carbon foam with 6 wt% iron c. carbon foam with 15 wt% iron	43
	3	Effect of the iron content of the carbon foam at sorbent dosage of 20 mg, concentration of 10 mg/L, and contact time of 30 minutes	44
	4	The leaching of iron ions, concentration of 10 mg/L, and contact time of 180 minutes	45
	5	Effect of the iron content of the carbon foam at sorbent dosage, concentration of 10 mg/L, and contact time of 30 minutes	46

Lists of Figures

Chapter	Figure	Title	Page	
4	6	Effect of Iron content on carbon foam at sorbent of 50 mg, 10 mg/L dye concentration and contact time of 180 minutes and Effect of Iron content on carbon foam at sorbent of 20 mg, 100 mg/L dye concentration and contact time of 180 minutes.	47	
	7	Effect of contact time, sorbent dosage (50mg), concentration of dye solution (10 mg/L), and volume of solution (20 mL).	47	
	8	Figure 8 Nonlinear fit of pseudo-first order and pseudo-second order for dye adsorption on carbon foam with 15wt% iron, 20 mg/L solution, initial concentration of 10 mg/L	48	
	9	Plot of the intraparticle diffusion model for methylene blue onto iron supported by carbon foam (50 mg), 10 mg/L solution, room temperature	50	
	10	Fitting of adsorption isotherms into experimental data	51	
	11	Flowrate breakthrough curve for 6wt% iron	53	
	12	Figure 12 Flowrate breakthrough curve for 15wt% iron	53	
	13	Height breakthrough curve for 6wt% iron	54	
	14	Height breakthrough curve for 15wt% iron	55	
	5	1	MET image conducted on a Jeol 2100 HRTEM operating at 200KV, a. Sample 1, b. Sample 2, c. Sample 3, d. Sample 4, and e. Sample 5	66
		2	Effect of initial concentration on phenol adsorption	67
		3	The effect of initial concentration on percentage of phenol adsorbed (50ml of phenol solution and 0.1 magnetic nanopowder)	67
		4	Effect of contact time on adsorption of phenol at concentration of 75mg/L, and 100mg	68

Lists of Figures

Chapter	Figure	Title	Page
5	5	Nonlinear fitting of pseudo-first order and pseudo-second order for phenol adsorption of sample 3 at a 75mg/L of concentration, and 100mg sorbent	69
	6	Plot of the intraparticle diffusion model for phenol onto iron supported by carbon foam (75mg/L of concentration, and 100mg sorbent)	70
	7	Fitting of adsorption isotherms into experimental data for sample 3	72
6	1	Dye removal using 40 mg/L solution under the effect of contact time	80
	2	Dye removal using a varying number of nanoparticles in increments of 10 mg	81
	3	Magnetite sample temperature effects	83
	4	Fitting of pseudo-first order and pseudo-second order for magnetite sample	86
	5	Intraparticle diffusion for magnetite sample	87

Lists of Tables

Chapter	Table	Title	Page
4	1	BET analysis	42
	2	Pseudo-first order parameters	49
	3	Pseudo-second order parameters	49
	4	Temkin and Freundlich isotherm parameters	52
5	1	Iron and magnetite added into carbon form for each sample	64
	2	Pseudo-first order parameters	69
	3	Pseudo-second order parameters	70
	4	Temkin, Freundlich, and Langmuir model parameters	72
6	1	Sample A, Sample B, Sample C, and Sample D sample	78
	2	Aqueous solutions of known concentrations	79
	3	Initial concentration test	82
	4	Isothermal equilibrium parameters	84
	5	Thermodynamic parameters	85
	6	Pseudo-first order and pseudo second order parameters	86

Abstract

The dyes in textile effluents have a deleterious impact on water bodies and impede photosynthesis by decreasing sunlight penetration. This work examined the adsorption capacity of an iron oxide sorbent immobilised on carbon foam generated from natural sources for to remove organic methylene blue dye from water. In this investigation, the carbon precursor and iron oxide precursor were combined in a single tank and carbonised. The carbon foam created had a self-assembled structure with flour as a basic constituent. This study examined the thermal and mechanical properties of carbon-based foam created from an inexpensive, green, and template-free carbonisation technique using natural grain and pyrolytic char. In addition, the adsorption capability of an iron oxide sorbent immobilised on natural carbon foam to remove organic methylene blue dye from water and the adsorption of phenol was investigated. The preparation method for iron-based nanoparticles substantially impacts particle shape and size, size distribution, active sites, and subsequent applications. As the number of nanoparticles grew, the dye adsorption increased due to the increased number of active sites. At high temperatures, the molecules of the pigment worked together more efficiently, making it simpler to eliminate.

The possible application of magnetic nanopowder for phenol adsorption mobilised on natural grain carbon foam from an aqueous solution was also examined. Priority pollutants with high toxicity, even at low concentrations, are phenolic chemicals. A magnetic nanopowder was synthesised by dissolving an iron sponge in nitric acid to form iron nitrate, which was then added to a natural grain mixture consisting primarily of flour. Investigating the effect of starting concentration under constant adsorbent dosage revealed that absorbance values rose with increasing concentration. In each of these tests, the amount of phenol adsorbed increased as the original concentration rose. In addition, absorption increased when the carbon foam iron level increased. Using an equation relating to a pseudo first-order chemical reaction, a kinetic investigation determined that the phenol adsorption data sufficiently covered all carbon foam samples evaluated. The Freundlich, Langmuir, and Temkin equations were evaluated for modelling equilibrium adsorption isotherms, and it was determined that the Temkin model satisfactorily fit the experimental data.

Sorbents with 0, 6 and 15 wt iron were produced. Transmission electron microscopy (TEM) and Brunauer-Emmett-Teller (BET) techniques were utilised to analyse the physical characteristics and surface morphology of the synthesised carbon foam. In batch testing, the adsorption capacities were examined by identifying the effects of a rise in iron content, sorbent dosage, contact time, and dye concentration. Breakthrough curves were obtained by adjusting the height of the sorbent bed and varying the flowrate of the dye solution. A higher bed height equates to a bigger amount of adsorbent. With increasing bed height, the breakthrough and equilibrium adsorption capabilities were shown to rise. When the flow rate is high, the dye solution leaves the column before equilibrium, resulting in shorter breakthrough and saturation durations. Higher bed heights and lower flow rates resulted in excellent dye removal in the flow through the system. Breakthrough time increases as iron content rises. The 15 wt.% iron sample had more adsorption capabilities than the 6 wt.% iron sample, but the 0 wt.% iron control sample exhibited minimum adsorption properties. This investigation was best represented by the pseudo-first order kinetic model ($R^2 > 0.96$), while the Freundlich isotherm best describes the adsorption equilibrium ($R^2 > 0.99$). The results show that an iron oxide sorbent immobilised on natural carbon foam effectively removes blue methylene dye.

Variable amounts of iron, nitric acid and magnetite were added to each sample. Additionally, aqueous solutions with varying amounts of methylene blue dye were produced. Based on the change in Gibbs free energy, all samples demonstrated exothermic adsorption except for the magnetite sample, which

displayed endothermic adsorption. As the temperature increases, the viscosity of the dye mixture reduces, allowing more adsorbate to flow through the outer boundary layer and internal pores of the adsorbent. In the adsorption of methylene blue onto iron supported by carbon foam, intraparticle diffusion was not the single rate-limiting step for all samples; rather, the adsorption rate was limited by a multistep elementary reaction mechanism in which numerous processes happened simultaneously. The pseudo-second order kinetic model best describes this experiment ($R^2 > 0.96$), while the Freundlich isotherm best describes the adsorption equilibrium ($R^2 > 0.999$). According to the results, an iron oxide sorbent immobilised on natural carbon foam effectively eliminates methylene dye.

Chapter One
Introduction and Background of Study

Introduction

1.1 Background study

The rise in global population, civilization, science, and industry has led to an increase in home and industrial wastewater production. The environmental disturbance combined with the escalating pollution issue has become a crucial. Toxic contamination from industrial, agricultural, or urban sources can have acute or chronic effects on the ecosystem. Wastewater can be classified based on its chemical, physical, and biological components. Chemical products (pharmaceutical goods, etc.), heavy metals (lead, copper, mercury, etc.), and organic compounds are common pollutants in wastewater (hydrocarbons, dyes, solvents etc.).

The textile sector is one of the largest contributors to global water pollution. Among other processes, the textile dyeing business utilises a great deal of water during the various dyeing and finishing steps. The nonbiodegradability and resistance to light and oxidising chemicals of dyes hinder the selection of a suitable removal strategy. Moreover, toxicity bioassays have demonstrated that most are hazardous (Mahmoodi & Arami, 2010). Due to limited light penetration, dyes can substantially impact the photosynthetic processes of aquatic organisms (Vasques et al., 2009). Therefore, eliminating colour from waste effluents has become increasingly crucial for environmental preservation (Sanghi & Bhattacharya, 2002). Most industries dispose of their trash in water bodies such as rivers and lakes. This garbage is loaded with colourants, salts, and other hazardous substances, which affect the water's purity and pH. Some communities obtain their drinking water from rivers and lakes. Consumption of these untreated effluents by people and animals poses potential health concerns. Therefore, the invention and implementation of new wastewater treatment systems are of the utmost importance. Through hydrolysis, oxidation, and other reactions, certain dyes generate toxic, carcinogenic, and mutagenic intermediates (Wang et al., 2005). Therefore, it is essential to remove dyes from wastewater before returning it to the natural environment (Yacouta-Nour, 2009).

Various industries, such as oil refining, petrochemicals, medicines, coking operations, resin production, plastics, paint, pulp, paper, and wood products, can all produce effluents containing these substances (Fathy Mubarak et al., 2021). Phenolic compounds are hazardous to human health and pose a threat to human life even at low doses. Significant health risks are likely to be posed to both human and animal populations, as well as aquatic environments, if these substances are released without first being managed. International regulatory organisations have demanded the creation of stringent phenol discharge restrictions to ensure that the environment remains habitable (Villegas et al., 2016). To protect humans and aquatic life from the phenolic compounds pollution, which are toxic, makes it is essential to eliminate them from water. In addition to making it easier to dispose of trash and reducing the hazards of the chemicals themselves, creating additional methods to dispose of phenolic compounds will produce more valuable phenolic compounds that can be used as secondary products.

Numerous techniques, including coagulation/flocculation, biological treatment, ozonation, photocatalysis, filtering, electrochemical, membrane processing, and adsorption (Sadeghi-Kiakhani et al., 2012), have been employed to remove dyes from coloured wastewaters. Therefore, among other strategies, the adsorption process has been demonstrated to be effective due to its efficiency, capacity, and large-scale application for dye removal, as well as the possibility for adsorbent regeneration, recovery, and recycling (Olasehinde et al., 2019). The ability of several adsorbents to remove dye from wastewater has been evaluated. To obtain a high-performance adsorbent, it is essential to select less expensive, more efficient adsorbents with greater adsorption capacity

(Olasehinde et al., 2019). An ideal adsorbent should have both a large surface area and a small volume. Other requirements must include strong mechanical strength, chemical and thermal stability, high porosity, and small pore diameter, resulting in more exposed surface area and, therefore, acceptable surface chemistry, resulting in a high adsorption capacity (Abegunde et al., 2020). Researchers are interested in (Li et al., 2014) materials with mechanical and thermal strength, a large surface area, a good, ordered structure, magnetic properties, optical qualities, and the capacity to be manipulated for specific properties. Nanoparticles are microscopic particles with dimensions between 1 and 100 nm (Naseri et al., 2015). Due to their distinctive features, they are useful for a variety of commercial and domestic uses, including catalysis, medicinal, imaging, agricultural, and engineering applications (Li et al., 2014). Nanoparticles are one of the most studied materials of the 20th century due to their novel features and diverse applications (Yaqoob et al., 2020).

Adsorption is contingent on the type of adsorbent used. Recent research with an inexpensive adsorbent has been conducted. Commercially available adsorbent materials include activated carbon, zeolites, silica gel, and activated alumina, which are typically expensive. Consequently, the use of sustainable and inexpensive materials in this project also addresses the issue of cost.

1.2 Research motivation

Biological and chemical agents are readily available for wastewater treatment. However, these agents are costly and frequently cause environmental damage. Adsorption is currently used to remove organic dyes due to its low cost, accuracy, viability, and straightforward design. Activated carbon is the preferred adsorbent for wastewater treatment, but its high cost restricts its industrial application. So, the textile industry is always looking for cheaper ways to replace activated carbon. The feasibility of metal oxides immobilised on natural grain-based carbon foam (mentioned) as a suitable adsorbent to remove organic dyes and phenol from wastewater has received scant attention. Metal oxides are readily accessible and inexpensive, but the difficulty of recovery is a concern due to their small size. The recovery of used adsorbent would be enhanced by immobilising these particles on a support. For carbon derived from natural sources, there are few studies on kinetic models, equilibrium isotherms, temperature effects, initial concentration effects, and sorbent effects. This research entails the preparing and characterizing of an iron oxide sorbent immobilised on a carbon foam support derived from natural sources. The sorbent's adsorption capabilities were examined, and a flow-through apparatus was used to determine the sorbent's breakthrough and saturation points. Knowing how the carbon foam is made and what it can absorb will make it more likely that it will be used in industry.

1.3 Statement of research problem

Adsorption is the most effective method for removing organic and inorganic contaminants from wastewater because it is easy to set up, inexpensive, does not require much time, and the adsorbent used in the process is not harmful to the environment and can be recovered and reused without a decrease in effectiveness. Consequently, the search for inexpensive and readily available adsorbents has prompted numerous researchers to seek more cost-effective and efficient strategies for utilising natural and synthetic materials as adsorbents. The nanomaterial composed of iron-based oxide exhibited various sorption properties for simultaneously removing colours, organic contaminants, and inorganic pollutants. Nanoparticles tend to aggregate in solutions, decreasing their reactivity. As the rate of aggregation and deposition decreases with increasing material stability, the stability of nanoparticles is crucial to their high reactivity and mobility. The preparation method for iron oxide nanoparticles significantly impacts particle shape and size, size distribution, surface chemistry, and,

consequently, their applications. Iron-based nanoparticles have great sorption abilities because they have a large specific surface area, a lot of holes, and a strong magnetic response. This gives them a great sorption capacity. It is believed that magnetic nanopowder is one of the most efficient adsorbents for removing organic and inorganic pollutants from aquatic environments. It is inexpensive, abundant, made from renewable sources, stable at high temperatures, resistant to most chemicals, and has a large surface area and a high porosity. So, in this study, the use of magnetic nanopowder for phenol adsorption on natural grain carbon foam was investigated to lower the amount of phenol in different solutions.

Based on the research problems, the present work addresses the following research questions:

- What are the structural characteristics of carbon foam made from natural grain and char?
- What is the structural characterisation of nanoparticles immobilised on natural grain carbon?
- Which nanoparticle possesses the highest adsorption capacity?
- How do kinetic models, intraparticle diffusion, and equilibrium isotherms influence the adsorption of methylene blue and phenol?
- What are the implications of varying the operation parameters for dye and phenol adsorption?
- What are the breakthrough curves?

1.4 Aims and Objectives of Research

This study aims to develop a sustainable, low-cost, and recoverable sorbent derived from naturally occurring carbon foam to remove organic pollutants (methylene blue dye and phenol) from water. This research aims to assess the adsorption effectiveness of an iron oxide sorbent immobilised on carbon foam obtained from natural sources to remove organic dye from an aqueous solution.

The following are the goals:

- Preparation and characterization of carbon foam and sorbent oxides for various wastewater treatment applications. Using Transformation Electron Microscopy and Brunauer-Emmett-Teller.
- Examine the structural durability of carbon foam.
- Application of structural resilience of carbon foam
- Evaluate the efficacy of the adsorbent in the removal of dye and phenol.
- Determine the effect of altering the adsorbent's duration, concentration, and amount on its adsorption capabilities.
- Determine the influence of dye concentration on the adsorption process by conducting experiments with dye solutions of varying concentrations.
- Examine the sorbent's ability to absorb by changing the iron percentage of the sorbent, the contact time, temperature and the amount of sorbent in the adsorption process
- Identify the adsorption isotherms and kinetic models applicable to each adsorbent.
- In a continuous adsorption process, find out how the initial adsorbate concentration (C_0), bed height (Z), and characteristic ratio (Z/D) affect breakthrough.
- Develop an adsorption model.

1.5 Thesis Overview

The first chapter of this dissertation, which comprises of six (6) chapters and appendices, provides an overview of the entire work, including the study's context, rationale, and motivation for the research effort. The overarching purpose and objectives of the project, as well as its scope. There is a description of the research objectives achieved in accordance with the research problem description.

The thesis is a collection of research results required by the University of KwaZulu-Natal to award the specified degree. The initiative resulted in four research publications addressing the study's distinct objective. Two has been peer-reviewed and published, while others are still undergoing peer reviews.

In Chapter 2, which is the first contribution, a comprehensive literature review on waste removal and adsorption studies is presented. There is a discussion of the various conventional and enhanced processes.

Chapter 3: "Preparation and Structural Properties of Carbon Foam Derived from Natural Grain and Waste Pyrolytic Char."

Chapter 4 is "Synthesis of Novel Carbon-Supported Iron Oxide Sorbents for Adsorption of Dye from Aqueous Solutions: Equilibrium and Flow-Through Studies."

Chapter 5: "Preparation and Application of Iron on Carbon Foam for the Removal of Phenol from Water: Batch Studies"

Chapter 6: "Preparation and Use of Iron on Carbon Foam for the Removal of Organic Dye from Water Batch Studies"

References

- Abegunde, S.M. *et al.* 2020. A review on the influence of chemical modification on the performance of adsorbents, *Resources, Environment and Sustainability*. 1, p. 100001. Available at: <https://doi.org/10.1016/j.resenv.2020.100001>.
- ADAMS, S.P. 2006. Cleveland, grover. *African American Studies Center* [Preprint]. Available at: <https://doi.org/10.1093/acref/9780195301731.013.44633>.
- FATHY MUBARAK, M., MAHER AHMED, A. AND SAAD GABR, S. 2021. Nanoporous carbon materials toward phenolic compounds adsorption. *Nanopores* [Preprint]. Available at: <https://doi.org/10.5772/intechopen.96380>.
- LI, N., ZHAO, P. AND ASTRUC, D. 2014. Anisotropic gold nanoparticles: Synthesis, properties, applications, and toxicity. *Angewandte Chemie International Edition*, 53(7), pp. 1756–1789. Available at: <https://doi.org/10.1002/anie.201300441>.
- MAHMOODI, N.M. AND ARAMI, M. 2010. Immobilized Titania nanophotocatalysis: Degradation, modeling and toxicity reduction of agricultural pollutants. *Journal of Alloys and Compounds*, 506(1), pp. 155–159. Available at: <https://doi.org/10.1016/j.jallcom.2010.06.164>.

- NASERI, N., VALIZADEH, H. AND ZAKERI-MILANI, P. 2015. Solid lipid nanoparticles and nanostructured lipid carriers: Structure, preparation and application. *Advanced Pharmaceutical Bulletin*, 5(3), pp. 305–313. Available at: <https://doi.org/10.15171/apb.2015.043>.
- OLASEHINDE, E.F. AND ABEGUNDE, S.M. 2019. Preparation and characterization of a new adsorbent from raphia taedigera seed. *Research on Engineering Structures and Materials* [Preprint]. Available at: <https://doi.org/10.17515/resm2019.139ma0713>.
- SADEGHI-KIAKHANI, M., ARAMI, M. AND GHARANJIG, K. 2012. Dye removal from colored-textile wastewater using chitosan-PPI dendrimer hybrid as a biopolymer: Optimization, kinetic, and isotherm studies. *Journal of Applied Polymer Science*, 127(4), pp. 2607–2619. Available at: <https://doi.org/10.1002/app.37615>.
- SANGHI, R. AND BHATTACHARYA, B. 2002. Review on decolorisation of aqueous dye solutions by low cost adsorbents. *Coloration Technology*, 118(5), pp. 256–269. Available at: <https://doi.org/10.1111/j.1478-4408.2002.tb00109.x>.
- VASQUES, A.R. *et al.* 2009. Removal of dyes from the textile industry by adsorption in fixed bed columns: A sustainable process. *Chemical Product and Process Modeling*, 4(4). Available at: <https://doi.org/10.2202/1934-2659.1301>.
- VILLEGAS, L.G. *et al.* 2016. A short review of techniques for phenol removal from wastewater. *Current Pollution Reports*, 2(3), pp. 157–167. Available at: <https://doi.org/10.1007/s40726-016-0035-3>.
- WANG, S., BOYJOO, Y. AND CHOUEIB, A. 2005. A comparative study of dye removal using fly ash treated by different methods. *Chemosphere*, 60(10), pp. 1401–1407. Available at: <https://doi.org/10.1016/j.chemosphere.2005.01.091>.
- YACOUTA-NOUR, A. 2009. Elimination des colorants acides en solution aqueuse par la bentonite et le kaolin,” *Comptes Rendus Chimie*. 12(6-7), pp. 762–771. Available at: <https://doi.org/10.1016/j.crci.2008.11.008>.
- YAQOOB, A.A. *et al.* 2020. Role of nanomaterials in the treatment of wastewater: A Review, *Water*, 12(2), p. 495. Available at: <https://doi.org/10.3390/w12020495>.

Chapter Two

Literature Review

2 Literature review

2.1 Introduction

Textile effluents are one of the primary causes of water pollution on a global scale. The industrial sector needs huge quantities of water for finishing processes such as sizing, dyeing, and printing (Vasques et al., 2009). These processes generate enormous quantities of pollutants, such as dyes, starches, detergents, salts, toxic organic compounds, biocides, and ionic metals (Villegas et al., 2012). These vividly coloured effluents pose a threat to the environment because they alter the pH, diminish the transparency of water bodies, increase the oxygen demand in receiving waters, and obstruct the entry of sunlight. Reduced solar penetration changes photosynthetic processes, ultimately contributing to the extinction of aquatic life. It is vital to remove these hazardous compounds to prevent environmental degradation and human and animal health risks. In the past, water was considered clean and uncontaminated if it lacked colour, odour, and flavour. Nonetheless, the water may contain organic pollutants, toxic metals, radioactive nuclides, etc.

In recent years, the elimination of phenol has been acknowledged as a significant subject of research within the field of chemical engineering. Phenolic chemicals are high on the list of priority pollutants because, even in minute quantities, they pose a substantial threat (Fathy Mubarak et al., 2021). By mixing with the metal ions emitted by other businesses, the phenol found in wastewater can form complex compounds. Then, these complicated molecules can be released into the environment. Numerous potential removal strategies for phenol have been investigated, including distillation, absorption, extraction, chemical oxidation, and electrochemical oxidation (Febrianto, 2009). (Villegas et al., 2012) say that these compounds can be found in the wastewater from oil refining, petrochemicals, pharmaceuticals, coking operations, resin production, plastics, paint, pulp, paper, and wood products. There are several technologies used to recover phenolic compounds from wastewater before it is discharged into water resources (Fathy Mubarak et al., 2021). Biodegradation, steam distillation, liquid-liquid extraction, adsorption, solid-phase extraction, wet air oxidation, catalytic wet air oxidation, and wet air oxidation are typical removal techniques. Electrochemical oxidation, photo-oxidation, ozonation, UV/H₂O₂, the Fenton reaction, membrane processes, and enzymatic treatment are among the most sophisticated techniques for phenol removal (Villegas, 2012). Physical, chemical, and biological treatment are the three standard methods for removing phenolic contaminants from aqueous solutions. Most people believe that physical adsorption is the best, cheapest, and most prevalent method for eliminating phenolic and dye pollution (Vasques et al., 2009).

2.2 Conventional waste management methods

Eliminating dyes using typical waste management processes is tough. Dye molecules' complicated molecular structures render them non-biodegradable, resistant to aerobic digestion, and stable to oxidising chemicals and light (Jain et al., 2015). The standard ways for removing dye are coagulation, froth flotation, chemical oxidation, and adsorption (Jain, et al., 2015). Adsorption is the most versatile of these techniques, as it may be used to a variety of substances (Shah et al., 2016).

2.2.1 Coagulation and Flocculation

Coagulation or flocculation includes the application of a coagulant that promotes the formation of flocs by neutralising the forces between the colloids. Polymers build bridges between flocs and bind particles into large aggregates or clumps through the process of flocculation. The flocs are subsequently separated from the aqueous solution by physical sedimentation or flotation (Malakootian et al., 2021). This is one of the most prevalent wastewater treatment methods being employed. This process does not involve the decomposition of any colourants; hence, no harmful intermediates are created. Although the colour removal method is reasonably economical, it does have its limitations. This technique produces sludge, which must be disposed of at significant expense and environmental danger. Another constraint is the difficulty of removing particularly soluble, low-molecular-weight cationic dyes (Zhu et al., 2014).

2.2.2 Froth floatation

The process of froth floatation is basic. The dye's natural or generated hydrophobicity is utilised to render it water-repellent. Using surface-active chemicals, sometimes known as collectors, hydrophobicity is intentionally generated. When a stream of gas bubbles is injected into a solution, hydrophobic particles adhere to the surface of the gas bubbles and collect at the surface of the liquid pool. This produces a layer on the surface that is rich in the solute and can be regularly removed. (Mavros et al., 2008)

2.2.3 Chemical oxidation

The process of chemical oxidation involves the transfer of electrons from oxidising reagents like hydrogen peroxide, chlorine dioxide, and ozone to the oxidised chemical species. This wastewater treatment technique transforms pollutants into harmless or stable chemicals (Bennett, 2009). This approach is particularly advantageous for small, highly concentrated streams where biological oxidation is impractical. Chemical oxidation is the right choice for industrial effluents that contain toxic compounds that are hard to break down, but biological oxidation wouldn't work in these situations (Jafarinejad, 2017).

2.2.4 Chemical precipitation

Through chemical precipitation, soluble metal ions are recovered from effluent. To render metal ions insoluble, precipitating substances (such as sodium hydroxide) are used. By settling and/or filtering, the particles in a solution are removed (Hackett, 1997). However, it may not be a realistic choice for most applications that are not adaptable (Onyango et al., 2004). The limitations are the poisonous sludge produced and its disposal, which is both expensive and environmentally dangerous.

2.2.5 Ion exchange

Ion exchange is the process of exchanging ions between a liquid phase and a porous substance. Typically, polymeric resins and zeolites are employed in ion exchange systems (Ali & El-Bishtawi, 1997). Cation exchange resins are frequently used in residences and municipal water treatment plants to remove Ca^{2+} and Mg^{2+} ions from "hard" water, as well as in the industrial production of ultra-pure water (Sonune & Ghate, 2004). According to (Sandoval & Villanueva-Rodríguez, 2018), Amberlite XAD-4 resin is an effective

adsorbent for a wide variety of aromatic compounds, particularly phenols. In contrast to activated carbon, XAD-4 resin has hydrophobic surfaces and a low capacity for most organic molecules, which restricts its use in industrial wastewater treatment (Sandoval & Villanueva-Rodríguez, 2018). To increase adsorption capacity and improve selectivity for a specific organic pollutant, ordinary polymeric resins are often chemically changed by grafting unique functional groups onto the matrix of the resins (Pan et al., 2009). Ion exchange may remove heavy metal ions effectively and selectively, but the resins are costly (Kim et al., 2006). The cost of taking regeneration treatments out of the environment is also a problem (Sonune and Ghate, 2004).

2.2.6 Membrane separation techniques

Reverse osmosis (RO), ultrafiltration (UF), and nanofiltration (NF) are pressure-driven membrane processes; diffusion dialysis is a concentration-driven membrane process; electro dialysis is an electrically driven membrane process; and membrane distillation is a temperature-driven membrane process. Using membrane filtration (UF, RO, and NF), colour, chemical oxygen demand (COD), heavy metals, and total dissolved solids (TDS) are removed from wastewater simultaneously. Obtaining effluents devoid of particulates is a particularly desirable component of this process (Greenlee et al., 2009). In addition, membrane separation techniques offer various advantages, such as a small system, easy operation and maintenance control, and low chemical requirements. Inefficient removal of low molecular weight (organic) compounds (ultrafiltration) and high energy consumption (reverse osmosis) are downsides of membrane separation, despite its advantages (Cheng & Sabatini, 2007). The decrease in flow caused by membrane fouling, which can be caused by the plugging of membrane pores with organic and inorganic particles, is another limitation of membrane processes. This fouling reduces the economic efficiency of membrane operations by slowing down the production of treated water and shortening the lifetime of the membranes (Laslo and Hodur, 2007).

2.2.7 Electrochemical method

The electrochemical method of wastewater treatment was created by blending shipboard sewage with saltwater in a ratio of 3:1 and subjecting the mixture to electrolysis. Subsequently, electrochemical treatment became prevalent in the treatment of industrial wastewaters such as textile and olive mill effluent, tannery effluent, distillery effluent, and cattle effluent (Vijayaraghavan & Yun, 2008). Electrolytic techniques are expensive and necessitate specialised equipment and regular upkeep. Therefore, it is crucial to identify an alternative treatment for the condition. The removal of heavy metals is also possible through complexation, solvent extraction, foam flotation, electrodeposition, and cementation (Wan Ngah & Hanafiah, 2008), although these techniques have limitations such as slow kinetics and inadequate selectivity. Adsorption has become the first line of defense, especially for waste that cannot be removed by other means (Mohan & Singh, 2002).

2.3 Adsorption

Due to its adaptability in terms of the variety of colours adsorbed, adsorption is one of the most efficient strategies for cleaning industrial wastewater. Adsorption is an interfacial process in which gaseous or solute components are accumulated on the surface of solid adsorbents. It is a surface phenomenon in which surface forces play a major role, in contrast to absorption, in which molecules are collected by volume rather than surface. When an absorbable solute (adsorbate) is present in a solution and exposed to an adsorbent, the intermolecular forces of attraction cause solute particles to accumulate on the surface of the adsorbent.

Zeolites, charcoal, clays, and other byproducts are used to create adsorbents (Kandisa & Saibaba KV, 2016). Activated carbon adsorbents are the most recommended for dye removal. Figure 1 illustrates the adsorption in wastewater treatment.

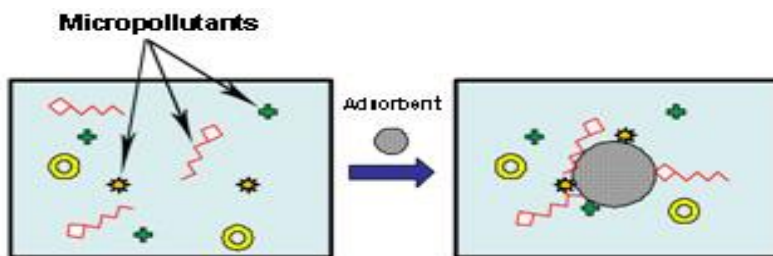


Figure 1. Adsorption in wastewater treatment (Kandisa & Saibaba KV, 2016)

Adsorption involves mass transfer and intraparticle diffusion. Mass transfer where adsorptive molecules are transferred to the external surface of the adsorbent granules. In intraparticle diffusion molecules diffuse within the adsorbent's pores. Adsorption capacity is determined by the physical and chemical properties of the adsorbent and the adsorbate, the concentration of the adsorbate in a liquid solution, experimental conditions such as temperature and pH, and the amount of time the adsorbate is in contact with the adsorbent (residence time) (Lodge, 1979). Since adsorption processes are the most prevalent in industry, they are the subject of the most research (Chiarle, 2000). Adsorbent selection is the initial step in the creation of an adsorption unit. Numerous adsorbents can be used to remediate industrial wastewater. Activated carbon is the most common adsorbent and has been demonstrated to be effective at removing heavy metals (Carvalho et al., 2007). Other researchers reported the usage of zeolites in wastewater treatment, whereas activated carbon was used to remove contaminants from wastewater (Qiu et al., 2007).

2.4 Types of Adsorptions

Adsorption is caused by the attraction between the atoms, molecules, and ions of the adsorbate and the surface or interface (Calvet, 1989). The classifications of adsorption are as follows:

- No electrons are exchanged between the adsorbent and the adsorbate during physical adsorption. If the adsorbate is held to the surface by physical and non-specific forces of type Van der Waals force and hydrogen bonding, several layers can be formed with almost the same adsorption heat. The maximum amount of heat of adsorption for physisorption is a few kcal mol^{-1} . Physical adsorption is a non-specific and reversible process.
- Chemical adsorption, also known as chemisorption, involves the contact or transfer of electrons between the adsorbed species and the adsorbent. Chemisorption bonds are frequently stronger than physical adsorption bonds (tens of kcal mol^{-1}) and thus significantly stronger and more stable at high temperatures.

2.5 Adsorption Isotherms

During the solute retention on solid particles examination, the residual solute concentration of the compound C (mol L⁻¹ or kg L⁻¹) can be linked with the retention concentration of this compound Q (mol kg⁻¹ or kg kg⁻¹). The expression $Q = f(C)$ describes the "sorption isotherm" (C). For this partnership to continue, many conditions must be met: (i) the various retention/release equilibria must have been attained, and (ii) all other physiochemical parameters must remain constant. Because of temperature on sorption reactions, the isotherm was chosen; the temperature must be kept constant (Werth et al., 1997).

2.5.1 Langmuir adsorption isotherm

To represent chemisorption, Langmuir's isotherm, often known as the "ideal localised monolayer model," was developed (Wang & Zhu, 2004). (Langmuir, 1918) investigated the sorption of gases on solid surfaces from a theoretical standpoint and considered sorption a chemical phenomenon. The Langmuir equation ties, at a fixed temperature, the number of molecules on a solid surface to the concentration of a medium above the solid surface. The Langmuir isotherm assumes localised monolayer adsorption; all surface sites can adsorb a single molecule; and all sites are identical and can only accommodate a single adsorbed molecule. The ability of a molecule to adsorb on a specific site is independent of the occupancy of adjacent sites. Adsorption is reversible, and molecules that have been adsorbed cannot migrate or interact with adjacent molecules (Febrianto et al., 2009). According to the hypothesis, the surface adsorption and desorption rates are equivalent. With these assumptions and the kinetic principle (equal rates of adsorption and desorption from the surface), the Langmuir equation can be written in hyperbolic form as follows:

$$q_e = \frac{q_m K_L C_e}{1 + K_L C_e} \quad (1)$$

Where q_e (mg/g) is the monolayer adsorption capacity, C_e (mg/L) is the equilibrium concentration of adsorbate, q_m (mg/g) is the monolayer adsorption capacity, and K_L is the Langmuir constants.

2.5.2 Freundlich adsorption isotherm

The Freundlich isotherm can be used to characterise the adsorption of organic and inorganic compounds on a wide variety of adsorbents (Febrianto et al., 2009). Originally an empirical form, the Freundlich isotherm was later interpreted as sorption to heterogeneous surfaces or surfaces with sites of differing affinities. According to (Liu et al., 2008), the stronger binding sites are likely to be filled first, and the bindings will weaken as the number of filled sites increases. According to this model, the quantity of mass adsorbed per mass of adsorbent is a power-law function of solute concentration. The empirical Freundlich model, which works well for low concentrations and is based on sorption on a rough surface, is shown by the following equation:

$$q_e = K_F C_e^{1/n} \quad (2)$$

Where C_e (mg/L) is the equilibrium adsorbate concentration, q_e (mg/g) is the equilibrium adsorption quantity. Adsorption capacity and adsorption intensity are proportional to the Freundlich constants K_F and

n, respectively. Freundlich's model is an empirical equation based on the equilibrium between solid and liquid solute distribution. The Freundlich model is used for heterogeneous surfaces, but its capacity to characterised adsorption data is restricted (Mahmoodi et al., 2013).

2.5.3 Temkin adsorption isotherm

The Temkin model reflects the properties of indirect adsorbate-adsorbent interactions on the adsorption isotherm. It assumes that the heat of adsorption of all molecules in the layer decreases linearly with coverage due to adsorbate-adsorbent interactions (Arora et al., 2016). Furthermore, a uniform distribution of binding energies, up to a maximum binding energy, characterises adsorption (Benguella & Yacouta-Nour, 2009). The Temkin model is expressed by the following equation:

$$q_e = \frac{RT}{b} \ln(AC_e) \quad (3)$$

q_e (mg/g) represents the amount of adsorption at equilibrium, C_e (mg/L) represents the equilibrium concentration of adsorbate, T (K) represents the temperature in Kelvin, R (J/mol/K) represents the universal gas constant, b (J/mol) represents the heat of adsorption, and A represents the equilibrium binding constant proportional to the maximum binding energy.

2.6 Adsorption kinetics

2.6.1 Pseudo-first order and pseudo-second order

For the research of adsorption kinetics modelling, Lagergren pseudo-first order and pseudo-second order models were utilised. The following equation represents pseudo-first order and pseudo-second order in their nonlinear version.

$$q_t = q_e(1 - e^{-K_1 t}) \quad (4)$$

The following equation demonstrates the nonlinear form of pseudo-second order.

$$q_t = \frac{q_e^2 K_2 t}{1 + K_2 q_e t} \quad (5)$$

Where q_t (mg/g) is the quantity absorbed at time t , q_e (mg/g) is the amount remaining after equilibrium of adsorption, and K_1 and K_2 are the pseudo-first and pseudo-second order model rate constants, respectively, represented in min^{-1} and g/mg/min .

Lagergren's first order and second order models, in the linear form, are expressed by equations 6 and 7, respectively:

$$\log(q_e - q_t) = \log q_e - K_1 t \quad (6)$$

$$\frac{t}{q_t} = \frac{1}{k_2 q_e} + \frac{1}{q_e} t \quad (7)$$

2.6.2 Intraparticle diffusion

The intraparticle diffusion resistance was evaluated utilising the intraparticle particle diffusion model by Weber and Morris, given by the following equation:

$$q_t = k_{id} t^{1/2} + c \quad (8)$$

Where q_t (mg/g) is the adsorption amount at time t (min), k_{id} (mg/g/min^{1/2}) is the adsorption rate constant of intraparticle diffusion model, and c is a constant related to the thickness of the boundary layer. If intraparticle diffusion is involved in the sorption process, a graph of adsorbate uptake vs the square root of time would have a linear connection, and intraparticle diffusion would be the rate-regulating step if this line passes through the origin (El Maguana et al., 2019). Furthermore, such a departure from the origin of the straight line suggests that pore diffusion is not the only factor affecting rate (El Maguana et al., 2019).

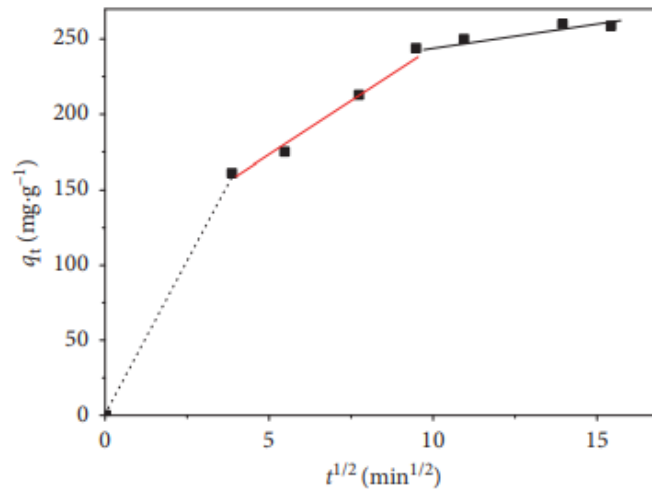


Figure 2. Plot of the intraparticle diffusion model for methylene blue adsorption onto activated carbon adapted from (El Maguana et al., 2019).

Figure 2 shows that the plot is multilinear with three linear segments over the time, showing that intraparticle diffusion was not the dominant rate-limiting component in the adsorption process. During the first stage, methylene blue diffuses through the solution to the adsorbent's external surface. The second component was caused by intraparticle diffusion. The third component corresponds to the final equilibrium stage, when intraparticle diffusion begins to slow due to a decrease in methylene blue concentration.

2.7 Activated carbon

Activated carbon is composed of purified, powdered charcoal. It is exposed to a physical or chemical process that induces the formation of small fractures that considerably increase its adsorptive surface area. Activated carbon is predominantly made of pure carbon and is currently the most effective adsorbent known (Agrawal et al., 2017). Due to its remarkable adsorption characteristics, activated carbon is the dominant dye-removal adsorbent (Arvanitoyannis & Varzakas, 2008). The carbon is processed to generate low-volume pores, which greatly increase the surface area and, thus, the number of adsorption sites. Activated carbon is used to treat poisonings and overdoses in the medical field, and its agricultural applications include pesticide and animal feed additive use. It is also applied in the purification of alcoholic beverages, where it is employed in the form of filters to polish the spirit by removing impurities that could affect its colour, aroma, or flavour. This adsorbent's expensive price typically hinders its broad application. Therefore, cheap alternatives to activated carbon are in high demand.

2.8 Metal oxides

As a result of the coordination tendency of metal ions, metal oxides are produced, with oxygen ions forming a coordination sphere around the metal ions and giving rise to a close-packed structure (Arora et al., 2016). The extensive range of chemical, optical, magnetic, and physical properties of metal oxides make them more susceptible to structural and compositional changes. Applications of metal oxides in industries such as the chemical, textile, and battery industries are appealing due to their multifunctional nature. Due to their limited solubility, amphoteric properties, and high activity, metal oxides have attracted considerable interest in recent years as potential adsorbents, especially for the removal of heavy metals from wastewater (Pirillo et al., 2009). Iron oxide, aluminium oxide, titanium oxide, manganese oxide, and zirconium oxide are currently being researched (Khulbe & Matsuura, 2018). Iron oxide was chosen for this experiment as the sorbent metal. It was produced by incorporating iron nitrate into the carbon support. Iron nitrate was utilised because of its inexpensive cost, availability, and high adsorption efficiency (Giles et al., 2011). Iron oxide sorbents are composed of minute particles, making their recovery from vast bodies of water challenging. To remedy the condition, assistance materials may be implemented. Desorption, which permits the sorbent to be cleaned and reused, is a crucial aspect of recovery. An approach for enhancing the desorption of contaminants from iron oxide sorbents uses a strong sodium hydroxide solution (Shanmugam et al., 2020).

2.9 Naturally derived carbon foam as a support

Carbon in its elemental form possesses several favourable properties, including easy accessibility, low cost, straightforward recycling, greater tolerance for both acidic and basic conditions, and low density. Carbon's characteristics make it a very versatile chemical element; as a result, different solid carbon forms (polymorphs) can be produced. Crystalline and amorphous are the two most frequent forms of carbon. There are numerous procedures for preparing carbon foams, and carbon foams are distinguished based on their preparation processes. These processes consist of blowing and carbonization, template carbonization, the compression of exfoliated graphite, and the construction of graphene nanosheets (Yunxia et al., 2016). Through these processes, physical properties such as density and pore size are regulated.

Due to the diverse porosity architectures and well-controlled pore diameters of amorphous carbon, carbon foam is regarded as an outstanding catalyst and adsorbent support material. Supports are commonly employed to facilitate the recovery of spent catalysts and adsorbents. As most textile industry activities are undertaken on a huge scale, there is a tremendous amount of wastewater that must be treated. Many adsorbents are powders or minute particles. By making the adsorbent particles bigger, adding a support makes it easier to get them out of the treated water and speed up the recovery process. This project's carbon foam support was created from a mixture of flour and yeast. The method of preparation was identical to that used by (Yuan et al., 2016). The production of valuable carbon-based compounds from natural components is a sustainable process since organic matter is abundant, environmentally friendly, and a renewable resource. There are a variety of methods for creating carbon foam from natural raw materials, including hydrothermal treatment, freeze-drying, and direct carbonization (Yuan et al., 2016). Direct carbonization is the most cost-effective method and therefore the most used. Metal oxide adsorbent deposition methods are required when employing supports. Various procedures are employed to glue adsorbents to supports. Examples include wet imbibition, dry ingestion, heating by means of a microwave. Other depositable materials available: Silica gel and Activated carbon.

2.10 Metal loadings

Metal loading on the support has an impact on the sorbent's adsorption capabilities. The greater metal loadings enhance the sorbent's adsorption capability (Afshar Taromi & Kaliaguine, 2018). However, agglomeration may occur if the metal concentration is too high. Agglomeration is the grouping of metal particles on a support, which increases particle size and decreases particle surface area. When the surface area of a sorbent decreases, so does its absorption capacity. As seen in Figure 1, as particle size increases, so does the susceptibility of the support material to pore blockage. Due to the inaccessibility of the microscopic holes, the metal oxide sorbent is squandered. Pore blockage on carbon support is shown in Figure 3.

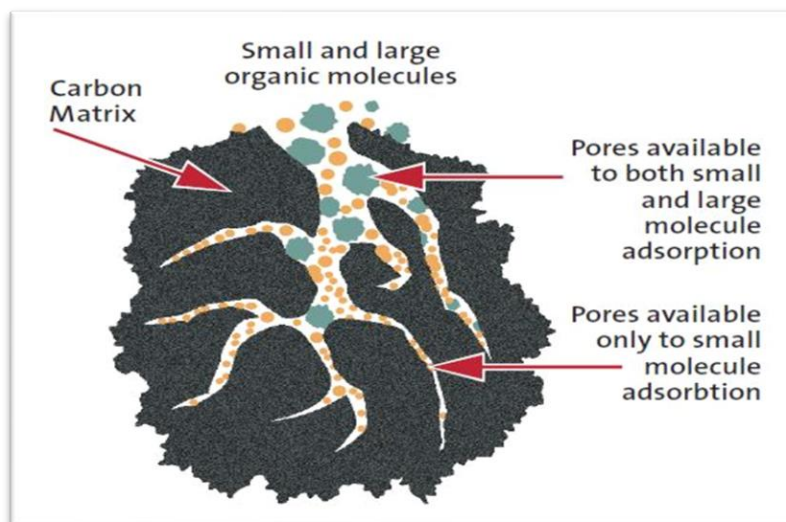


Figure 3. Pore blockage on carbon support (Afshar Taromi & Kaliaguine, 2018)

2.11 Column adsorption

During the dynamic adsorption experiments, the adsorbent is loaded into columns, and these columns form a bed. The aqueous solution containing the adsorbate is then passed through the bed. The solution constantly meets a new portion of the adsorbent as it travels through the bed, which causes a tendency for a new equilibrium to be established. A genuine equilibrium can never be reached, however, because the amount of time spent in contact with any one portion of the adsorbent is restricted. The adsorption zone goes downwards as the solution is continuously passed through it. After a given amount of time, t , the adsorption zone has just reached the bottom of the bed, and the concentration has abruptly and unexpectedly risen to a value that is appreciable for the first time. In actuality, the operation of the system is halted when the concentration of the effluent reaches a specific level, known as the breakthrough concentration (Vasques, 2009). This is the point at which it is no longer profitable to continue operating the system. The term "breakthrough time," abbreviated as "tb," refers to the amount of time it takes for the concentration of the effluent to reach the maximum level that is permissible for release. The maximum permitted discharge limit is taken into consideration as the breakthrough concentration in the process of computing the characteristic parameters of the system (Attia et al., 2008). As the adsorption zone moves through the bottom of the bed, the concentration of solutes in the effluent begins a rapid ascent that continues until it eventually reaches the concentration that it was at in the beginning ($C_i/C_o = 1$). Since the bed is, in all intents and purposes, totally in equilibrium with the feed solution by the time it reaches the final stage ($C_i/C_o = 0.9$), there is very little or no adsorption taking place at this point. The way a fixed bed adsorbent is operated is profoundly affected both by the form that the breakthrough curve takes and the moment at which it first becomes visible. In most cases, the curves are in the shape of a S; nevertheless, they may be sharp or relatively flat, and in rare instances, they are significantly warped (Attia et al., 2008).

2.12 Flow through apparatus for wastewater treatment

A flow-through apparatus is a fixed-bed column filled with adsorbent. Wastewater flows through the fixed bed, where pollutants adhere to the adsorbent and cleansed water is released into the environment. Due to the high amount of water required for textile finishing, textile decontamination and recycling must be conducted on a massive scale. Consequently, therapy effectiveness and cost become crucial. Adsorption in fixed-bed columns is one of the most prevalent commercial methods for eliminating contaminants from aqueous textile effluents without the use of chemical agents (Vasques et al., 2009). Activated carbon is the most effective method for cleaning textile effluents due to its high surface area. Most sorbents are chosen according to their adsorption potential, which is directly proportional to particle size, making industrial wastewater treatment challenging. Adsorbents with a high surface area operate well. A vast surface area requires tiny sorbent particles. The sorbent is then recovered. Large bodies of water make it difficult to extract particles. Multiple sorbent particles attached to a support facilitate recovery. A flow-through system eliminates the need for sorbent recovery. The sorbent will remain in the column, and water that has been cleaned can be discharged into the environment. The spent sorbent is renewed by replacing the fixed bed.

2.13 Breakthrough curve and saturation point

Using flow-through equipment, one can determine a breakthrough curve. This graph illustrates the relationship between time and the concentration of adsorbate (a contaminant) in the effluent stream. Initially, as the solution begins to flow through the column, there should be rapid adsorption due to the lack of contaminants on the sorbent surface, when the driving force for adsorption is greatest. This should result in an effluent with a low adsorbate concentration. At the breakthrough point, the adsorbate content in the effluent begins to increase. This indicates that the adsorption driving force has diminished. When the effluent concentration approaches that of the original solution, the sorbent is said to be reaching its saturation point. At saturation, the concentration of the effluent is the same as the concentration of the solution at the beginning, and no more adsorptions happen. Figure 4 displays the time-dependent characteristic of the breakthrough curve in the fixed bed column adsorption process.

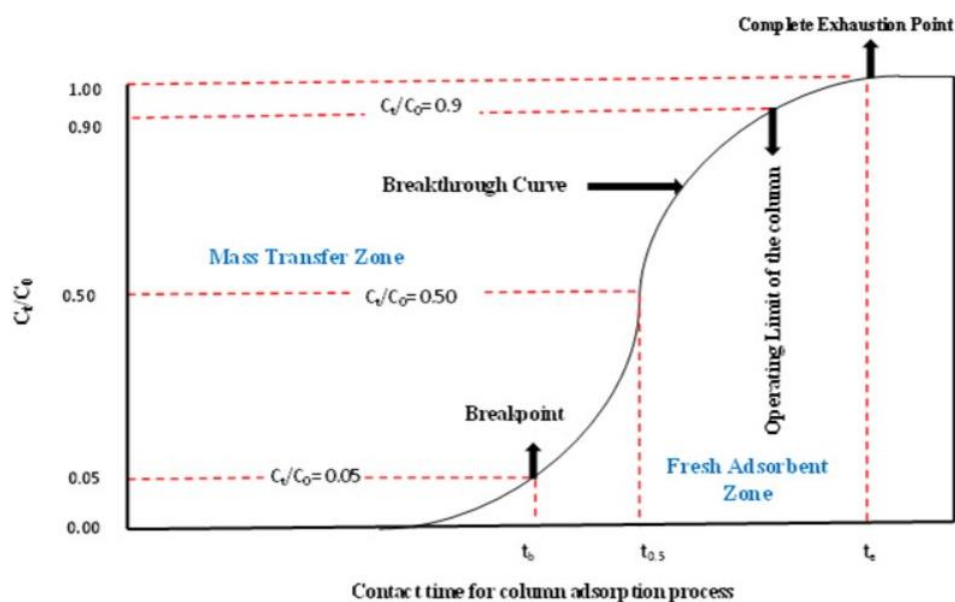


Figure 4. Characteristics of the breakthrough curve in the fixed bed column adsorption process in relation to time (Chowdhury et al. 2015)

2.14 Methylene Blue

Methylene blue's chemical formula is $C_{16}H_{18}N_3SCl$, and its molecular weight is 373.9 g/mol. It is widely used in the leather industry, as well as in calico and cotton printing and tanning. It is used in microscopy examinations to study RNA and DNA, and thus plays an important role in the healthcare industry. It has been established that minute doses of methylene blue are beneficial for health. Vitamin C is the strongest antioxidant; it increases cellular energy, which in turn improves long- and short-term memory and is neuroprotective (SmartDrugSmarts, 2017). Greater concentrations, on the other hand, pose a health risk because they reduce the ability of red blood cells to transport oxygen (SmartDrugSmarts, 2017). Extreme nausea, vomiting, and diarrhoea are obvious side effects that may occur after consuming a significant quantity. Furthermore, inhalation is discouraged because it may create breathing difficulties. The vivid

colour of methylene blue is chiefly responsible for the environmental risk it poses. As a component of industrial waste, it impacts water quality by lowering the amount of light that may enter. This threatens aquatic organisms whose biological processes require sunlight. Before trash is dumped into the ocean, it is vital to make a determined effort to remove any potentially hazardous compounds. This is when the absorption process comes into play. Figure 5 shows the structural formula of methylene blue

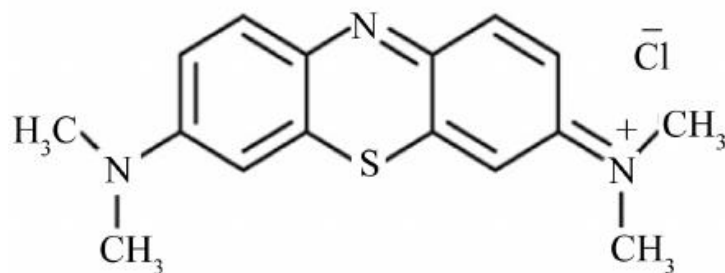


Figure 5. Structural formula of Methylene blue

References

- AFSHAR TAROMI, A. AND KALIAGUINE, S. 2018. Hydrodeoxygenation of triglycerides over reduced mesostructured ni/γ-alumina catalysts prepared via one-pot sol-gel route for Green Diesel production. *Applied Catalysis A: General*, 558, pp. 140–149. Available at: <https://doi.org/10.1016/j.apcata.2018.03.030>.
- AGRAWAL, S. *et al.* 2017. The role of Inoculum and reactor configuration for microbial community composition and dynamics in mainstream partial nitritation anammox reactors. *MicrobiologyOpen*, 6(4). Available at: <https://doi.org/10.1002/mbo3.456>.
- ALI, A.A.-H. AND EL-BISHTAWI, R. 1997. Removal of lead and nickel ions using Zeolite Tuff. *Journal of Chemical Technology & Biotechnology*, 69(1), pp. 27–34. Available at: [https://doi.org/10.1002/\(sici\)1097-4660\(199705\)69:1<27: aid-jctb682>3.0.co;2-j](https://doi.org/10.1002/(sici)1097-4660(199705)69:1<27: aid-jctb682>3.0.co;2-j).
- ARORA, A. *et al.* 2016. Applications of metal/mixed metal oxides as photocatalyst: A Review,” *Oriental Journal of Chemistry*, 32(4), pp. 2035–2042. Available at: <https://doi.org/10.13005/ojc/320430>.
- ARVANITOYANNIS, I.S. AND VARZAKAS, T.H. 2008. Vegetable waste management: Treatment methods and potential uses of treated waste. *Waste Management for the Food Industries*, pp. 703–761. Available at: <https://doi.org/10.1016/b978-012373654-3.50014-6>.
- ATTIA, A.A., GIRGIS, B.S. AND FATHY, N.A. 2008. Removal of methylene blue by carbons derived from peach stones by H₃PO₄ activation: Batch and column studies. *Dyes and Pigments*, 76(1), pp. 282–289. Available at: <https://doi.org/10.1016/j.dyepig.2006.08.039>.
- BENGUELLA, B. AND YACOUTA-NOUR, A. 2009. Elimination des colorants acides en solution aqueuse par la bentonite et le kaolin. *Comptes Rendus Chimie*, 12(6-7), pp. 762–771. Available at : <https://doi.org/10.1016/j.crci.2008.11.008>.

- BENNETT, G.F. 2009. Biosolids Engineering and Management, Handbook of Environmental Engineering Vol. 7, Humana Press, Totowa, NJ (2008) 820 pp., ISBN: 978-1-58829-861-4, USD 175.00. *Journal of Hazardous Materials*, 166(2-3), pp. 1567–1568. Available at: <https://doi.org/10.1016/j.jhazmat.2008.12.014>.
- CALVET, R. 1989. Adsorption of organic chemicals in soils. *Environmental Health Perspectives*, 83, pp. 145–177. Available at: <https://doi.org/10.1289/ehp.8983145>.
- CARVALHO, A.F. *et al.* 2007. Augmentation strategies for treatment-resistant depression: A literature review,” *Journal of Clinical Pharmacy and Therapeutics*, 32(5), pp. 415–428. Available at: <https://doi.org/10.1111/j.1365-2710.2007.00846.x>.
- CHENG, H. AND SABATINI, D.A. 2007. “Separation of organic compounds from Surfactant Solutions: A Review. *Separation Science and Technology*, 42(3), pp. 453–475. Available at: <https://doi.org/10.1080/01496390601120664>. Chiarle, S. (2000) “Mercury removal from water by ion exchange resins adsorption,” *Water Research*, 34(11), pp. 2971–2978. Available at: [https://doi.org/10.1016/s0043-1354\(00\)00044-0](https://doi.org/10.1016/s0043-1354(00)00044-0).
- CHOWDHURY, Z. Z., HAMID, S. B. A., AND ZAIN, S. M. 2015. Evaluating design parameters for breakthrough curve analysis and kinetics of fixed bed columns for Cu(II) cations using lignocellulosic wastes. *BioRes.* 10(1), 732-749.
- EL MAGUANA, Y. *et al.* 2019. Activated carbon from prickly pear seed cake: Optimization of preparation conditions using experimental design and its application in dye removal. *International Journal of Chemical Engineering*, 2019, pp. 1–12. Available at: <https://doi.org/10.1155/2019/8621951>.
- FATHY MUBARAK, M., MAHER AHMED, A. AND SAAD GABR, S. 2021. Nanoporous carbon materials toward phenolic compounds adsorption. *Nanopores* [Preprint]. Available at: <https://doi.org/10.5772/intechopen.96380>.
- FEBRIANTO, J. *et al.* 2009. Equilibrium and kinetic studies in adsorption of heavy metals using biosorbent: A summary of recent studies. *Journal of Hazardous Materials*, 162(2-3), pp. 616–645. Available at: <https://doi.org/10.1016/j.jhazmat.2008.06.042>.
- GILES, D.E. *et al.* 2011. Iron and aluminium based adsorption strategies for removing arsenic from water. *Journal of Environmental Management*, 92(12), pp. 3011–3022. Available at: <https://doi.org/10.1016/j.jenvman.2011.07.018>.
- GREENLEE, L.F. *et al.* 2009. Reverse osmosis desalination: Water sources, technology, and today's challenges. *Water Research*, 43(9), pp. 2317–2348. Available at: <https://doi.org/10.1016/j.watres.2009.03.010>.
- HACKETT, E.J. 1997. Peer Review in science and science policy. *Evaluating Science and Scientists*, pp. 51–60. Available at: <https://doi.org/10.7829/j.ctv280b88f.11>.
- HO, Y.S., JOHN WASE, D.A. AND FORSTER, C.F. 1995. Batch nickel removal from aqueous solution by sphagnum moss peat. *Water Research*, 29(5), pp. 1327–1332. Available at: [https://doi.org/10.1016/0043-1354\(94\)00236-z](https://doi.org/10.1016/0043-1354(94)00236-z).
- JAFARINEJAD, S. 2017. Cost-effective catalytic materials for AOP Treatment Units. *The Handbook of Environmental Chemistry*, pp. 309–343. Available at: https://doi.org/10.1007/698_2017_77.
- JAIN, M. *et al.* 2015. Adsorption of heavy metals from multi-metal aqueous solution by sunflower plant biomass-based carbons. *International Journal of Environmental Science and Technology*, 13(2), pp. 493–500. Available at: <https://doi.org/10.1007/s13762-015-0855-5>.

- KANDISA, R.V. AND SAIBABA KV, N. 2016. Dye removal by adsorption: A Review. *Journal of Bioremediation & Biodegradation*, 07(06). Available at: <https://doi.org/10.4172/2155-6199.1000371>.
- KHULBE, K.C. AND MATSUURA, T. (2018) “Removal of heavy metals and pollutants by membrane adsorption techniques,” *Applied Water Science*, 8(1). Available at: <https://doi.org/10.1007/s13201-018-0661-6>.
- KIM, J., MANN, J.D. AND SPENCER, J.G. 2006. Arsenic removal from water using lignocellulose adsorption medium (LAM). *Journal of Environmental Science and Health, Part A*, 41(8), pp. 1529–1542. Available at: <https://doi.org/10.1080/10934520600754284>.
- LANGMUIR, I. 1918. The adsorption of gases on plane surfaces of glass, mica and platinum. *Journal of the American Chemical Society*, 40(9), pp. 1361–1403. Available at: <https://doi.org/10.1021/ja02242a004>.
- LIU, A. *et al.* 2008. Hydrogen-bond detection, configuration assignment and rotamer correction of side-chain amides in large proteins by NMR spectroscopy through protium/deuterium isotope effects. *ChemBioChem*, 9(17), pp. 2860–2871. Available at: <https://doi.org/10.1002/cbic.200800467>.
- LIU, A. *et al.* 2008 Hydrogen-bond detection, configuration assignment and rotamer correction of side-chain amides in large proteins by NMR spectroscopy through protium/deuterium isotope effects. *ChemBioChem*, 9(17), pp. 2860–2871. Available at: <https://doi.org/10.1002/cbic.200800467>.
- LODGE, J.P. 1979. Air Pollution Sampling and analysis deskbook. *Atmospheric Environment (1967)*, 13(10), pp. 1481–1482. Available at: [https://doi.org/10.1016/0004-6981\(79\)90134-3](https://doi.org/10.1016/0004-6981(79)90134-3).
- LÁSZLÓ, Z. AND HODÚR, C. (2007) “Purification of thermal wastewater by membrane separation and ozonation. *Desalination*, 206(1-3), pp. 333–340. Available at: <https://doi.org/10.1016/j.desal.2006.03.572>.
- MAHMOODI, N.M., NAJAFI, F. AND NESHAT, A. 2013. Poly (amidoamine-co-acrylic acid) copolymer: Synthesis, characterization and dye removal ability. *Industrial Crops and Products*, 42, pp. 119–125. Available at: <https://doi.org/10.1016/j.indcrop.2012.05.025>.
- MALAKOOTIAN, M. *et al.* 2021. Ciprofloxacin removal from aqueous media by adsorption process: A systematic review and meta-analysis. *DESALINATION AND WATER TREATMENT*, 229, pp. 252–282. Available at: <https://doi.org/10.5004/dwt.2021.27334>.
- MARQUES, J.C. 2016. Suíça. *OEm Country Report* [Preprint]. Available at: <https://doi.org/10.15847/ciesoemcr032016>.
- MOHAN, D. AND SINGH, K.P. 2002. Single- and multi-component adsorption of cadmium and zinc using activated carbon derived from bagasse—an agricultural waste. *Water Research*, 36(9), pp. 2304–2318. Available at: [https://doi.org/10.1016/s0043-1354\(01\)00447-x](https://doi.org/10.1016/s0043-1354(01)00447-x).
- PAN, B. *et al.* 2009. Development of polymeric and polymer-based hybrid adsorbents for pollutants removal from waters. *Chemical Engineering Journal*, 151(1-3), pp. 19–29. Available at: <https://doi.org/10.1016/j.cej.2009.02.036>.
- PIRILLO, S., FERREIRA, M.L. AND RUEDA, E.H. 2009. The effect of ph in the adsorption of alizarin and Eriochrome Blue Black R onto iron oxides. *Journal of Hazardous Materials*, 168(1), pp. 168–178. Available at: <https://doi.org/10.1016/j.jhazmat.2009.02.007>.
- POURHAKKAK, P. *et al.* 2021. Fundamentals of Adsorption Technology. *Interface Science and Technology*, pp. 1–70. Available at: <https://doi.org/10.1016/b978-0-12-818805-7.00001-1>.
- QIU, J. *et al.* 2007. Carbon Nanotube Integrated Multifunctional Multiscale Composites. *Nanotechnology*, 18(27), p. 275708. Available at: <https://doi.org/10.1088/0957-4484/18/27/275708>.

- SANDOVAL, G. AND VILLANUEVA-RODRÍGUEZ, S.J. 2018. Extraction methods for phenolic compounds. *Phenolic Compounds in Food*, pp. 61–74. Available at: <https://doi.org/10.1201/9781315120157-4>.
- SHAH, V. *et al.* 2016. Adsorption of nonionic brij and tween surfactants at PTFE-water and air-water interfaces: Investigations on wetting, dispersion stability, foaming and drug solubilization. *Colloids and Surfaces A: Physicochemical and Engineering Aspects*, 508, pp. 159–166. Available at: <https://doi.org/10.1016/j.colsurfa.2016.08.057>.
- SHANMUGAM, K., MANIVANNAN, J. AND MANJULADEVI, M. 2020. Stupendous nanomaterials: Carbon nanotubes synthesis, characterization, and applications. *Nanomaterials - Toxicity, Human Health and Environment* [Preprint]. Available at: <https://doi.org/10.5772/intechopen.90318>.
- SONUNE, A. AND GHATE, R. 2004. Developments in wastewater treatment methods. *Desalination*, 167, pp. 55–63. Available at: <https://doi.org/10.1016/j.desal.2004.06.113>.
- VASQUES, A.R. *et al.* 2009. Removal of dyes from the textile industry by adsorption in fixed bed columns: A sustainable process. *Chemical Product and Process Modeling*, 4(4). Available at: <https://doi.org/10.2202/1934-2659.1301>.
- VIJAYARAGHAVAN, K. AND YUN, Y.S. 2008. Bacterial biosorbents and biosorption. *Biotechnology Advances*, 26(3), pp. 266–291. Available at: <https://doi.org/10.1016/j.biotechadv.2008.02.002>.
- VILLEGAS, L.G. *et al.* 2016. A short review of techniques for phenol removal from wastewater. *Current Pollution Reports*, 2(3), pp. 157–167. Available at: <https://doi.org/10.1007/s40726-016-0035-3>.
- WAN NGAH, W.S. AND HANAFIAH, M.A.K.M. 2008. Removal of heavy metal ions from wastewater by chemically modified plant wastes as adsorbents: A Review. *Bioresource Technology*, 99(10), pp. 3935–3948. Available at: <https://doi.org/10.1016/j.biortech.2007.06.011>.
- WANG, S. AND ZHU, D. 2004. Adsorption heat pump using an innovative coupling refrigeration cycle. *Adsorption*, 10(1), pp. 47–55. Available at: <https://doi.org/10.1023/b:adso.0000024034.39430.94>.
- WERTH, C.J. *et al.* 1997. Effects of grain-scale mass transfer on the transport of volatile organics through sediments: 2. column results. *Water Resources Research*, 33(12), pp. 2727–2740. Available at : <https://doi.org/10.1029/97wr02426>.
- YUAN, Y. *et al.* 2016. Multifunctional stiff carbon foam derived from bread. *ACS Applied Materials & Interfaces*, 8(26), pp. 16852–16861. Available at: <https://doi.org/10.1021/acsami.6b03985>.
- YUNXIA, W. AND SHANCHEN, H. 2015. Ecomusée en Chine : Entre Idéal et réalité. *Des patrimoines et des normes*, pp. 241–251. Available at: <https://doi.org/10.4000/books.putc.10119>.
- ZHU, X. *et al.* 2014. Effective adsorption and enhanced removal of organophosphorus pesticides from aqueous solution by ZR-based mofs of UIO-67. *ACS Applied Materials & Interfaces*, 7(1), pp. 223–231. Available at: <https://doi.org/10.1021/am5059074>.

Chapter Three

PREPARATION AND STRUCTURAL PROPERTIES OF CARBON FOAM DERIVED FROM NATURAL GRAIN AND PYROLYTIC WASTE CHAR

Khumalo, Siphesihle Praise-God*, Lokhat, David, Sewpersad, Ajay & Seevnarain, Aleshya

School of Engineering, University of KwaZulu-Natal, Howard College Campus, Durban, South Africa

Correspondence should be addressed to Khumalo S.P.: spgkhumalo@gmail.com

(Submitted and under review)

Abstract

This study investigates the thermal and mechanical properties of carbon foam derived by an affordable, green, and template-free carbonisation method using natural grain and pyrolytic char. The carbon foam prepared had a self-assembled structure with flour as a basic element, and its shape and original network structure are inherited from bread. It was observed that the grain-based carbon foam was mechanically firm and able to sustain a considerable load without appreciable deformation. It was also able to withstand high temperatures without its structures breaking down because of heat flow through the pores. Temperatures inside porous material are disturbed by the pore distribution; due to the uneven distribution of pores, the temperature distribution becomes irregular along the heat flow direction. An increase in porosity leads to a smaller thermal conductivity. The study illustrated that carbon foam from the natural grain mixture with pyrolytic char is a viable stand-in for foams made from other materials, can be mass-produced like regular bread, and is a feasible substitute for carbon foams made from other materials.

Keywords: Carbon foam, pyrolytic char, natural grain mixture, thermal and mechanical test

Introduction

Waste tyres are proving to be a critical environmental and social problems not only in South Africa but worldwide, with significant hazards associated with illegal dumping, stockpiling, and burning. Efforts are currently being directed toward waste tyre management, and pyrolysis is proving to be a promising form of waste tyre recycling that produces potentially valuable products (Martínez, 2013). Pyrolytic tyre char is a carbonaceous solid product originating from the carbon black filler within tyres, constituting 40% of the total mass produced by pyrolysis (Helleur, 2001). Pyrolytic tyre char can be used as a starting point for making carbon foam (Helleur, 2001).

Carbon foam is a porous carbon product containing regularly shaped, predominantly concave, homogeneously dispersed cells that interact to form a three-dimensional array throughout a carbon continuum (Klett J., 2000). The material possesses many unique characteristics, such as low density, high thermal stability, noise insulation, chemical inertness, tailorable electrical and thermal conductivity, as well as good mechanical properties (Diaz, 2007). Carbon foam has many structural and insulating applications in aerospace engineering, energy storage, and temperature maintenance due to its large geometric surface area and interconnected pores, which provide well-defined pathways for reactants to easily access active sites (Inagaki, 2015). Moreover, carbon-based materials can also be used in other applications, such as water purification and gas storage, as well as traditional support materials for metal catalysts and as solid acid catalysts (Agrawal, 2017). Carbon foam could also be used in many ways, such as in environmental, chemical, and renewable energy conversion applications (Ge M, 2007).

The synthesis of the carbon foam used in this study proceeds via a one-pot process where the carbon precursor and pyrolytic char are combined and then carbonised together. When the natural grain mixture is baked and carbonized, it forms a porous structure. This study aims to produce carbon foam from a mixture of natural grains and pyrolytic tyre char. The obtained carbon foam was characterised by physical, mechanical, thermal resistance, and morphological studies. Minerals in fine coal act like additives that change the properties of the finished product.

Materials and methods

Materials and Chemicals

The following materials were used: 300 g baking flour, and 5 g dry yeast. The following reactants were utilised for this study: Pyrolytic char, argon gas, pressurised air, ethylene blue dye (powder), and water. All chemicals were used as supplied with no further purification.

Methods

Carbon foam Preparation

Waste tyre pyrolysis produces pyrolytic char (Helleur, 2001). Pyrolytic char can be used as a coal-like carbon-neutral fuel, an alternative to coke in the metals industry, an adsorbent, and a soil amendment, among other things (Antal, 2003). Baking flour weighing 300 g and varying amounts of pyrolytic tyre char (100 g, 150 g, and 300 g) were mixed in a large bucket. Figure 1 depicts the schematic diagram illustrating the process of carbon foam preparation. A mixture of 5 g of dry yeast in 115 mL of water was prepared and stirred until the yeast was dissolved. Then, the dissolved yeast was added to the dry ingredients, followed by water. To ensure a uniform distribution of each material and an even texture throughout, the mixture

was placed under an electrically powered stirrer for 5 to 10 min. The paste was then deflated and placed in an aluminium baking tray for 60 min at 60 °C in an oven. This process ensures paste fermentation, due to the dry yeast added, and forms the porous structures within the carbon foam. The mixture was further baked for 40 min at 180 °C; at this stage, the foam formed resembled that of a bread mixture. The foam was then placed in an oven for another 18 h at 80 °C to remove excess moisture. The foam was cut into a small strip and placed in a laboratory tube furnace to allow the carbonisation process to occur, and nickel grease was applied around the edges of the tube to make sure no gas escaped.

The carbonisation process occurred in an argon gas atmosphere at a flow rate of 0.4 cm³/min and a heating rate of 10 °C/min. The flow rate was adjusted to ensure a continuous flow of argon gas throughout the tube furnace. The carbon foam reached a maximum temperature of 600 °C inside the tube furnace, and that temperature was kept constant for 90 min, also known as the holding time. The carbon foam was then cooled naturally in an argon atmosphere until it reached room temperature. Three samples were prepared, and each sample had a varied amount of pyrolytic tyre char added. The preparation procedure remained the same; only the amount of pyrolytic tyre char was varied for each sample. The samples were used to determine the thermal and mechanical properties. The mass fraction of char added to sample A, B and C were 0.25, 0.33 and 0.5 respectively.

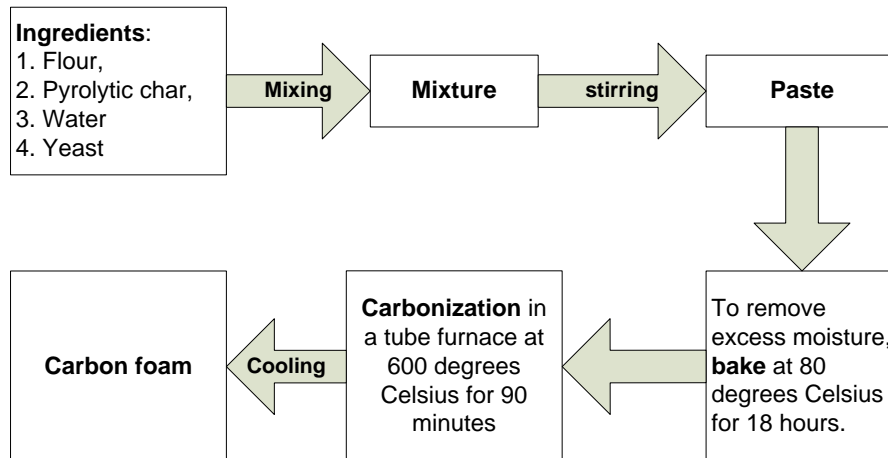


Figure 1. Scheme of carbon foam preparation

The preliminary fabrication step is based on a bread making process, following a carbonization process as illustrated in Figure 2, flour-based (containing glucose and protein) bread was used as a carbon source. The lack of oxygen prevented the material from burning like burnt toast; hence an argon atmosphere was used for the carbonization step.

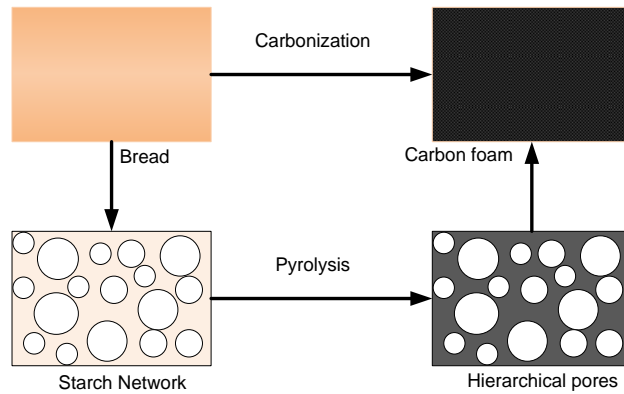


Figure 2. Fabrication of carbon foam derived from bread, adapted from (Yuan, 2016)

Laboratory tube furnace setup

A rotameter was attached to an Argon gas cylinder, to ensure a continuous gas flow throughout the carbonisation process. The carbon foam was placed inside the metal tube, connected to the rotameter, and then the metal tube was placed into the furnace. At the furnace outlet, rubber tubes were connected to a glass chamber, which contained water. The bubbling water inside the glass chamber indicated that Argon gas was unobstructed through the tubes. Hence, the amount and size of foam added were important, to prevent any blocking and build-up of pressure. The tubes were connected to an outlet of the glass chamber, which released the argon gas into the atmosphere. Figure 3 depicts the laboratory tube furnace.

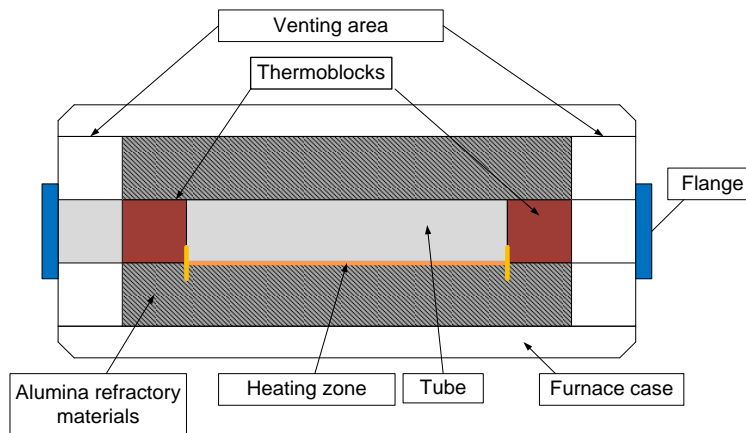


Figure 3. Scheme of tube furnace carbonisation

Results and Discussion

Open Flame Test

An initial temperature of 22°C was measured and recorded before the start of each test. This temperature was used as a reference since it was constant. A direct flame from a gas lighter, was applied on the upper surface of the carbonised foam. A thermocouple, placed underneath the carbonised foam, was used to record the temperatures that each sample can withstand. The needle-like end (temperature-sensitive part) was pierced through the side of an aluminium baking tray before switching on the thermocouple. The tested

sample was placed on top of the needle-like end, and thereafter the thermocouple was switched on. A gaslighter was used to provide the heat (flame), and it was applied directly to the carbon foam. The flame was applied to the foam for approximately one minute, and changes to the foam structure were recorded. Observations of odour, colour, and structural change were recorded. The sample was simply pinched between fingers to test whether it was hard or brittle.

The temperature increased from the initial temperature of 22°C, after 28 seconds for sample A. The sample reached a maximum temperature of 35.2°C. No deformation of the foam structure was observed while heating the sample. Despite the sample reaching a relatively high temperature, no odour was released. During the heating process, the surface that was directly exposed to the flame enflamed, while the rest of the sample remained unchanged. The carbon foam was not hot after the flame was removed, and the temperature remained the same as the reference temperature. Like sample A, sample B showed an increase in temperature after 28 seconds, and the highest temperature reached was 31.8°C. While the sample was being heated, it did not show any signs of "redness," hence it remained in its original state throughout the process. No deformation of its structure was observed.

The maximum temperature obtained for sample C was 41.5°C. The temperature increased drastically approximately 16 seconds after the flame was applied. During the heating process, the entire sample was slightly red, showing that the heat travelled throughout the sample in a very short space of time. No observable odour was released during this process. After the flame was removed, the entire sample was hot; however, there were no changes in its structure. The low temperatures found in samples A and B indicated that these samples were temperature resistant. Samples A and B contained a much greater porous structure than sample C. These porous structures trapped some of the heat within them and directed the flow of heat throughout the entire material, which may also be lost to the surroundings. Hence, these samples had a much lower temperature since the temperature was "evenly" distributed within the material. Samples A and B possess some insulating properties compared to sample C. Figure 4 depicts the outcomes of the open flame and ethanol-soaked burnt tests.

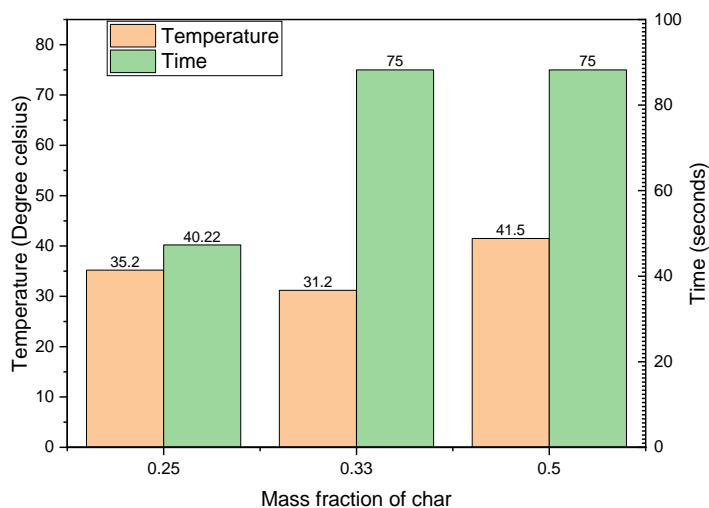


Figure 4. Results of open flame test and ethanol-soaked burnt test

In complex structures, the thermal conductivity of a porous material depends not only on porosity and thermal property but also on pore structures (Kang, 2015). For heat flow inside the porous material, the existence of non-uniform pore structures leads to complicated heat conduction, which plays a significant role in the heat transfer performance of the porous material (Eksilioglu A., 2006). Conduction involves solid conduction and gas conduction. It is known that the thermal conductivity of a gas is much lower than that of a solid. Thus, the hierarchical pores will significantly contribute to thermal resistance (Beechem T., 2005).

Ethanol-soaked Burn Test

Each sample was immersed in a beaker filled with 100 ml of ethanol for 15 seconds. Each sample was in the “ethanol bath” for 20–30 seconds. The sample was then removed and placed onto an evaporating glass dish, and thereafter it was immediately ignited. After sample A was set alight, 25 seconds later, the edges turned red. The flame took approximately 40.22 seconds to go out. During the burning process, no appreciable odour was observed, as well as no breakdown of the structures within the sample. However, immediately after the flame went out, the sample did feel slightly warm.

The aspects mentioned above were also tested for sample B, resulting in similar results. It was noted that the time taken for the flame to last was 75 seconds, which is twice if for it took sample A. The sample remained its original colour, with no shape change. Sample C: The flame took 75 seconds to extinguish. It was observed that after 17 seconds, the sample turned red, resulting in the sample being relatively hot after the flame went out. The overall structure of the shape was maintained throughout the burning process. Based on the findings, it can be concluded that the materials containing the most pyrolytic tyre char had a longer-lasting flame than the other samples. Samples B and C took a long time for the flame to go out. Hence, more ethanol was absorbed within the structure, indicating that these samples contain a clustered porous structure. For sample A, only a small amount of ethanol was absorbed within the material, which clearly shows that the resulting material was highly porous. Neither odour nor shape changes were observed before or after the test conducted.

Carbon foam non-uniform pore structure triggers different heat flows inside the porous material (Kang, 2015). Carbon foam thermal conductivities remain relatively low (Eksilioglu A., 2006). A challenge for general thermal insulating materials is their poor resistance to fire. The burn tests that were performed, namely the open flame test and the ethanol-soaked test, indicate that the carbon foam has a high fire-resistance performance. These findings indicate that carbon foam is an excellent candidate for thermal insulation materials (Beechem T., 2005). The results obtained demonstrate a promising method to manufacture an economical, robust carbon material for applications in industry, as well as topics regarding environmental protection and the improvement of energy efficiency.

Strength Test

Weights, ranging from 5 g to 1000 g, were placed on top of each sample to determine the stiffness of carbonised foam. All observations were noted and recorded. Weights, varying from 5 g to 1000 g, were provided to determine the stiffness of the carbon foam. Each weight of a specific size was placed on top of

each sample. Any changes in the appearance of the foam were noted. Figure 5 depicts the weights utilised during the strength test.

Weights ranging from 5 g to 500 g were placed on the top of sample A. The sample was able to withstand all weights under 500 g without deforming. However, when a 500 g weight was on placed the sample, it was slightly crushed. When a 1000 g weight was placed, the carbon foam was completely crushed into crumbs. Similar results were obtained for sample B. The material started to break down when a 500 g sample was placed on top of sample B. At 1000 g, the sample was fully crushed. Figure 5 depicts the samples that were used for the strength test.

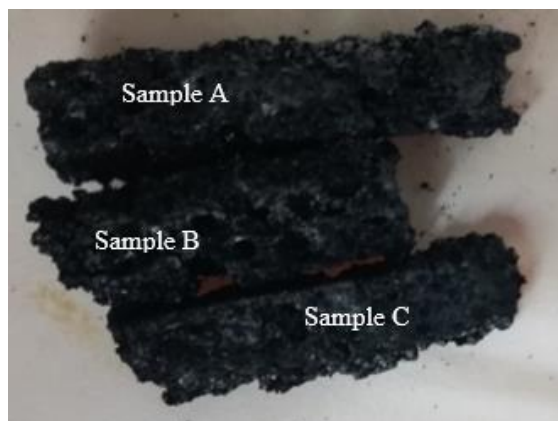


Figure 5. Photograph of char samples, soon after removal from the tube furnace

The maximum weight that sample C could withstand was 200 g. This sample's composition was broken down much faster than the previous two samples. In this test, samples A and B were successful because they could withstand more weight than sample C. It is stiff and lightweight, making it good for structural applications. Figure 6 illustrates the graphical representation of the strength test.

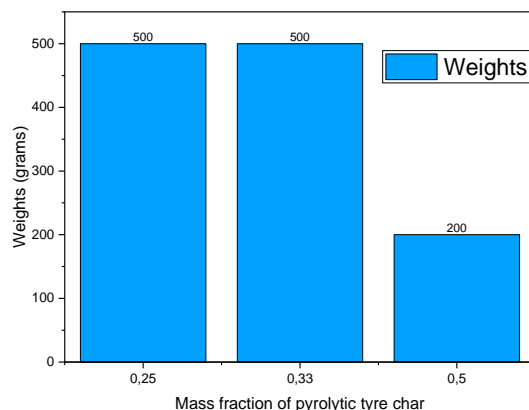


Figure 6. Mass fraction versus the maximum weight the samples can withstand

Sample C had the least number of airy pockets because it had the most pyrolytic tyre char added. These airy pockets lie within the foam and render it mechanically stiff. The size of the material tested is also a factor that plays a vital role in determining strength. Hence, small weights were used in this test due to the small sample sizes. It can be concluded that samples A and B contained a higher amount of porous structure

within their material, hence being to withstand a much larger weight (Wang Y., 2009). The lack of oxygen prevented the material from burning like burnt toast; hence, an Argon atmosphere was used for the carbonisation step. Pore size and pore distribution are important factors determining the properties of porous carbon materials (Inagaki, 2009). Many factors can influence hierarchical pore structures (Li J., 2009). The hierarchical pore structures can be tuned by many factors (Zygmunt Marczenko, 2000). By varying the amounts of yeast, water, and pyrolytic char in the mixture, the size of the holes in the foam can vary (Yunxia, 2011). Near-round pores of a few hundred micrometres in size can be visible to the naked eye (Wang Y., 2009).

Characterisation

The results shed information on the pore structure of natural-grain-based carbon foam. The carbon foam has enhanced micropore volume and surface area (Yuan, 2016). Figure 7 depicts Transmission electron microscopy (TEM) image of the natural-grain carbon foam. The granular carbon foam produced a lot more pores. The surface of the material contained an amorphous, porous structure and geometrical features with an irregular form, large agglomerates, and a rough surface, which would provide extra sites for the adsorbing medium (Chen, 2006). These characteristics have been demonstrated to be helpful for synthetic carbon foam.

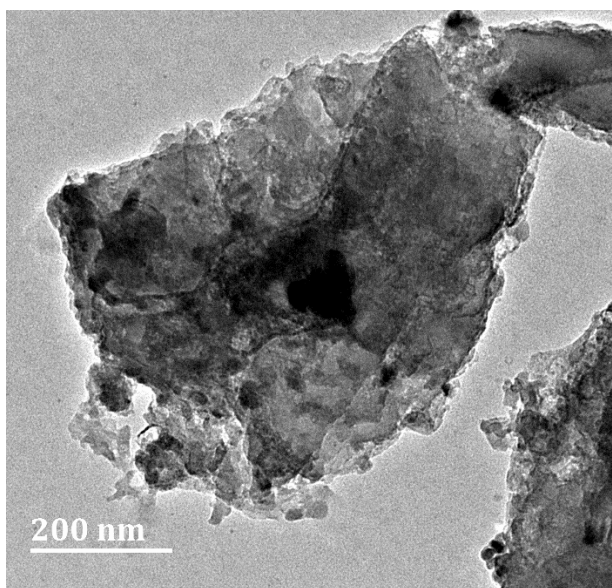


Figure 7. TEM image conducted on a Jeal 2100 HRTEM operating at 200 KV carbon foam based on natural grain and pyrolytic char

Conclusion

Carbon foam was prepared from natural grains and varying compositions of pyrolytic char. The products obtained were characterised by TEM analysis, open flame test, ethanol-soaked burn test, and strength test. Temperature transfer inside porous materials is hampered by pore distribution. Due to the uneven distribution of pores, the temperature inside the porous material is no longer uniform, and temperature

distribution is irregular along the heat flow direction. An increase in porosity leads to a smaller thermal conductivity. Carbon foam could be mass-produced like regular bread and is a feasible substitute for foams made from other materials. Carbon foam is relatively stable and non-flammable. Pore size can be varied by controlling the temperature, pressure, precursor, water, and pyrolytic tyre char content. This allows the carbon foam to be used for a variety of applications.

References

- AGRAWAL, V. R., VAIRAGADE, V. S., & KEDAR, A.P. 2017. Activated Carbon as Adsorbent in Advance Treatment. *Journal of Mechanical and Civil Engineering (IOSR-JMCE)*, 14, 36-40.
- ANTAL, M. J. A. M. G. G. 2003. The Art, Science, and Technology of Charcoal Production. *Industrial & Engineering Chemistry Research* 42, 1619-1640.
- BEECHEM T., L. K., & ELGAFY A 2005. Bubble growth mechanism in carbon foams. *Carbon*, 43, 1055-1064.
- CHEN, C., KENNEL, E. B., STILLER, A. H., STANSBERRY, P. G., & ZONDLO, J. W. 2006. Carbon foam derived from various precursors. *Carbon*, 44, 1535-1543.
- DIAZ, J., ALVIM-FERRAZ, M., ALMEIDA, M., RIVERA-UTRILLA, J. & SÁNCHEZ-POLO, M 2007. Waste materials for activated carbon preparation and its use in aqueous-phase treatment: A review. *Journal of Environmental Management*, 85, 833-846.
- EKSILOGLU A., G. N., YARDIM M.F, & EKINCI E. 2006. Mesophase AR pitch derived carbon foam: effect of temperature, pressure, and pressure release time. *journal of Materials Science*, 41, 2743-2748.
- GE M, S. Z., CHI WD, AND LIU H. 2007. Anisotropy of mesophase pitch-derived carbon foams. *Carbon*, 45, 141-145.
- HELLEUR, R. E. A. 2001. Characterization and potential applications of pyrolytic char from ablative pyrolysis of used tires. *Journal of Analytical and Applied Pyrolysis*, 58-59, 813-824.
- INAGAKI, M. 2009. Pores in carbon materials-importance of their control. *New Carbon Materials*, 24, 193-232.
- INAGAKI, M., QIU, J. AND GUO, Q. 2015. Carbon foam: Preparation and application. *Carbon*, 87, 128-152.
- KANG, M. I. A. F. 2015. Pore development in carbon materials. *Carbon Materials Science and Engineering*, 87, 123-152.
- KLETT J., H. R., ROMINE E., WALLS C., AND BURCHELL T 2000. High-thermal conductivity, mesophase-pitch-derived carbon foams: effect of precursor on structure and properties. *Carbon*, 38, 953-973.
- LI J., W. C., ZHAN L., QIAO W.M., LIANG X.Y., & LING L.C. 2009. Carbon foams prepared by supercritical foaming method. *Carbon*, 47, 1204-6.
- MARTÍNEZ, J. D. E. A. 2013. Waste tyre pyrolysis – A Review. *Renewable and Sustainable Energy Reviews*, 23, 179-213.
- WANG Y., M. Z., CAO M., & XU D. 2009. Effect of heating conditions on pore structure and performance of carbon foams. *New Carbon Mater*, 24, 321-6.
- YUAN, Y., DING, Y., WANG, C., XU, F., LIN, Z., QIN, Y., LI, Y., YANG, M., HE, X., PENG, Q. & LI, Y. 2016. Multifunctional Stiff Carbon Foam Derived from Bread. *ACS Applied Materials & Interfaces*, 8, 16852-16861.
- YUNXIA, Y., KEN, C., & NICK, B. 2011. Porous carbon- supported catalysts for energy and environmental applications. *Catalysis Today*, 178, 197-205.

ZYGMUNT MARCZENKO, M. B. 2000. *Separation, Preconcentration and Spectrophotometry in Inorganic Analysis*, Elsevier.

Chapter Four

SYNTHESIS OF NOVEL CARBON-SUPPORTED IRON OXIDE SORBENTS FOR ADSORPTION OF DYE FROM AQUEOUS SOLUTIONS: EQUILIBRIUM AND FLOW-THROUGH STUDIES

Siphesihle Praise-God Khumalo*, David Lokhat, Kimbelin Chetty & Latisha Chetty, Scientific Reports 12, 20009(2022). <https://doi.org/10.1038/s41598-022-24257-8>

School of Engineering, University of KwaZulu-Natal, Howard College Campus, Durban, South Africa

Correspondence should be addressed to Khumalo S.P.: spgkhumalo@gmail.com

Published on the 21 November 2022

Abstract

Textile effluents contain dyes that negatively affect water bodies and inhibit photosynthesis by reducing sunlight penetration. This study investigated the adsorption capacity of an iron oxide sorbent immobilised on naturally derived carbon foam to remove organic methylene blue dye from water. In this study, the carbon and iron oxide precursors were mixed and carbonised in a single vessel. Baking and carbonization of the natural grain combination produce a porous structure that can effectively support the iron oxide particles. The carbon foam prepared had a self-assembled structure with flour as a basic element. Sorbents of 6 weight (wt.) %, 15wt% iron, and a 0wt% iron control sample were prepared. Transmission electron microscopy (TEM) and Brunauer-Emmett-Teller (BET) techniques were used to examine the physical properties and surface morphology of the synthesised carbon foam. The adsorption capabilities were investigated in batch tests by determining the effects of an increase in iron content, sorbent dosage, contact time, and dye concentration. Breakthrough curves were obtained by varying the height of the sorbent bed and varying the flowrate of the dye solution. A higher bed height corresponds to a greater amount of adsorbent. The breakthrough and equilibrium adsorption capacities were found to increase with increasing bed height. When the flow rate is high, the dye solution leaves the column before equilibrium, resulting in shorter breakthrough and saturation times. Higher bed heights and lower flow rates resulted in optimal dye removal in the flow through the system. Breakthrough time increases with increasing iron content. The 15 wt% iron sample displayed superior adsorption capabilities than the 6 wt% sample, while the 0 wt% iron control sample displayed minimal adsorptive capabilities. The pseudo-first order kinetic model was the best fit model for this study ($R^2 > 0.96$), and the adsorption equilibrium is best described by the Freundlich isotherm ($R^2 > 0.99$). The results showed that an iron oxide sorbent immobilised on carbon foam made from natural sources is a good adsorbent for removing methylene dye.

Keywords: *TEM, BET, adsorption, methylene blue, dye, breakthrough*

Introduction

Water pollution is a global issue, and the textile industry is one of the major contributors. The textile dyeing industry uses much water during the different dyeing and finishing stages, among other things (Taman, 2015). Dyes' nonbiodegradability and resistance to light and oxidising agents complicate the selection of an appropriate method for their removal. Furthermore, toxicity bioassays have shown that most dyes are toxic (Mahmoodi, 2010). Because of reduced light penetration, dyes can significantly impact photosynthetic processes in aquatic life (Mahmoodi, 2010). As a result, removing colour from waste effluents has become increasingly important for the environment (Vasques, 2009). Most industries use water bodies, such as rivers and lakes, to dispose of their wastes (Al-Kadhi, 2019). This waste is saturated with colorants, salts, and other toxicants, which alter the clarity and pH of the water. Some communities rely on rivers and lakes as sources of drinking water. The discharge of these untreated effluents can pose health risks when ingested by humans and animals. Therefore, the discovery and implementation of new wastewater treatment methods is a high priority. Some dyes generate toxic, carcinogenic, and mutagenic intermediates through hydrolysis, oxidation, and other processes (Sanghi, 2002). Because of this, it is important to get rid of wastewater dyes before putting them back into the natural environment (Wang, 2005).

Furthermore, dyes can evade conventional wastewater treatment methods because they are designed to withstand physicochemical and biological degradation (Benguella, 2009). Adsorption is an enticing, simple, and effective method of removing pollutants from wastewater. Low-cost adsorbents are made from low-cost materials or even waste and appear to be economically appealing for practical application (Tara, 2020). Several materials have been used as adsorbents, including agricultural wastes, natural compounds, and activated carbon (Uğurlu, 2009). Removing dyes using conventional waste management methods can prove challenging as dyes comprise complex molecular structures, which makes them non-biodegradable (Mahmoodia, 2013), resistant to aerobic digestion, and stable to oxidising agents and light. Possible dye removal methods include coagulation, froth floatation, chemical oxidation, and adsorption (Jain, 2015). Adsorption is the most flexible method because it can be used on a wider range of compounds (Shah, 2016).

Many methods have been used to remove dyes from coloured wastewater, including coagulation/flocculation, biological treatment, ozonation, photocatalysis, filtration, electrochemical, membrane processing, and adsorption (Mahmoodi, 2014). Thus, among other techniques, the adsorption process has been shown to be effective due to its efficiency, capacity, and large-scale applicability for dye removal, as well as the potential for adsorbent regeneration, recovery, and recycling (Tan, 2000). Various adsorbents have been tested for their ability to remove dye from wastewater. To obtain a high-performance adsorbent, it is critical to choose more efficient and less expensive adsorbents with higher adsorption ability (Tan, 2000). A suitable adsorbent material should have a large surface area as well as a small volume (Sadeghi-Kiakhani, 2013). Other characteristics must include high mechanical strength, chemical and thermal stability, high porosity, and small pore diameter, which results in more exposed surface area and thus suitable surface chemistry, resulting in high adsorption capacity (Olasehinde, 2020). The properties of mechanical and thermal strength, high surface area, suitable ordered structure, magnetic properties, optical properties, and the ability to manipulate them for required properties have all piqued the interest of researchers (Segun M., 2020). Nanoparticles are small particles with diameters ranging from 1 to 100 nm (Ahmed, 2022). They are suitable materials for various commercial and domestic applications due to their unique properties, including catalysis, medical, imaging, agricultural, and engineering applications (Segun

M., 2020). Nanoparticles are one of the most studied materials of the 20th century because they have unique and new properties and can be used in many ways (Ahmed, 2022).

This study intends to determine the adsorption efficiency of an iron oxide sorbent immobilised on naturally derived carbon foam for the removal of organic dye from an aqueous solution (Li, 2014). The effects of varying the iron content of the sorbent, contact time, dye concentrations, and sorbent dosage were studied. Also, the determination of saturation and breakthrough points of the sorbent were investigated. A carbon foam was synthesized, and its dye adsorption ability was investigated. The isotherm and adsorption kinetics of dye were thoroughly investigated.

This carbon source was tested as a model compound to prove the concept, particularly because it was easy to obtain and manipulate. The intention is to eventually progress to a different type of natural grain, one that is not used as a food source and can be used to produce the same or similar quality of carbon foam (as a support for the iron). The synthesis of the iron oxide on the carbon foam used in this study proceeds via a one-pot process where the carbon precursor and iron oxide precursor are combined and then carbonised together. When the natural grain mixture is baked and carbonized, it forms a porous structure that the iron oxide particles can use to stick to.

Materials and Methods

Materials and chemicals

The following ingredients were used: flour (300 g), yeast (5 g), water (400 mL), 99.99% pure iron nitrate crystals (14g), and deionised water.

Iron nitrate of analytical grade purity and methylene blue dye were purchased from Sigma-Aldrich. The argon gas used for the carbonisation process was purchased from Afrox.

Sorbent preparation

The natural grain mixture made of flour, water, and yeast were mixed in a large beaker for 10 minutes using the overhead stirrer. The mixture was then transferred to the aluminium trays. The sample was placed in an oven, which was set at 35 °C for 60 min to promote activation of the yeast. Thereafter, the sample was transferred to a second oven, which was set at 180 °C to bake. The oven rack was lined with aluminium foil to contain spills as the mixture rose significantly during the baking process. The second oven temperature was changed to 80 °C after 40 min, and the sample was left to dry in these conditions for 18 h. Carbonisation of the dried sample took place in the u-tube furnace under argon flow. A rotameter regulated the flow of argon gas. The analytical balance was used to measure how much iron was in the sorbent by weighing the samples.

Spectrophotometric analysis

The UV-Vis spectrophotometer was switched on and given 15 min to warm up. The sorbent was removed from the treated solution through vacuum filtration. The setup included a Buchner flask and funnel. Stainless steel mesh was placed in the Buchner funnel as a filter. Cuvettes were used to test the filtered solutions, and the digital absorbance readings were recorded.

Calibration of the Spectrophotometer

Methylene blue powder was mixed with deionised water to produce aqueous solutions of the following concentrations: (5, 10, 15, 20, 30, 40) mg/L. The spectrophotometer was switched on and allowed to warm up for 10-15 min. The spectrophotometric analysis was performed at the wavelength of maximum adsorption, which was 662 nm for methylene blue dye (Naseri, 2015). A cuvette filled with distilled water was used as the reference solution. This cuvette was inserted into the spectrophotometer and the device was set to show an absorbance value of zero. The cuvette was then removed. A second cuvette was filled with the 5 mg/L solutions, placed in the spectrophotometer and the device was run. The digital reading obtained, which indicated the amount of light absorbed by the solution, was recorded. For each concentration of methylene blue solution, all the steps were done again. For each sample, a new cuvette was used so that the solution wouldn't get diluted.

Batch Tests

Glass beakers (50 mL) were used to conduct the iron content, sorbent dosage, and contact time tests. The beakers were covered with parafilm to avoid contamination. For the contact time test, a magnetic stirrer was employed to agitate solutions. The tests were carried out for each of the 3 samples at concentrations of dye solutions of 10 mg/L and 20 mg/L, respectively.

When the concentration of the solution after adsorption is known, the absorbance can be calculated. Absorbance is a measurement of the milligrams of dye adsorbed per gramme of sorbent. The following equation was used to determine the absorbance capacity of the sorbent (Marczenka, 2000).

$$q_t = \frac{(C_0 - C_t) \times V}{m} \quad (1)$$

$$q_e = \frac{(C_0 - C_e) \times V}{m} \quad (2)$$

Where q_t (mg/g) is an adsorption density, q_e (mg/g) is an adsorption density at equilibrium, C_0 (mg/L) is the initial concentration of aqueous solution, C_t (mg/L) is the concentration of aqueous solution at time t , C_e (mg/L) is an equilibrium concentration of aqueous solution, V (L) is the volume of solution, and m (g) is the mass of adsorbent.

To obtain the percentage removal of dye, the initial and final concentration of the solution were required. The calculation was carried out using the following equation (Yaqoob, 2020):

$$\%R = \frac{(C_0 - C_t) \times 100}{C_0} \quad (3)$$

Where % R is the percentage of methylene blue dye removed, C_0 (mg/L) is the initial concentration of aqueous solution, and C_t (mg/L) is the concentration of aqueous solution at time t .

Flow-through Tests

A flow-through apparatus was used to determine the breakthrough and saturation points of the sorbent. Figure 1 below shows the setup of the apparatus. The suction pipe of the peristaltic pump was placed in a beaker filled with a 10 mg/L solution, and the release pipe was placed at the top of the glass column. Another beaker was placed at the exit point of the glass column to collect the treated water. This set-up made sure that the solution was pumped from beaker 1 to the glass column at a certain flow rate, where it went through the sorbent bed and ended up in beaker 2.

For the breakthrough tests, the effluent from the glass tube was tested at regular intervals to find out when the concentration of the effluent started to rise, or when the breakthrough happened, and when the sorbent reached its saturation point.

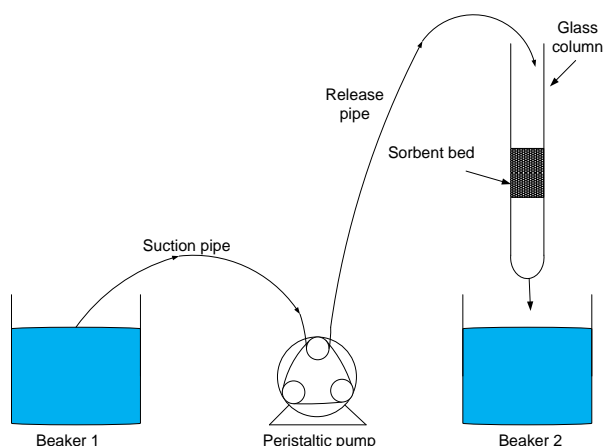
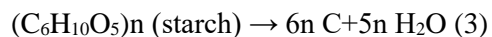


Figure 1. Flow-through apparatus setup

Results and Discussion

Preparation of sorbent

Preparation of the sorbent was carried out according to the procedure outlined (Marczenka, 2000). To determine the effect of iron content on the adsorption process, the samples were required to comprise different quantities of metal loadings. This was achieved by varying the amount of iron nitrate added to each sample. The iron nitrate was thermally decomposed to form iron oxide through a pyrolysis process under argon flow. A scaling calculation was used to obtain the final weight percentage of iron in the samples. Three samples were prepared. Sample A contained 6 wt. Sample B contained fifteen wt% iron, and sample C was produced as a control sample, which contained no iron. The natural grain mixture served as a carbon source due to the glucose and protein it contains. Carbonisation under argon flow transformed the mixture into the desired sorbent. The following equation shows the reaction that occurred during the carbonisation process.



Discussion

The samples exhibited visual differences after the baking process and before carbonisation. A colour difference was observed. The 0 wt% sample, which contained no iron, was the lightest in colour and the most brittle. After the process of carbonisation, the samples became visually identical, black in colour, and resembled charcoal. The carbon foam was very light and had a soft, powdery feel, which made it easy to break up into smaller pieces.

Advantages and disadvantages

Nanomaterials offer excellent antifouling capabilities for many membranes and applications. Iron oxide gives iron immobilised in natural grain-based carbon foam both mechanical strength and stability. Since adsorption is a surface event, the nanoparticles presence increases the surface area (Idan, 2017). If an abundant source of the natural grain precursor material can be identified, it has the potential to be a sustainable sorbent. Since it has less surface area than activated carbon, this could make it harder to sell.

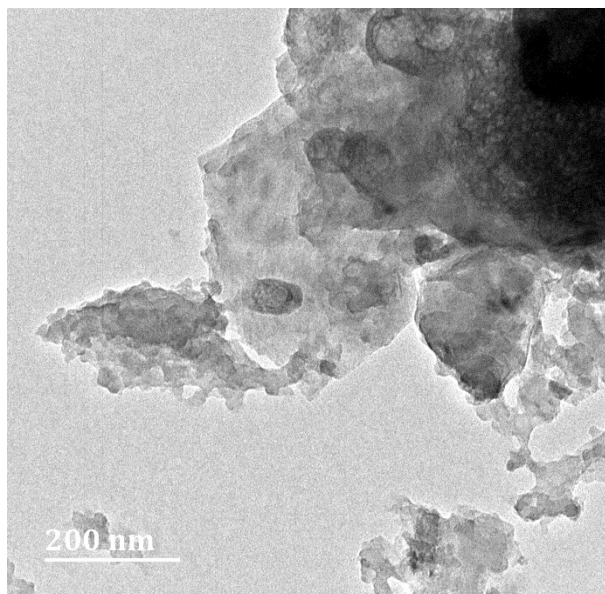
Characterisation of an adsorbent

Table 1 displays the findings of the investigations into the BET surface area, micropore volume, and pore radius. The results provide light on the pore structure of the carbon foam made from natural grains. The surface area of the samples with 15 wt% and 6 wt% iron is greater than that of the sample with 0 wt% iron. Additionally, the micropore volume of both 6 wt% and 15 wt% of iron was greater than 0 wt% of iron content of 0 wt%. The carbon foam has increased surface area, micropore volume. The presence of iron enhances the action of the yeast, i.e., the consumption of sugars in the grain mixture and the production of carbon dioxide, which is responsible for developing the pore structure in the carbonised material.

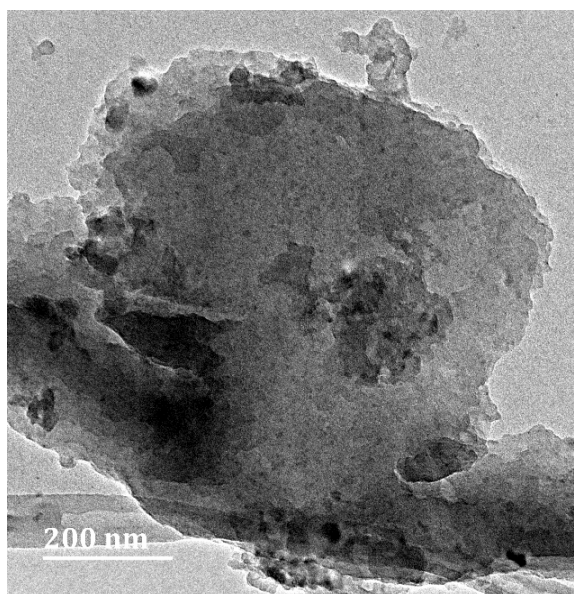
Table 1. BET analysis

Parameters	0 wt% iron	6 wt.% iron	15 wt.% iron
BET surface area m ² /g	0.0211	4.546	3.759
Average pore volume cm ³ /g	0.014 x 10 ⁻³	1.145 x 10 ⁻³	1.211 x 10 ⁻³
Average pore diameter	25.891	12.272	11.985
Average hydraulic pore radius	0	3.792	4.791

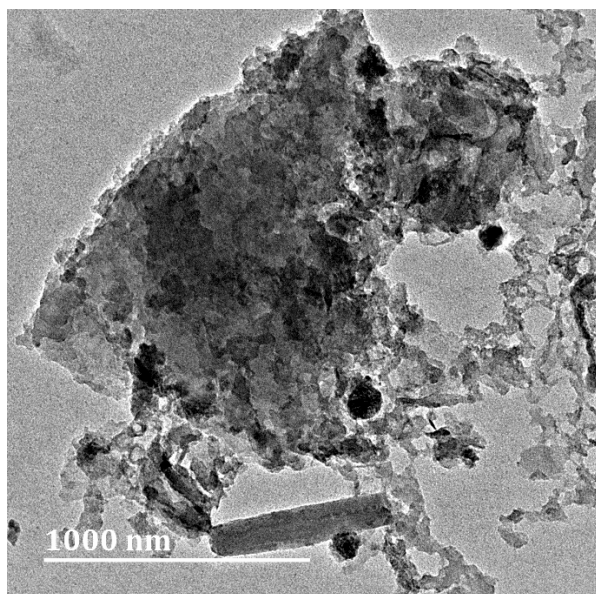
The TEM micrographs of the natural grain carbon foam are shown in Figure 2. It is evident that the addition of iron nitrate particles to the grain carbon foam resulted in a more amorphous and porous structure. The material surface possessed geometrical characteristics with an uneven shape, big agglomerates, and a rugged surface, which would provide additional sites for adsorbing heavy metal ions. These attributes were shown to be advantageous for the synthesised carbon foam.



(a)



(b)



(c)

Figure 2. TEM image conducted on a Jeol 2100 HRTEM operating at 200KV (a) carbon foam with 0 wt% iron (b) carbon foam with 6 wt% iron (c) carbon foam with 15 wt% iron

Effect of Iron content

Three samples of 0 wt%, 6 wt%, and 15 wt% iron on carbon foam of 20 mg were investigated using 10 mg/L and 20 mL of methylene blue dye. The contact time for each sample was 30 min. Thereafter, the solutions were vacuum filtered and absorbance readings were taken using the spectrophotometer. A control sample was used to determine the adsorption efficiency of the carbon support. Figure 3 shows that the control sample adsorbed less than 1% of the dye after 30 min, whereas the 6 wt% iron sample adsorbed

11.05 % and the 15 wt% iron sample adsorbed 20.26 %. This miniature effect on dye removal indicates that the carbon support was beginning to absorb after 30 min. During the same time, the 15 wt. 1% iron sample adsorbed approximately 9.21% more dye than the 6 wt.% iron sample. This suggested that an increase in iron content within the sample increased the adsorptive properties of the sorbent (Alkhouzaam, 2021). However, studies carried out by Taromi and Kaliaguine (2018) showed that if the metal content of the sample is excessive, then agglomeration may occur, which increases the size of the iron particles, thereby reducing the surface area (Mohajershojaei, 2015). Because of this, metal oxide is wasted, and the ability of a sorbent to take up water is also reduced.

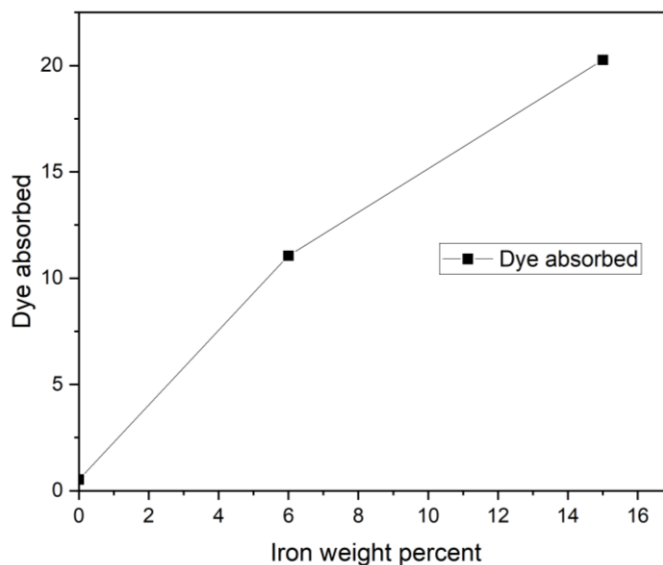


Figure 3. Effect of the iron content of the carbon foam at sorbent dosage of 20 mg, concentration of 10 mg/L, and contact time of 30 minutes

Figure 4 displays the concentration of iron ions as a function of reaction time. The decrease in iron ion leaching as the reaction progressed suggests that iron ions in the solution may be redeposited on the iron-carbon foam surface (Taromi, 2018). At the end of Figure 4, the variation of iron ion concentration with reaction time is depicted. The decrease in iron ion leaching as the reaction progressed suggests that iron ions in the solution may be redeposited on the iron-carbon foam surface. At the conclusion of the reaction (180 min), iron leaching was less than 3.61 mg/L for a 15 wt.% sample and 4.64 mg/L for a 6 wt.% sample, with a negligible difference from a 0 wt.% iron control sample. This low level of leaching showed the stability and reusability of the iron-carbon foam particle electrodes, which was in line with the BET and TEM analyses.

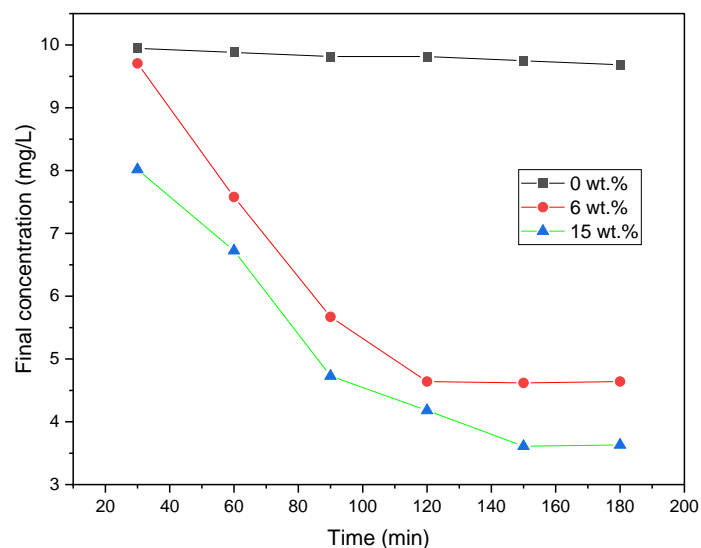


Figure 4. The leaching of iron ions, concentration of 10 mg/L, and contact time of 180 minutes.

Effect of sorbent dosage

Sorbent dosage test experimental design was conducted for 20, 40, 60, 80, and 100 mg of sorbent dosage. The concentrations of 10 mg/L and 20 mg/L methylene blue dye were utilised with a volume of 20 mL and contact time of 180 minutes. Three absorbance readings were taken for each filtered solution, and an average value was calculated. An increase in the amount of sorbent added to the aqueous solution improved the percentage of dye adsorbed over a period of 180 minutes for all the samples, see Figure 5 (Pirillo, 2009a). For the 6 wt% sample, at 20 mg of sorbent, 5.13 % of the dye was adsorbed from the 10 mg/L solution. This percentage increased to 40.44 % when a 100 mg dose was used. The rise in adsorption can be accredited to the increased availability of adsorptive sites that is the resultant of a higher dosage (Pathania, 2017). Initially, the removal of dye is rapid as the dosage increases from 20 mg to 80 mg; thereafter, there is an observable decrease in gradient. Such behaviour implies a decrease in adsorption efficiency. The adsorption efficiency of a sorbent is known to decrease when the sorbent approaches its saturation point. The driving force for adsorption declines as the dye molecules accumulate within the pores of the sorbent. This lessens the intensity of the attractive forces between the dye molecules and the sorbent, resulting in adsorption occurring at a slower pace. Figure 5 shows that samples of 6 wt% and 15 wt% displayed similar trends. The deviation between the samples was the amount of dye removed. A sample of 15 wt.% of iron, which consisted of a higher metal loading than the sample of 6 wt% of iron, adsorbed significantly more dye. The largest difference occurred at a sorbent dose of 100 mg, where 15 wt% of the iron adsorbed 54.69% of the dye. This was a deviation of approximately 14.25%. Therefore, the sample of 15 wt% of iron had a higher adsorptive capacity due to its higher metal loading. The control sample showed a slight increase in adsorption with increasing dosage. However, the highest dosage of 100 mg resulted in only 2.5% of the dye being removed. This indicated that the carbon support did not have a major impact on the adsorption efficiency of the sorbent. Adsorbent dosage increases dye adsorption due to increased adsorbent surface and the availability of more adsorption sites (Oyelude, 2011). When the adsorption capacity was expressed in milligrams adsorbed per gramme of material, the capacity decreased with increasing adsorbent amount. It happens when adsorption sites overlap or group together, which makes less

adsorbent surface area available to the dye and makes the length of the dye path of diffusion longer (Tara, 2020).

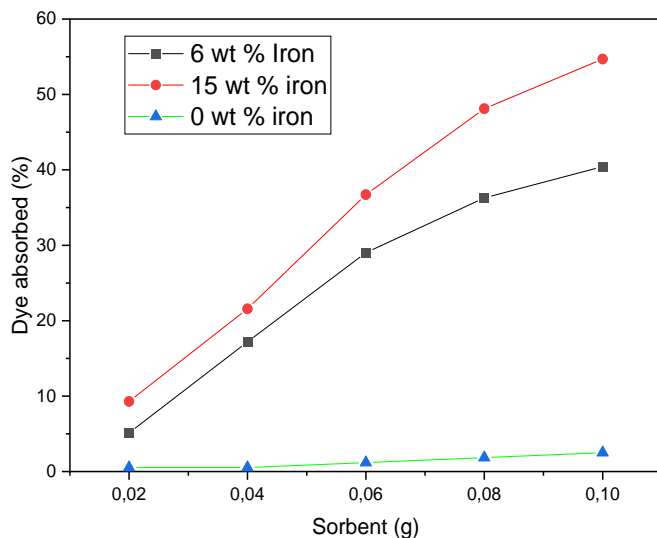


Figure 5. Effect of the iron content of the carbon foam at sorbent dosage, concentration of 10 mg/L, and contact time of 30 minutes

Effect of contact time

Figure 6 displays the effect of contact time and concentration on the adsorption of methylene blue dye per gramme of sorbent. It was found that absorbance increased with increasing contact time. For the 10 mg/L solution, a steady increase in dye removal was observed during the first 90 minutes, after which the slope of the graph lessened and eventually levelled off at 120 minutes. Since the sorbent initially has no dye coating its surface, there are strong attractive forces between the surface of the sorbent and the dye molecules. As the sorbent becomes saturated, the large driving force for adsorption diminishes, and the adsorption efficiency decreases after 90 minutes. When the sorbent reached its saturation point at 120 minutes and an absorbance value of approximately 2.14 mg/g, no further adsorption took place. This is illustrated by the horizontal line displayed from the 120 minutes mark to the 180 minutes mark. The 20 mg/L solution shows higher absorbance during the first 90 minutes, see Figure 6. This is a result of the increased number of dye molecules in the solution. The larger concentration gradient promoted more rapid adsorption. Before the sorbent became saturated, the adsorption efficiency for the 20 mg/L solution was much higher than the maximum efficiency for the 10 mg/L solution. This rise with increasing concentration is the result of an increased driving force for adsorption. This test showed that a solution with a higher concentration made the sorbent work better because it took less time for the sorbent to reach its maximum dye-removing ability.

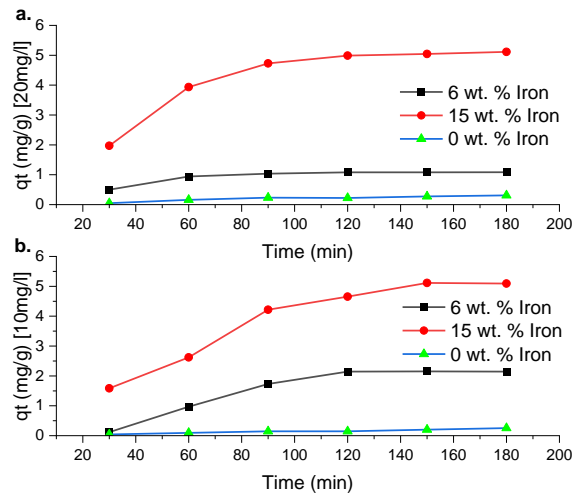


Figure 6 Effect of Iron content on carbon foam at sorbent of 50 mg, 10 mg/L dye concentration and contact time of 180 minutes and Effect of Iron content on carbon foam at sorbent of 20 mg, 100 mg/L dye concentration and contact time of 180 minutes.

The percentage of dye adsorbed for each of the samples is shown in Figure 7. A distinct difference in dye removal is noted for each of the 3 samples. As shown by the iron content test, the 15 wt% iron sample had the highest percentage removal of 63.68% after 180 minutes. Sample A removed 53.60% of the dye, and sample C continued to display minimal adsorption capabilities with a dye removal percentage of just 3.14%. The sorbent dosage was kept constant for this test at 20 mg, and it was noted that the saturation point differed for samples with 6 wt% and 15 wt% of iron. Sample A reached saturation at 120 minutes, while Sample B reached its saturation point at 150 minutes. This showed that an increase in iron content not only increases the amount of dye removed per gramme of sorbent but also extends the lifespan of the sorbent.

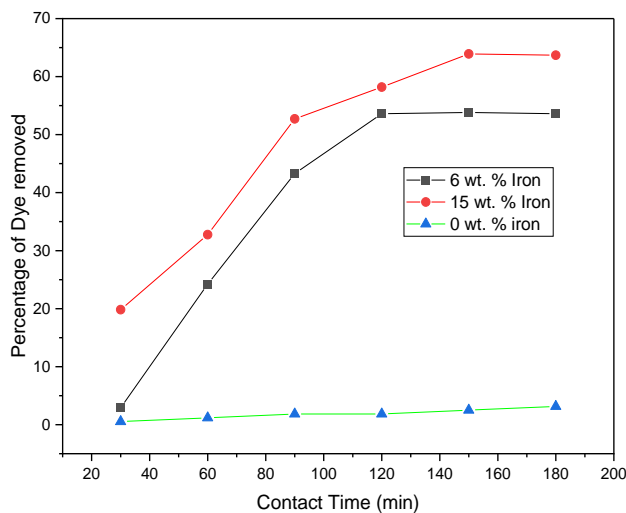


Figure 7. Effect of contact time, sorbent dosage (50mg), concentration of dye solution (10 mg/L), and volume of solution (20 mL).

Adsorption kinetics

Adsorption kinetics were investigated to determine the relationship between contact time and dye uptake. At a constant temperature of 25 °C, the initial concentration influence of the reagent on the adsorption kinetics was investigated.

Pseudo-first and pseudo-second order equations

For the investigation of modelling of adsorption kinetics, Lager Gren pseudo-first order and pseudo-second order models were used for the investigation. The nonlinear form of pseudo-first order is given by the following equation:

$$q_t = q_e(1 - e^{-K_1 t}) \quad (4)$$

The nonlinear form of pseudo-second order is given by the following equation:

$$q_t = \frac{q_e^2 K_2 t}{1 + K_2 q_e t} \quad (5)$$

Where q_t (mg/g) is the amount absorbed at time t , q_e (mg/g) is the amount remaining after equilibrium of adsorption, and K_1 and K_2 are the pseudo-first and pseudo-second order model rate constants, expressed in min^{-1} and g/mg/min , respectively. Table 2 and Table 3 illustrate the calculated values of q_e , K_1 , K_2 , and the regression coefficient R^2 values. Figure 8 shows the plot of pseudo-first order and pseudo-second order. The validity of a model is judged by evaluating correlation coefficients R^2 and the comparability of experimental and calculated values of q_e . Therefore, a pseudo-first order model is the best fit for the adsorption process of methylene blue on carbon foam.

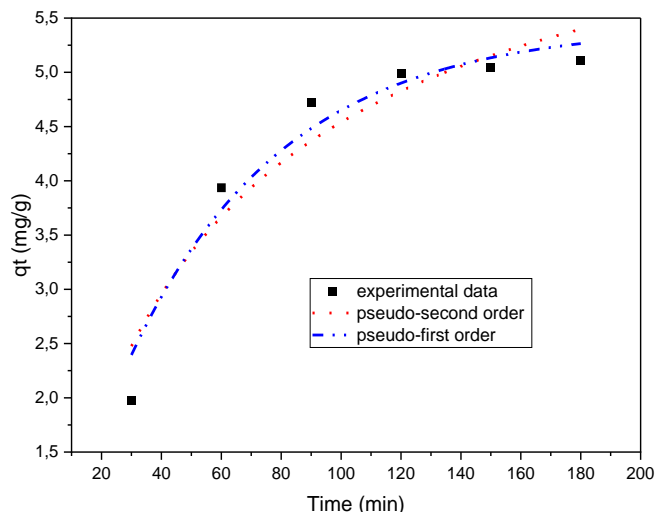


Figure 8. Nonlinear fit of pseudo-first order and pseudo-second order for dye adsorption on carbon foam with 15 wt% iron, 20 mg/L solution, initial concentration of 10 mg/L

Table 2. Pseudo-first order parameters

Pseudo First order				
Iron wt%	Exp. qe (mg/g)	Calc. qe (mg/g)	K₁ (min⁻¹)	R²
10 mg/L solution concentration				
6%	2.263	3.501	0.006	0.875
15%	5.390	6.252	0.011	0.967
20 mg/L solution concentration				
6%	1.107	1.129	0.245	0.943
15%	5.355	5.404	0.019	0.957
0%	0.391	0.423	0.007	0.937

Table 3. Pseudo-second order parameters

Pseudo Second order				
Iron wt%	Exp. qe (mg/g)	Calc. qe (mg/g)	K₂ (mg/g/min)	R²
10 mg/L solution concentration				
6%	2.263	6.088	0.001	0.870
15%	5.239	9.274	0.001	0.958
0%		2.012	3.795	0.965
20 mg/L solution concentration				
6%	1.107	1.393	0.019	0.888
15%	5.355	7.062	0.003	0.922
0%	0.391	0.423	0.007	0.934

Intraparticle diffusion

The intraparticle diffusion resistance was evaluated using the intraparticle particle diffusion model by Weber and Morris (Crini, 2008), given by the following equation:

$$q_t = k_{id}t^{1/2} + c \quad (6)$$

Where q_t (mg/g) is the adsorption amount at time t (min), k_{id} (mg/g/min^{1/2}) is the adsorption rate constant of the intraparticle diffusion model, and c is a constant related to the thickness of the boundary layer. The plot of q_t versus $t^{1/2}$ is the sole rate-limiting step of the adsorption process if it is linear and passes through the origin (Weber, 1963a). When the lines of uptake pass through the origin, the rate-controlling step is intraparticle diffusion. When the plots do not pass through the origin, it indicates that the intraparticle diffusion is not the only rate-limiting step, but that other kinetic models may also control the rate of adsorption, all of which may be operating concurrently (Mahmoodia, 2013). The plots of intraparticle diffusion illustrated in Figure 9 are non-linear and do not pass through the origin. This indicates that

intraparticle diffusion was not the only rate-limiting step of the adsorption process of methylene blue onto iron supported by carbon foam but that other mechanisms may also control the rate of the adsorption, all of which may be operating simultaneously (Rathi, 2020).

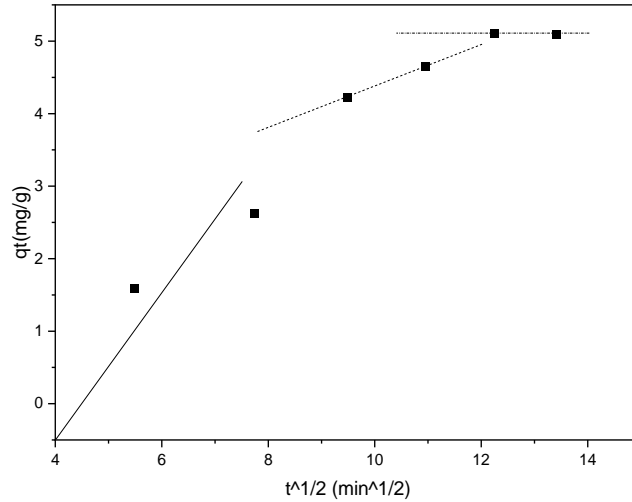


Figure 9. Plot of the intraparticle diffusion model for methylene blue onto iron supported by carbon foam (50 mg), 10 mg/L solution, room temperature

Equilibrium Adsorption

Adsorption equilibrium occurs between the adsorbed molecules and the adsorbent surface when an adsorbate is in contact with the adsorbent. The adsorption isotherm is the equilibrium relationship between the amount of adsorbed (q_e) and the residual adsorbate concentration (C_e) at constant temperature (Dutta, 2013). In general, adsorption isotherms provide information on the affinity and the binding energy between the adsorbate and the adsorbent, on the adsorption capacity, and on the surface phase, which may be considered as a monolayer or multilayer (Narasimharao, 2022). The modelling of the adsorption isotherms consists of describing the exponential data using theoretical or empirical mathematical equations and allowing the determination of isotherm parameters to compare the efficiency of different adsorbents. The adsorption isotherm investigates the relationship between the amount of dye adsorbed onto an adsorbent and the concentration of dye in the liquid phase (Tara, 2020).

The empirical Freundlich model, which is good for low concentrations and is based on sorption on the uneven surface, is shown by the following equation:

$$q_e = K_F C_e^{1/n} \quad (7)$$

Where C_e (mg/L) is the equilibrium concentration of adsorbate, q_e (mg/g) is the amount of adsorption at equilibrium. K_F and n are Freundlich constants related to the adsorption capacity and adsorption intensity, respectively. The Freundlich model is an empirical equation based on the solute distribution at equilibrium between the solid and aqueous phases (Fatima, 2019). The Freundlich model is applied to heterogeneous surfaces, but it can only describe adsorption data over a limited range (Uğurlu, 2009).

All the parameters of the isotherm models were calculated from nonlinear fitting of q_e versus C_e in Origin Lab. The Temkin model reflects the properties of indirect adsorbate-adsorbent interactions on the adsorption isotherm. It assumes that the heat of adsorption of all molecules in the layer decreases linearly with coverage due to adsorbate-adsorbent interactions (Fatima, 2019). Furthermore, a uniform distribution of binding energies, up to a maximum binding energy, characterises adsorption (Wang, 2005). The Temkin model is expressed by the following equation:

$$q_e = \frac{RT}{b} \ln(AC_e) \quad (8)$$

q_e (mg/g) represents the amount of adsorption at equilibrium, C_e (mg/L) represents the equilibrium concentration of adsorbate, T (K) represents the temperature in Kelvin, R (J/mol/K) represents the universal gas constant, b (J/mol) represents the heat of adsorption, and K_T represents the equilibrium binding constant proportional to the maximum binding energy.

Figure 10 illustrates the curves of Freundlich and Temkin using equations 7 and 8, respectively. Table 4 depicts calculated parameters of Freundlich and Temkin isotherms, R^2 values, obtained by the nonlinear fitting method. Based on the R^2 value comparisons, the Freundlich model represents a better fit of experimental data at equilibrium compared to the Temkin model. Thus, the adsorption process of methylene blue can be best described by the Freundlich isotherm, which indicates the multilayer adsorption on the heterogenous surface with a different energy distribution. The Freundlich constant, n , is a measure of adsorption intensity (Taman, 2015). A value of $1/n$ was found to be between 0 and 1, indicating the favourable adsorption of methylene blue (Arora, 2016).

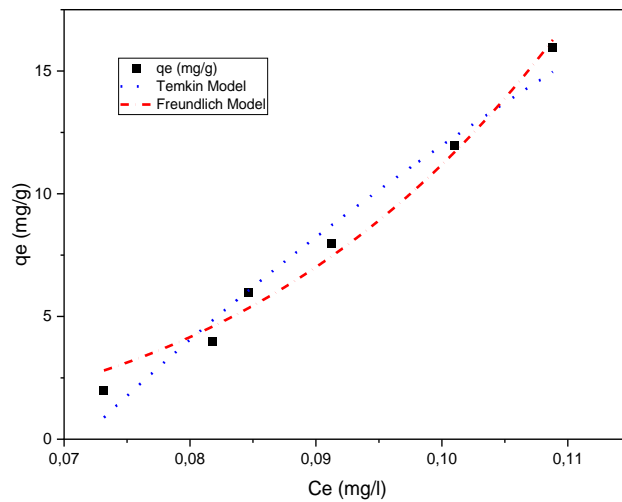


Figure 10. Fitting of adsorption isotherms into experimental data

Table 4. Temkin and Freundlich isotherm parameters

Temkin Model			Freundlich		
b	A	R ²	1/n	K _F	R ²
69,85	14,01	0,97	0.23	303192,56	0,99

Adsorption mechanism

The adsorption rate was governed a multistep elementary reaction mechanism, since intraparticle diffusion was not the only rate-limiting step of the adsorption process of methylene blue onto iron supported by carbon foam but that other mechanisms may also control the rate of the adsorption, all of which may be operating simultaneously (Gurses, 2006b). Also, as the Freundlich isotherm was the best fit for this study and is used to represent adsorption processes that occur on heterogeneous surfaces and active sites with varying energies based on multilayer adsorption and equilibrium, it was the most appropriate model for this investigation. These complicated processes may involve lateral contacts, numerous binding sites, and/or non-random adsorbate contributions. In recent years, it has been considered that multi-step adsorption contributes to the estimation of the adsorption rate.

Flow-through apparatus

The performance of the flow-through apparatus was studied by examining breakthrough curves and saturation points of the sorbent. Breakthrough curves represent the ratio of effluent concentration to initial concentration over a specified period. A flow-through apparatus acts as a fixed bed column where the bed is made up of an adsorbent. The treated water flows through the fixed bed and the contaminants adhere to the surface of the adsorbent, releasing the treated water into the environment. The detoxication and recycling processes present in the textile industry must be implemented on a large scale due to the exorbitant amount of water required for finishing processes. Therefore, the efficiency and cost-effectiveness of treatment processes become a major consideration. The breakthrough point is defined as the phenomenon when the solute begins to appear in the effluent, while the exhaustion point occurs when the outflow concentration reaches the inflow concentration (Taman, 2015). The studies were carried out at room temperature.

The transport of solute from bulk solution through liquid film to the adsorbent exterior surface is represented by the first portion of the plot on the left. The second part is attributed to intraparticle diffusion as a slower process. The slope of the linear part shows the rate of the adsorption process; the lower slope corresponds to a slower adsorption process. Thus, initially at the rate of diffusion of methylene blue molecules, they are quickly adsorbed onto the interior of adsorbent particles. Last, the last part is due to the final equilibrium stage, when the intraparticle diffusion slows down because there isn't much dye in the water.

Effect of Flowrate

Variation of the flowrate was achieved by altering the speed of the peristaltic pump. For this test, three-speed settings of 5 mL/min, 10 mL/min, and 15 mL/min were used for this test, whilst the concentration and bed height were kept constant at 10 mg/L and 2 cm, respectively. Figure 11 provides a visual representation of the time taken for the concentration of the effluent to begin to increase to its original concentration. This point in time is referred to as the "breakthrough time." The trend portrayed by Figure 11 suggests that an increase in flow rate resulted in a decrease in the breakthrough time. At 5 mL/min, the breakthrough time was between 30 and 40 minutes, whereas, for the 15 mL/min run, the breakthrough occurred much sooner, between 10 to 20 minutes. A consequence of higher flowrates is the decrease in contact time between the dye molecules and the adsorbent. This significantly reduces the amount of adsorption occurring as the solution passes through a fixed bed. This results in an increased effluent concentration, which can be seen by the decreasing gradient of the curves in Figure 11 as the flowrate increases. The faster breakthrough can also be explained in terms of mass transfer, where it is known that mass transfer increases with increasing flowrates and this results in poor residence time. This then leads to increased effluent concentration and faster breakthrough (El Maguana, 2019).

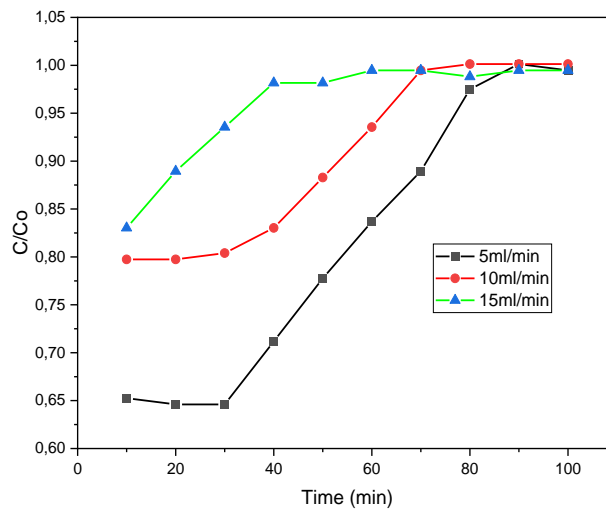


Figure 11. Flowrate breakthrough curve for 6 wt% iron

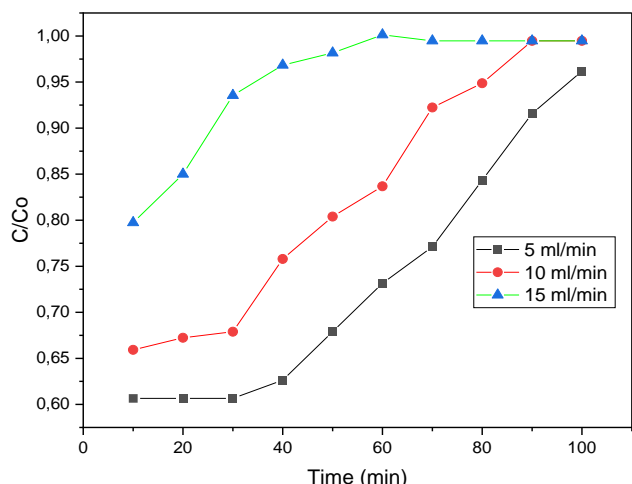


Figure 12. Flowrate breakthrough curve for 15 wt% iron

The sample of 15 wt.% iron shown in Figure 12, all 3 flowrates, showed additional dye removal compared to the sample of 6 wt% iron in Figure 11. This agrees with the conclusion of the iron content test, where it was reported that sorbents of higher metal loadings displayed increased adsorption capabilities. The gradients in Figure 11 appear to level out at the point of saturation for each of the tested flowrates. This did not occur in Figure 12 for the 5 mL/min flowrate, thus indicating that saturation was not reached within 100 minutes. Although the dye removal was superior for the sample of 15 wt.% iron, there was little to no improvement in the breakthrough points or each flowrate as they occurred within the same time ranges as the sample of 5 wt.% iron. Even though the breakthrough points didn't change for the sample with 15 wt.% iron, sample B was better at adsorption because it removed more dye and could be used for longer.

Effect of bed height

A breakthrough curve can be obtained when using a flow-through apparatus. This curve illustrates the relationship between time and the concentration of the adsorbate (contaminant) in the effluent stream. Initially, when the solution begins to flow through the column, rapid adsorption should occur as the driving force for adsorption is largest at this point due to the absence of contaminants on the sorbent surface. This should result in a low concentration of adsorbate in the effluent. The breakthrough point refers to the point at which the concentration of the adsorbate in the effluent begins to rise. This is an indication of a decrease in the driving force for adsorption. Once the concentration of the effluent approaches the concentration of the original solution, the sorbent is said to be approaching its saturation point. When saturation is near, the concentration of the effluent is the same as the concentration of the original solution. At this point, no more adsorptions can happen.

The bed heights used for this test were 1 cm, 2 cm, and 3 cm, whilst other variables such as methylene blue dye concentration and flowrate were kept constant at 10 mg/L and 10 mL/min, respectively. At 10-minute intervals, cuvettes were used to collect the effluent from the tube, and these samples were tested with the spectrophotometer. Three readings were taken, and average values were calculated. This procedure was repeated for bed heights of 2 cm and 3 cm.

Figure 13 illustrates the relationship between time and the amount of organic dye in the effluent for each of the 3-bed heights investigated. It was observed that an increase in bed height resulted in an increase in the breakthrough time. This is plausible because at greater bed heights, the solution remains in contact with the sorbent for a longer duration, which results in a greater percentage of dye removal. Higher bed heights imply more sorbent. Hence, as with the sorbent dosage test, the increase in surface area increases the availability of adsorption sites, thereby increasing the adsorption efficiency. The slope of the breakthrough curve was found to increase with increasing bed height. In terms of mass transfer, this can be attributed to the increased length of the mass transfer zone. The breakthrough time increased from the range of 10 to 20 minutes to 30 to 40 minutes as the bed height increased from 1 cm to 3 cm. Therefore, to obtain an effluent of lower concentration for a longer time, a larger bed height was necessary. Because there is more adsorbent in a bed with a higher height, the breakthrough and equilibrium adsorption rates go up.

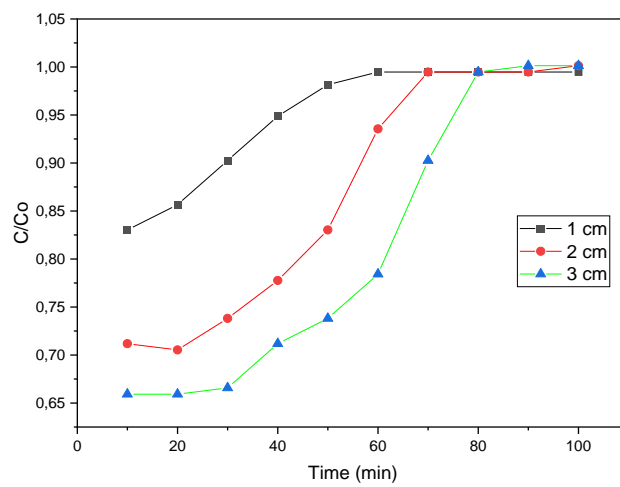


Figure 13. Height breakthrough curve for 6 wt% iron

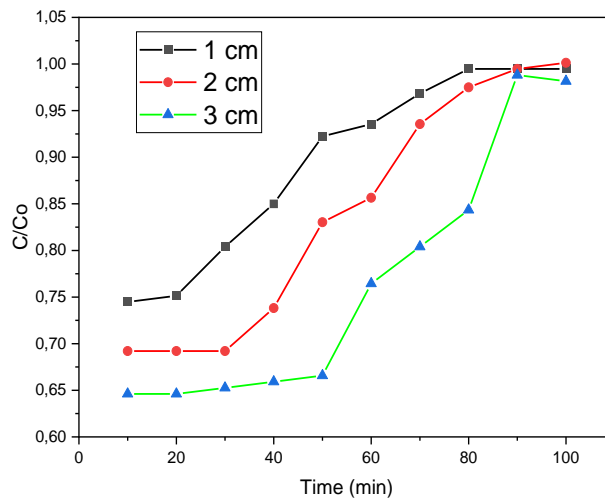


Figure 14. Height breakthrough curve for 15 wt% iron

The increased iron content of the sample at 15 wt.% increased the amount of adsorption occurring at bed heights of 1 cm and 2 cm. It was observed that the breakthrough time for these bed heights also increased.

Figure 14 shows that the breakthrough occurred between 20 and 30 minutes for the 1 cm bed, whereas for sample A, at the same bed height, the breakthrough occurred between 10 and 20 minutes. This is a result of the increased iron content, which increases the surface area available for adsorption. For the 3 cm run, it was observed that initially the same amount of dye was adsorbed as sample A. This was implied by the C/C_0 ratio, which reflected a value of 0.65 on Figures 13 and 14. As the flowrate was constant at 10 mL/min for both runs, this may have impacted the adsorption of dye molecules by limiting the interaction between the molecules and the sorbent. Therefore, the limited contact time may have inhibited the dye adsorption for the 15 wt.% iron sample. Figure 14 showed that the breakthrough occurred between 50 and 60 minutes for a 15 wt.% iron sample, which was much later than the breakthrough for a sample of 6 wt.% iron, which was between 30 and 40 minutes. Refer to Figure 11. It should also be noted that the saturation points of the 15 wt.% sorbent were reached much later than the 6 wt.% sample. The 3 cm bed height failed to reach saturation in the 100-minute testing period. Therefore, the 15 wt. Due to the higher metal loading of the sorbent, the 1% sample was better at attracting metal than the 6 wt.% sample.

Industrial application of flow-through apparatus

Since the addition of chemical compounds is not a requirement in the separation process, adsorption in fixed bed columns is one of the most widely used industrial processes for the removal of contaminants from aqueous textile effluents (Patel, 2019). The sorbent bed generally comprises activated carbon as this is the most effective sorbent for the treatment of textile effluents due to its large surface area. On an industrial scale, the treatment of wastewater through adsorption can be problematic as most sorbents are selected based on adsorption potential, which is directly related to the size of the sorbent particles. The best performing sorbents are generally those that have the greatest surface area (Mavros, 2008). To have a large surface area, the size of the sorbent particles would have to be minuscule. This then presents the issue of sorbent recovery. In large bodies of water, minute particles will be difficult to retrieve. The use of support will aid in recovery as multiple sorbent particles will accumulate on the support, making it easier to retrieve. However, the use of a flow-through apparatus will alleviate the need for sorbent recovery. The sorbent will be confined to the column and, once the water has been treated, it can be released directly into the environment. The spent sorbent can be renewed by simply replacing the fixed bed.

Recovery of sorbents after they have been released into wastewater becomes problematic when using traditional batch adsorption techniques, which refer to the treatment of a fixed volume of water using a fixed amount of sorbent (Qiao, 2015). Therefore, to alleviate the need for sorbent recovery, flow through adsorption systems is being investigated. The advantage of using the flow-through apparatus is that this technique of wastewater treatment is relatively inexpensive and simple to implement. In the fixed bed system used for this experiment, the sorbent was confined to the column and the dye solution continuously flowed through the sorbent bed at a constant flowrate. This process of dye removal is viable for large-scale industrial use because the large quantities of industrial wastewater would be difficult to treat using conventional batch sorption methods. Flow-through systems make sure that the dye molecules are always in contact with a certain amount of new adsorbent. This makes sure that the dye is taken out as well as possible (Qiao, 2015).

Thermodynamic Analysis

Thermodynamic parameters such as the Gibbs energy (ΔG), enthalpy (ΔH), and entropy (ΔS) are the actual indicators for the adsorption process's practical application. Which process will occur spontaneously can be predicted based on the values of these parameters (Kandisa, 2016). The following equations (Kandisa, 2016) were used to calculate the thermodynamic parameters:

$$\Delta G = \Delta H - T\Delta S \quad (9)$$

$$K_c = \frac{q_e}{c_e} \quad (10)$$

$$\ln K_c = \frac{\Delta S}{R} - \frac{\Delta H}{RT} \quad (11)$$

$$\Delta G = -RT \ln K_c \quad (12)$$

Where K_c , R , and T represent the equilibrium constant, the amount of dye adsorbed on the adsorbent of the solution at equilibrium (mol/L), the equilibrium concentration of dye in the solution (mol/L), the gas constant (8.314 J/mol K), and the absolute temperature (K). The slopes and intercepts of a graph of $\ln K_c$ versus $1/T$ can be used to estimate the ΔH and ΔS values. The Gibbs free energy of change is used to evaluate the spontaneity and feasibility of adsorption processes. Both 15 wt.% and 6 wt.% iron samples yielded negative ΔG value, -21.335 J/mol and -30.253 J/mol. The graphs of $\ln K_c$ vs $1/T$ with slopes and intercept are provided in Appendix D, Figures D.12 and D.13. Thermodynamic studies can indicate the adsorption process's spontaneity ($\Delta G < 0$), endothermic nature ($\Delta H > 0$), or exothermic nature ($\Delta H < 0$). For all samples, the Gibbs free energy of change reflects the spontaneity and practicability of adsorption processes. All the samples had exothermic adsorption.

Conclusion

Iron oxide immobilised on naturally derived carbon foam exhibits reasonable adsorption capabilities for the removal of organic dyes from aqueous solutions. Adsorption studies revealed that increasing the iron dosage resulted in the highest removal efficiency. Adsorption isotherm and kinetic model studies revealed that the Langmuir isotherm and pseudo-first order kinetic models provided the best fit for the study. The percentage of dye removal for the 15 wt.% iron content was 9.21% greater than that of the 6 wt.% sample, which indicated that sorbent efficiency increased with increasing iron content. Contact time and sorbent dosage tests showed greater adsorption occurring at higher concentrations of dye solution because of greater concentration gradients. Amplifying sorbent dosage enhanced the adsorptive properties of the sorbent due to the increased availability of adsorption sites. Increased contact time allowed for sorbent saturation to occur, therefore maximising the adsorption potential of the sorbent. Increased bed height imposes a longer contact time between the dye and sorbent, therefore increasing breakthrough time. Higher flowrates reduced the efficiency of the sorbent and decreased the breakthrough time as contact time between dye molecules and the surface of the sorbent was reduced. The use of the flow-through apparatus is inexpensive and alleviates the need for sorbent recovery. It is suitable for large quantities of water, which makes it suitable

for large-scale industrial use. The data showed that the adsorption process could be improved by using lower flowrates and increasing the contact time, concentration of the dye solution, iron content of the sample, and sorbent dosage. TEM and BET techniques were utilised to evaluate the physical characteristics and surface morphology of synthesised carbon foam. The adsorption rate was governed by a multistep elementary reaction mechanism, as intraparticle diffusion was not the only rate-limiting step in the adsorption process of methylene blue onto iron supported by carbon foam, but that other mechanisms may also control the adsorption rate, with all of them operating simultaneously. This investigation was best represented by the pseudo-first order kinetic model ($R^2 > 0.96$), while the Freundlich isotherm best describes the adsorption equilibrium ($R^2 > 0.99$). Results indicated that an iron oxide sorbent immobilised on natural carbon foam is an effective sorbent for removing methylene dye.

References

- ADELEYE, A. S., CONWAY, J.R., GARNER, K., HUANG, Y., SU, Y., KELLER, A.A. 2016. Engineered nanomaterials for water treatment and remediation: costs, benefits, and applicability. *Journal of Chemical Engineering*, 286, 640-662.
- AGRAWAL, V. R., VAIRAGADE, V. S., & KEDAR, A.P. 2017. Activated Carbon as Adsorbent in Advance Treatment. *Journal of Mechanical and Civil Engineering (IOSR-JMCE)*, 14, 36-40.
- AHMED, R. E. A. 2022. Biodegradable acid based nanocomposite-cuo-zno-ni(oh)₂/PA: A novel material for water cleansing. *Journal of Cleaner Production*, 341, 130860.
- AL-KADHI, N., S. 2019. The kinetic and thermodynamic study of the adsorption Lissamine Green B dye by micro-particle of wild plants from aqueous solutions. *The Egyptian Journal of Aquatic Research*, 45, 231-238.
- ALKHOUZAAM, A. Q., H. 2021. Functional Go-based membranes for water treatment and desalination: Fabrication Methods, performance, and advantages. A Review. *Chemosphere*, 274, 129853.
- ANTAL, M. J. A. M. G. G. 2003. The Art, Science, and Technology of Charcoal Production. *Industrial & Engineering Chemistry Research* 42, 1619-1640.
- ANTONIO TURCO , A. G. M., ELISABETTA MAZZOTTA, GIUSEPPE MARUCCIO, COSIMINO MALITESTA 2018. An Innovative Porous Nanocomposite Material for the Removal of Phenolic Compounds from Aqueous Solutions. *Nanomaterials*, 8, 334.
- ARORA, A. K., JASWAL, V. S., SINGH, K., & SINGH, R. 2016. Metal/Mixed Metal Oxides and their Applications as Adsorbents. *international Journal of Chemical Science*, 3215-3227.
- ASENCIOS, Y. J. O., LOURENÇO, V. S. & CARVALHO, W. A. 2022. Removal of phenol in seawater by heterogeneous photocatalysis using activated carbon materials modified with TiO₂. *Catalysis Today*, 388-389, 247-258.
- ASHRAF, I., SINGH, N.B. & AGARWAL, A. 2022. Green synthesis of iron oxide nanoparticles using Amla seed for methylene blue dye removal from water. *Materials Today: Proceedings*.
- ASOKAN, K. 2011. *Mass Transfer Concepts*, University press.
- BABU, S. G. A. B. 2010. Experimental, kinetic, equilibrium and regeneration studies for adsorption of Cr(VI) from aqueous solutions using low cost adsorbent (activated flyash). *Desalination and Water Treatment*, 20, 168-178.
- BAHRAM BAGHERI, S. A. H., HABIB MEHRIZADEH 2020. A Comparison of the Catalytic Activity of Cu-X₂ (X=Mn, Co) Nano Mixed Oxides toward Phenol Remediation from Wastewater by Catalytic Wet Peroxide Oxidation. *J. Water Environ Nanotechnol.*, 5, 139-146.
- BANAT, F., AL-BASHIR, B., AL-ASHEH, S. AND HAYAJNEH, O. 2000. Adsorption of Phenol by Bentonite. *Environmental Pollution*, 107, 391-398.
- BASKAR, P. P. S. A. R. B. P. P. S. A. R. 2019. Mass Transfer Enhancement for CO₂ Absorption in Structured Packed Absorption Column. *Journal of the chemical society of pakistan*, 41, 820-820.
- BEECHEM T., L. K., & ELGAFY A 2005. Bubble growth mechanism in carbon foams. *Carbon*, 43, 1055-1064.

- BENGUELLA, B., & YACOUTA-NOUR, A. 2009. *Comptes Rendus Chimie* 12, 62-771.
- BRUNO LELLIS, C. Z. F.-P., JOÃO ALENCAR PAMPFILE, JULIO CESAR POLONIO 2019. Effects of textile dyes on health and the environment and bioremediation potential of living organisms. *Biotechnology Research and Innovation*, 3, 275-290.
- CHEN, C., KENNEL, E. B., STILLER, A. H., STANSBERRY, P. G., & ZONDLO, J. W. 2006. Carbon foam derived from various precursors. *Carbon*, 44, 1535-1543.
- CHONG, M. N., JIN, B., CHOW, C.W.K. & SAINT, C. 2010. Recent developments in Photocatalytic Water Treatment Technology: A Review. *Water Research*, 44, 2997–3027.
- CRINI, G., ROBERT, C., GIMBERT, F., MARTEL, B., ADAM, O., & DE GIORGI, F. 2008. The removal of Basic Blue dye from aqueous solutions by chitosan-based adsorbent: batch studies. *Journal of Hazardous Materials*, 153, 96-106.
- DIAZ, J., ALVIM-FERRAZ, M., ALMEIDA, M., RIVERA-UTRILLA, J. & SÁNCHEZ-POLO, M 2007. Waste materials for activated carbon preparation and its use in aqueous-phase treatment: A review. *Journal of Environmental Management*, 85, 833-846.
- DUTTA, M. B., J.K. 2013. Fixed-bed column study for the adsorptive removal of acid fuchsin using carbon–alumina composite pellet. *International Journal of Environmental Science and Technology*, 11, 87-96.
- E. O. OYELUDE, U. R. O. 2011. ADSORPTION OF METHYLENE BLUE FROM AQUEOUS SOLUTION USING ACID MODIFIED CALOTROPIS PROCERA LEAF POWDER. *Journal of Applied Sciences in Environmental Sanitation*, 6, 477-484.
- EKSILIOGLU A., G. N., YARDIM M.F, & EKINCI E. 2006. Mesophase AR pitch derived carbon foam: effect of temperature, pressure, and pressure release time. *journal of Materials Science*, 41, 2743-2748.
- EL MAGUANA, Y., ELHADIRI, N., BOUCHDOUG, M., & BENCHANAA, M. 2019. Activated carbon from prickly pear seed cake: optimization of preparation conditions using experimental design and its application in dye removal. *International Journal of Chemical Engineering*, 12.
- FARAG, R. T. A. M. E. O. A. M. S. M. A. H. A. 2015. Metal Oxide Nano-particles as an Adsorbent for Removal of Heavy Metals. *Journal of Advanced Chemical Engineering* 5(3), 5.
- FATHY MUBARAK, M., MAHER AHMED, A. AND SAAD GABR, S. 2021. Nanoporous carbon materials toward phenolic compounds adsorption. *Nanopores*.
- FATIMA, B., SIDDIQUI, S. I., AHMED, R. & CHAUDHRY, S. A. 2019. Green synthesis of F-CdWO₄ for photocatalytic degradation and adsorptive removal of Bismarck Brown R dye from water. *Water Resources and Industry* 22, 100119.
- GE M, S. Z., CHI WD, AND LIU H. 2007. Anisotropy of mesophase pitch-derived carbon foams. *Carbon*, 45, 141-145.
- GIRI, S. K., DAS, N.N., AND PRADHAN, G.C. 2011. Synthesis and characterization of magnetite nanoparticles using iron ore tailings for adsorptive removal of dyes from aqueous solutions. *Colloids and Surfaces A: Engineering, Materials Science*, 389, 43-49.
- GURSES, A., DOGAR, C., YALCIN, M., ACIKYILDIZ, M., BAYRAK, R. & KARACA, S. 2006a. The adsorption kinetics of the cationic dye, methylene blue, onto Clay. *Journal of Hazardous Materials*, 131, 217-228.
- GURSES, A., DOGAR, M., YALCIN, M., BAYAQRAC, R., & KARACA, S 2006b. The adsorption of kinetics of the cationic dye, methylene blue, onto clay. *Journal of Hazardous Materials*, 131, 217-228.
- HELLEUR, R. E. A. 2001. Characterization and potential applications of pyrolytic char from ablative pyrolysis of used tires. *Journal of Analytical and Applied Pyrolysis*, 58-59, 813-824.
- IDAN, I., J., JAMIL, S., N., ABDULLAH, L.C., & CHOONG, T., S., Y. 2017. Removal of Reactive Anionic Dyes from Binary Solutions by Adsorption onto Quaternized Kenaf Core Fiber. *International Journal of Chemical Engineering*.
- INAGAKI, M. 2009. Pores in carbon materials-importance of their control. *New Carbon Materials*, 24, 193-232.

- INAGAKI, M., QIU, J. AND GUO, Q. 2015. Carbon foam: Preparation and application. *Carbon*, 87, 128-152.
- JAIN, N., DWIVEDI, M. K., AGARWAL, R., & SHARMA, P. 2015. Removal of Malachite Green from Aqueous Solution by Zeolite- Iron Oxide Magnetic Nanocomposite. *Journal of Environmental Science, Toxicology and Food Technology*, 9, 42.
- K.V., R. V. K. A. N. S. 2016. Dye Removal by Adsorption: A Review. *Journal of Bioremediation & Biodegradation*, 7.
- KANDISA, R. V., SAIBABA, N. K., SHAIK, K., B., & GOPINATH, R. 2016. Dye Removal by Adsorption: A Review. *Journal of Bioremediation & Biodegradation*, 7.
- KANG, M. I. A. F. 2015. Pore development in carbon materials. *Carbon Materials Science and Engineering*, 87, 123-152.
- KLETT J., H. R., ROMINE E., WALLS C., AND BURCHELL T 2000. High-thermal conductivity, mesophase-pitch-derived carbon foams: effect of precursor on structure and properties. *Carbon*, 38, 953-973.
- LAURA G. CORDOVA VILLEGAS, N. M., MIAO CHEN, DEBJANI MUKHERJEE, KEITH E. TAYLOR & NIHAR BISWAS 2016. A Short Review of Techniques for Phenol Removal from Wastewater. *Current Pollution Reports*, 2, 157-167.
- LI J., W. C., ZHAN L., QIAO W.M., LIANG X.Y., & LING L.C. 2009. Carbon foams prepared by supercritical foaming method. *Carbon*, 47, 1204-6.
- LI, N., ZHAO, P., & ASTRUC, D. 2014. Anisotropic gold nanoparticles: Synthesis, properties, applications, and toxicity. *Angewandte Chemie International Edition*, 53, 1756-1789.
- LOPEZ, F. J. A. A. F. A. 2020. Adsorption Processes in the Removal of Organic Dyes from Wastewaters: Very Recent Developments. In: SUMMERS, I. A. M. A. J. K. (ed.) *Promising Techniques for Wastewater Treatment and Water Quality Assessment*.
- LUZ-ASUNCIÓN, M. D., SÁNCHEZ-MENDIETA, V., MARTÍNEZ-HERNÁNDEZ, A.L., CASTAÑO, V.M., & VELASCO-SANTOS, C. 2015. Adsorption of phenol from aqueous solutions by carbon nanomaterials of one and two dimensions: kinetic and equilibrium studies. *Journal of Nanomaterials*, 16, 422.
- MAHMOODI, N., M., ARAMI, M 2010. Immobilized titania nanophotocatalysis: Degradation, modeling and toxicity reduction of agricultural pollutants. *Journal Alloys Compd*, 506, 155-156.
- MAHMOODI, N. M., NAJAFI, F. & NESHAT, A. 2013. Poly (amidoamine-co-acrylic acid) copolymer: Synthesis, characterization and dye removal ability. *Industrial Crops and Products*, 42, 119-125.
- MAHMOODI, N. M., SADEGHI, U., MALEKI, A., HAYATI, B. & NAJAFI, F 2014. Synthesis of cationic polymeric adsorbent and dye removal isotherm, kinetic and thermodynamic. *Journal of Industrial and Engineering Chemistry* 20, 2745-2753.
- MAHMOODIA, N., M., NAJAFIB, F., & NESHATC, A. 2013. Poly (amidoamine-co-acrylic acid) copolymer: Synthesis, characterization and dye removal ability. *Industrial Crops and Products*, 42, 119-125.
- MARCZENKA, Z. 2000. Separation, Preconcentration and Spectrophotometry in Inorganic Analysis. *Elsevier*.
- MARTÍNEZ, J. D. E. A. 2013. Waste tyre pyrolysis – A Review. *Renewable and Sustainable Energy Reviews*, 23, 179-213.
- MAVROS, P., DANIILIDOU, A., C. 2008. Colour removal from aqueous solutions. Part I. Part I. Flotation. *Environmental Technology*, 15, 601-616.
- MCKAY, Y. S. H. A. G. 1998. Kinetic models for the sorption of dye from aqueous solution by wood. *Process Safety and Environmental Protection*, 76, 183-191.
- MEDJOR, W., WEPUAKA, C. AND GODWILL, S. 2015. Spectrophotometric Determination of Phenol in Natural Waters by Trichloromethane Extraction Method after Steam Distillation. *International Research Journal of Pure and Applied Chemistry*, 7, 150-156.

- MOHAJERSHOJAEI, K., MAHMOODI, N.M. AND KHOSRAVI, A. 2015. Immobilization of Laccase enzyme onto Titania nanoparticle and decolorization of dyes from single and Binary Systems. *Biotechnology and Bioprocess Engineering*, 20, 109-116.
- MOHAMMED M. RAHMAN, S. B. K., ASLAM JAMAL, AND ABDULLAH M. AISIRI 2011. Iron Oxide Nanoparticles. *Nanomaterials*.
- MP, S. 2016. Industrial Wastewater Treatment: A Challenging Task in the Industrial Waste Management. *Advances in Recycling & Waste Management*, 2.
- MP, S. 2017. Industrial wastewater treatment: A challenging task in the Industrial Waste Management. . *Advances in Recycling & Waste Management*, 01.
- NARASIMHARAO, K. E. A. 2022. Fe₃O₄@date seeds powder: A sustainable nanocomposite material for wastewater treatment. *Journal of Materials Research and Technology*, 18, 3581-3597.
- NASERI, N., VALIZADEH, H., & ZAKERI-MILANI, P. 2015. Solid lipid nanoparticles and nanostructured lipid carriers: Structure, preparation and application. *Advance Pharmaceutical Bulletin*, 5, 305.
- NIZAMUDDIN, S., SIDDIQUI, M.T.H., MUBARAK, N.M., BALOCH, H.A., ABDULLAH, E.C., MAZARI, S.A., GRIFFIN, G.J., SRINIVASAN, M.P. 2019. Iron oxide nanomaterials for the removal of heavy metals and dyes from wastewater. *Nanoscale Materials in Water Purification*, 447-472.
- OLASEHINDE, E., F., & ABEGUNDE, S., M. 2020. Adsorption of methylene blue onto acid modified raphia taedigera seed activated carbon. *Advance Journal Chemical Analysis*, 3, 663-679.
- OYELUDE, E. O., & OWUSU, U. R. 2011. Adsorption of Methylene Blue from Aqueous Solution Using Acid Modified Calotropis Procera Leaf Powder. *Water Contamination*, 6, 477-484.
- PATEL, H. 2019. Fixed-bed column adsorption study: a comprehensive review. *Applied water science*
- PATHANIA, D., SHARMA, S. & SINGH, P. 2017. Removal of methylene blue by adsorption onto activated carbon developed from ficus carica bast. *Arabian Journal of Chemistry* 10.
- PIRILLO, S., PEDRONI, V., RUEDA, E. & LUJÁN FERREIRA, M. 2009a. Elimination of dyes from aqueous solutions using iron oxides and chitosan as adsorbents: A comparative study. *Química Nova*, 32, 1239-1244.
- PIRILLO, S., PEDRONI, V., RUEDA, E., & FERREIRA, M. L. 2009b. Elimination of dyes from aqueous solutions using iron oxides and chitosan as adsorbents: a comparative study. *Química Nova*, 35, 1239-1244.
- QIAO, N., CHANG, J., HU, M. & MA, H. 2015. Novel bentonite particle electrodes based on Fenton catalyst and its application in Orange II removal. *Desalination and Water Treatment* 1-9.
- RATHI, G., SIDDIQUI, S. I., PHAM, Q. & NAM, V. T. 2020. Nigella sativa seeds based antibacterial composites: A sustainable technology for water cleansing - A Review. *Sustainable Chemistry and Pharmacy*, 18, 100332.
- RENDO, D. 2021. Adsorption of Methylene Blue Dye using Fe₃O₄ Magnetized Natural Zeolite Adsorbent. *Jurnal Kimia Sains dan Aplikasi*, 24, 51-57.
- S. F. HASANY, I. A., RAJAN J, AND A. REHMAN 2012. Systematic Review of the Preparation Techniques of IronOxide Magnetic Nanoparticles. *Nanoscience and Nanotechnology*, 2, 148-158.
- SADEGHI-KIAKHANI, M., ARAMI, M., & GHARANJIG, K. 2013. *Journal of Applied Polymer Science* 127, 2607-2619.
- SAIF, S., TAHIR, A., & CHEN, Y. 2016. Green Synthesis of Iron Nanoparticles and Their Environmental Applications and Implications. *Nanomaterials*, 6, 209.
- SANGHI, R., & BHATTACHARYA, B. 2002. Review on decolorisation of aqueous dye solutions by low cost adsorbents. *Colour Technology*, 118, 256-269.
- SEGUN M., A., KAYODE S., I., OLORUNSOLA M., A, & TINUADE, A. 2020. A review on the influence of chemical modification on the performance of adsorbents. *Resources, Environment and Sustainability*, 1.

- SHAH, M. 2016. Industrial Wastewater Treatment. *A Challenging Task in the Industrial Waste Management*
- SHOHREH MOHAMMADI, A. K., HAMIDREZA SANAEEPUR, KHALIL ABBASSIAN, ATEFEH NAJAFI & ELHAM MOFARRAH 2015. Phenol removal from industrial wastewaters: a short review. *Desalination and Water Treatment*, 53, 2215-2234.
- SONG, W., GAO, B., XU, X., XING, L., HAN, S., DUAN, P., SONG, W. & JIA, R. 2016. Adsorption-desorption behavior of magnetic amine/Fe₃O₄ functionalized biopolymer resin towards anionic dyes from wastewater. *Bioresource Technology*, 210, 123-130.
- TAMAN, R., OSSMAN, M., MANSOUR, M., & FARAG, H. 2015. Metal Oxide Nano-particles as an Adsorbent for Removal of Heavy Metals. *Journal of Advanced Chemical Engineering* 5(3), 5.
- TAN, B. H., TENG, T. T., & MOHD, O. A. 2000. Removal of Dyes and Industrial Dye Wastes by Magnesium Chloride. *PII: S0043-1354*, 99, 597-601.
- TANKSALE, S. N. A. M. T. H. S. A. N. M. M. A. H. A. B. A. E. C. A. A. S. A. M. A. G. G. A. M. S. A. A. 2019. Iron Oxide Nanomaterials for the Removal of Heavy Metals and Dyes From Wastewater. *Nanoscale Materials in Water Purification*.
- TARA, N., SIDDIQUI, S. I., BACH, Q.-V. & CHAUDHRY, S. A. 2020. Reduce graphene oxide-manganese oxide-black cumin based hybrid composite (RGO-MNO₂/BC): A novel material for water remediation. *Materials Today Communications*, 25.
- TAROMI, A. A., & KALIAGUINE, S. 2018. Hydrodeoxygenation of triglycerides over reduced mesostructured Ni/γ-alumina catalysts prepared via one-pot sol-gel route for green diesel production. *Applied Catalysis*, 140-149.
- UĞURLU, M. 2009. Adsorption of a textile dye onto activated sepiolite. *Microporous and Mesoporous Materials*, 119, 31-59.
- V. FIERRO, V. T.-F., D. MONTANÉ AND A. CELZARD 2007. Adsorption of phenol onto activated carbons having different textural and surface properties. *Microporous and Mesoporous Materials*, 111, 276-284.
- V. FIERRO, V. T.-F., D. MONTANÉ AND A. CELZARD 2008. Adsorption of phenol onto activated carbons having different textural and surface properties. *Microporous and Mesoporous Materials*, 111, 276-284.
- VANITHA KATHERESAN, J. K., AND SIE YON LAU 2018. Efficiency of various recent wastewater dye removal methods: A review. *Journal of Environmental Chemical Engineering*, 6, 4676-4697
- VASQUES, A., R., ULSON DE SOUZA, S. M., VALLE, J. E., & ULSON DE SOUZA, A. A 2009. Removal of Dyes from the Textile Industry by Adsorption in Fixed Bed Columns: A Sustainable Process. *Chemical Product and Process Modeling*, 4.
- VIKASH R AGRAWAL, V. S. V., AND AMOL P KEDAR 2017. Activated Carbon as Adsorbent In Advance Treatment of Wastewater. *Journal of Mechanical and Civil Engineering (IOSR-JMCE)*, 14, 36-40.
- WANG, S., BOYJOO, Y. CHOUAIB, A. 2005. *Chemosphere*, 60, 1401-1407.
- WANG Y., M. Z., CAO M., & XU D. 2009. Effect of heating conditions on pore structure and performance of carbon foams. *New Carbon Mater*, 24, 321-6.
- WEBER, W., J., & M, J. C. 1963a. Kinetics of Adsorption on Carbon from Solutions. *Journal of the Sanitary Engineering Division, American Society of Civil Engineers*, 89, 31-60.
- WEBER, W. J., & MORRIS, J.C. (1963). KINETICS OF ADSORPTION ON CARBON FROM SOLUTION. JOURNAL OF THE SANITARY ENGINEERING DIVISION, 89, 31-59. 1963b. Kinetics of Adsorption on Carbon from Solution. *Journal of the Sanitary Engineering Division*, 89, 31-59.
- Y. EL MAGUANA, N. E., M. BOUCHDOUG, M. BENCHANAA, AND A. JAOUAD 2019. Activated Carbon from Prickly Pear Seed Cake: Optimization of Preparation Conditions Using Experimental Design and Its Application in Dye Removal. *International Journal of Chemical Engineering*, 12.
- Y. ELSAYED, A. T. B. 2001. A Study of Acetaldehyde Adsorption on Activated Carbons. *Journal of Colloid and Interface Science*.

- YAO, T., GUO, S., ZENG, C., WANG, C. & ZHANG, L. 2015. Investigation on efficient adsorption of cationic dyes on porous magnetic polyacrylamide microspheres. *Journal of Hazardous Materials*, 292, 90–97.
- YAQOUB, A., A., PARVEEN, T., UMAR, K., & MOHAMAD, I., M., N 2020. Role of nanomaterials in the treatment of wastewater: A review. *Water*, 12, 495.
- YUAN, Y., DING, Y., WANG, C., XU, F., LIN, Z., QIN, Y., LI, Y., YANG, M., HE, X., PENG, Q. & LI, Y. 2016. Multifunctional Stiff Carbon Foam Derived from Bread. *ACS Applied Materials & Interfaces*, 8, 16852-16861.
- YUNXIA, Y., KEN, C., & NICK, B. 2011. Porous carbon- supported catalysts for energy and environmental applications. *Catalysis Today*, 178, 197-205.
- ZYGMUNT MARCZENKO, M. B. 2000. *Separation, Preconcentration and Spectrophotometry in Inorganic Analysis*, Elsevier.

Chapter Five

PREPARATION AND APPLICATION OF IRON ON CARBON FOAM FOR REMOVAL OF PHENOL FROM WATER: BATCH STUDIES

Khumalo, Siphesihle Praise-God, Lokhat, David, Anwar, Chante, Jasmine, Reddy, Huvin. Synthesis of Iron on Carbon Foam for Use in the Removal of Phenol from Aqueous Solutions. *Molecules* 2023, 28, 1272. <https://doi.org/10.3390/molecules28031272>

School of Engineering, University of KwaZulu-Natal, Howard College Campus, Durban, South Africa

Correspondence should be addressed to Khumalo S.P.: spgkhumalo@gmail.com

(published 28 January 2022))

Abstract

Abstract: The potential use of magnetic nanopowder for phenol adsorption mobilised on natural grain carbon foam from an aqueous solution was studied. Phenolic compounds are priority pollutants with high toxicity even at low concentrations. A magnetic nanopowder was synthesised by dissolving an iron sponge in nitric acid to produce iron nitrate, which was added to a natural grain mixture with flour as the main ingredient. The synthesised carbon foam was investigated for the effects of initial concentration, time, and TEM (transmission electron microscopy) characterization. The phenol adsorption increased as the iron content of the carbon foam and the initial concentration increased. A kinetic study showed that the phenol adsorption data adequately covered all the carbon foam samples tested using an equation corresponding to a pseudo-first order chemical reaction. The Freundlich, Langmuir, and Temkin equations were tested for modelling the adsorption isotherms at equilibrium, and it was concluded that the Temkin model fit the experimental data adequately. $R^2 > 0.94$ indicates that the Freundlich isotherm provides the best fit to the equilibrium data.

Keywords: *adsorption, phenol, carbon foam, nanopowder*

Introduction

In recent years, the removal of phenol has become recognised as an important area of research within the discipline of chemical engineering (Fathy Mubarak, 2021). Phenolic compounds are high on the priority pollutants list because they can pose a significant risk even in small amounts (Bahram Bagheri, 2020). Phenol that is contained in wastewater can form complicated compounds by combining with the metal ions that are discharged from other industries (V. Fierro, 2007). These complex compounds can then be discharged back into the environment. Various sectors, including oil refining, petrochemicals, pharmaceuticals, coking operations, resin manufacture, plastics, paint, pulp, paper, and wood products, can all produce effluents that contain these compounds (K.V., 2016). Even at low concentrations, phenolic chemicals are harmful. If these compounds are released without first being handled, it is probable that significant health problems may be posed to both human and animal populations as well as to aquatic ecosystems (Adeleye, 2016). The establishment of rigorous discharge regulations for phenols has been mandated by international regulatory organisations to make certain that the environment will remain habitable (Laura G. Cordova Villegas, 2016).

To properly extract phenolic compounds from wastewater before it is disposed of in water resources, a variety of technologies are used (Asencios, 2022). Typical removal methods include steam distillation, liquid-liquid extraction, adsorption, solid-phase extraction, wet air oxidation, catalytic wet air oxidation, and biodegradation (Pirillo, 2009b). Electrochemical oxidation, photo-oxidation, ozonation, UV/H₂O₂, the Fenton reaction, membrane processes, and enzymatic treatment are among the most advanced methods for removing phenols (Shohreh Mohammadi, 2015). Physical, chemical, and biological treatment are the three conventional categories for the elimination of phenolic contaminants from aqueous solutions (E. O. Oyelude, 2011).

Adsorption is the most efficient method for removing organic and inorganic contaminants from wastewater because it is simple to set up, inexpensive, does not require much time, and the adsorbent used in the process is not harmful to the environment and can be recovered and reused without a reduction in efficiency (Antonio Turco 2018). Therefore, the hunt for inexpensive and readily accessible adsorbents has prompted numerous researchers to seek more cost-effective and effective strategies for employing natural and synthetic materials as adsorbents (Babu, 2010). The most extensively employed adsorbent is activated carbon. It has a high capacity for the adsorption of organic molecules (Mckay, 1998).

Magnetic nanopowder is thought to be one of the most effective and cost-efficient adsorbents for removing organic and inorganic pollutants from aquatic environments (Frag, 2015). It has a high surface area and a high porosity, and it is cheap, abundant, made from renewable sources, stable at high temperatures, and resistant to all chemicals (Fathy Mubarak, 2021). Hence, in this study, the use of magnetic nanopowder for phenol adsorption on natural grain carbon foam to reduce the concentration of phenol in diverse solutions was investigated. In addition to altering the phenol content in the solution while maintaining the nanoparticle mass, stirring time, and stirring speed constant, additional studies were conducted to determine the impact of nanoparticle contact time with the phenol solution. In this study, the carbon precursor and magnetic nanopowder precursor were mixed and carbonised in a single vessel. When the natural grain is baked and carbonised at the same time, a porous structure is formed that can support the iron oxide particles well.

Materials and Methods

Materials and chemicals

The following materials were used: deionized water, phenol, iron oxide nanoparticles, iron sponge, nitric acid, magnetite, flour, and yeast.

Preparation of Carbon Foam

Phenol removal is a topic of particular interest in the field of preventing and getting rid of pollution because it is toxic to water quality and can hurt people even in small amounts. Adsorption is still one of the best ways to get rid of something. It became possible when magnetic nanopowder was made in a carbon foam suspension. The 5 grammes of dry yeast were dissolved in 115 ml of water with continuous stirring. Once the yeast and water were completely dissolved, the mixture was added to 300 grammes of flour. A varying amount of iron nitrate was added into the flour-yeast mixture. This was done by mixing iron sponge with nitric acid to make iron nitrate, which was then added to a mixture of natural grains to bake. The mixture was then mixed with water, and the mechanical mixer was used to knead the mixture until it formed a paste. The porous structure was made by letting the paste ferment in an oven at 35 °C for an hour. The bread was then allowed to bake in an oven set at 180 °C for 40 minutes. Thereafter, the bread was allowed to dry in an oven at 80 °C for 18 hours. A U-tube furnace under argon gas conditions was set up. The dry bread was placed into the furnace and allowed to carbonise at 10 °C/min. The oven was set to heat up at a rate of 10 °C per minute and reach a maximum temperature of 600 °C. The holding time for the maximum temperature was set at 120 minutes. The sample was allowed to cool in the argon atmosphere until it reached room temperature. When different amounts of liquid iron nitrate were added to the flour, yeast, and water mix, four different organic samples were made. To make a second sample, magnetite was added to the dry ingredients, and then water was added. Table 4 depicts the iron contents for each sample.

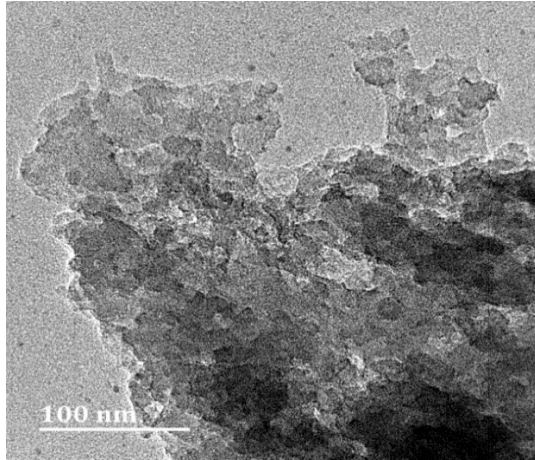
Table 1. Iron and magnetite added into carbon form for each sample

Sample 1	Sample 2	Sample 3	Sample 4	Sample 5
Magnetite	3g pure iron	3g iron sponge dissolved in nitric acid	1g iron sponge dissolved in nitric acid	2g of iron sponge dissolved in nitric acid

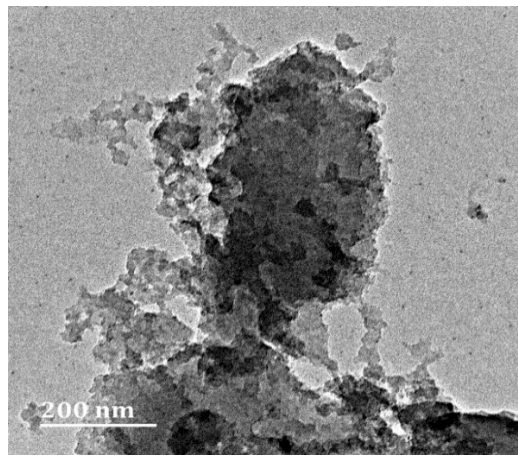
Results and discussion

Characterization of carbon foam

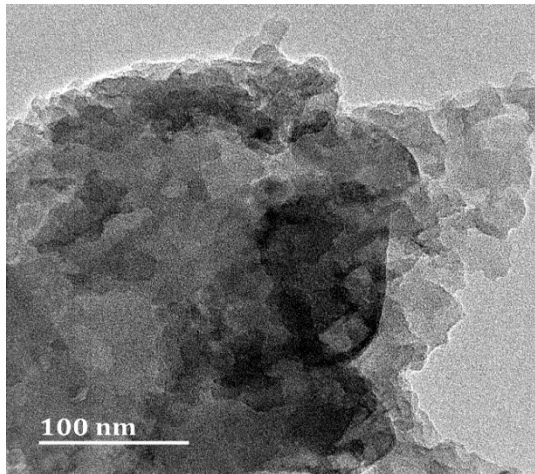
The existence of cavities in the carbon structure is advantageous for the adsorption process because they allow phenol molecules to penetrate the adsorbent. Figure 1 (a), (b), (c), (d), and (e) depict the TEM micrographs of the iron immobilised in natural grain carbon foam. It is evident that the addition of iron nitrate particles to carbon foam produced a structure that is more amorphous and porous; see Figure 1 (c), (d), and (e). The surface of the material featured geometrical properties such as an irregular form, large agglomerates, and a rough surface, which would provide extra sites for adsorbing heavy metal ions (Zygmunt Marczenko, 2000). These characteristics have been demonstrated to be helpful for synthetic carbon foam.



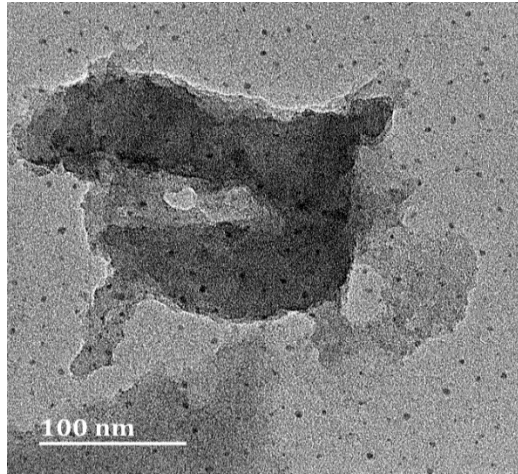
(a)



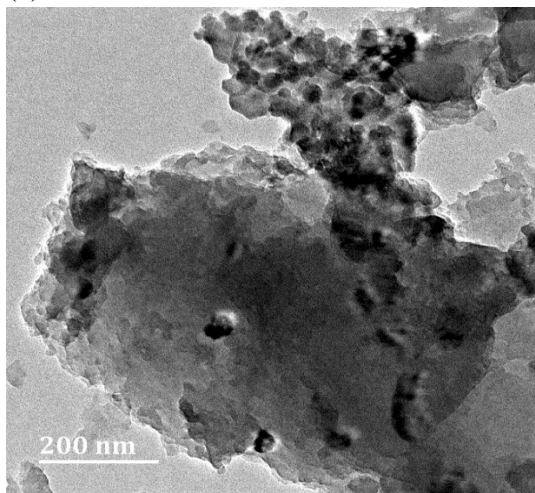
(b)



(c)



(d)



(e)

Figure 1. TEM image conducted on a Jeol 2100 HRTEM operating at 200KV, (a) Sample 1, (b) Sample 2, (c) Sample 3, (d) Sample 4, and (e) Sample 5

Effect of Initial Concentration

Shaking the adsorbent-adsorbate solution until equilibrium is reached for increments of the initial adsorbate concentration at similar adsorbent dosage and time can be used to study the effect of the initial concentration (Rendo, 2021). Adsorption depends on the initial concentration of an adsorbate, since lowering the initial concentration of phenol molecules lowers the surface area. As the initial concentration increases, the driving force of mass transfer increases, enhancing adsorption (Baskar, 2019). Figure 2 shows the effect of the initial concentration of phenol, where an initial concentration of 25, 50, 75, and 100 mg/L were absorbed by iron mobilised on natural grain carbon foam in 4 different samples. There was an increase in adsorption with an increase in the initial concentration at room temperature with a contact time of 10 minutes and 25 mg/L of solution. The amount of available surface area on adsorbents goes down as the initial concentration increases. This means that more adsorbate is taken up and less phenol is removed.

The following equation was used to calculate the amount of phenol adsorbed (Zygmunt Marczenko, 2000).

$$q_t = \frac{(C_o - C) \times V}{w} \quad (1)$$

Where q_t (mg/g) is the adsorption density, C_o (mg/L) is the initial concentration of aqueous solution, C (mg/L) denotes the final aqueous solution concentration (mg/L), $v(l)$ the volume of solution, and $w(g)$ the mass of adsorbent.

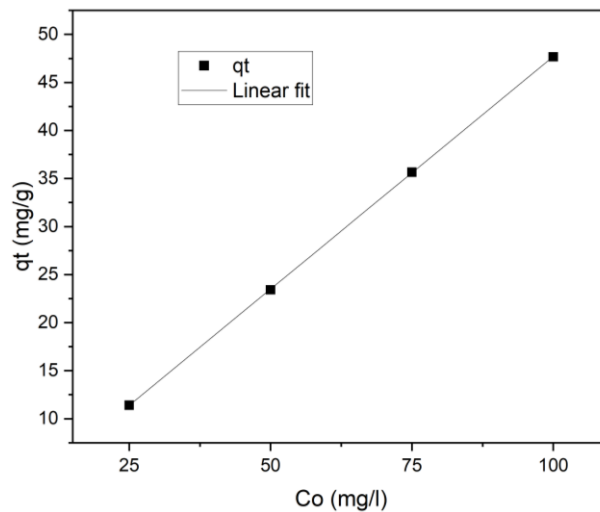


Figure 2. Effect of initial concentration on phenol adsorption

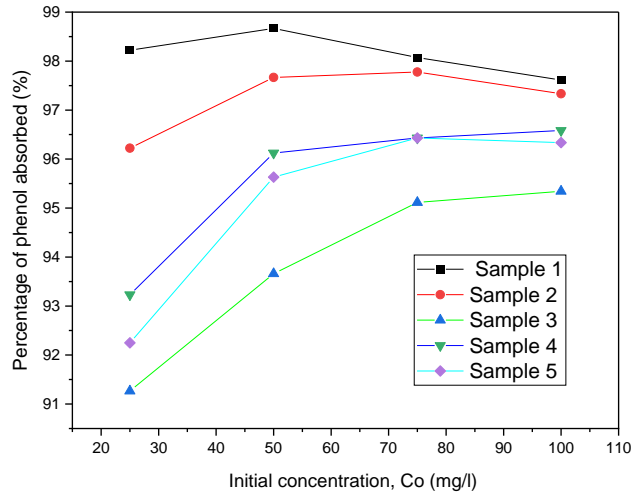


Figure 3. The effect of initial concentration on percentage of phenol adsorbed (50ml of phenol solution and 0.1 magnetic nanopowder).

Four phenol solutions were prepared with concentrations ranging from 25, 50, 75, and 100 mg/L. A plot of the percentage of phenol adsorbed versus the initial concentration was made for each sample of nanopowder in each solution concentration. Figure 3 indicates that the percentage of phenol adsorbed increased for each sample as the initial concentration increased. This demonstrates that more light is being absorbed by a solution of greater concentration. This makes sense because when the concentration of a solution goes up, there are more particles for the light to hit, so there are more chances for absorption (Asokan, 2011)

Effect of time on adsorption

Adsorbate rate rises with longer contact times because it deposits on the accessible adsorption sites on the adsorbent material; nevertheless, longer contact times will not result in an increase in uptake (Y. Elsayed, 2001). The amount of adsorbate adsorbed onto the adsorbent is in equilibrium with the amount of adsorbate desorbing from the adsorbent. The effectiveness of adsorbate removal is substantially impacted by the length of time that the two components are in contact (V.Fierro, 2008).

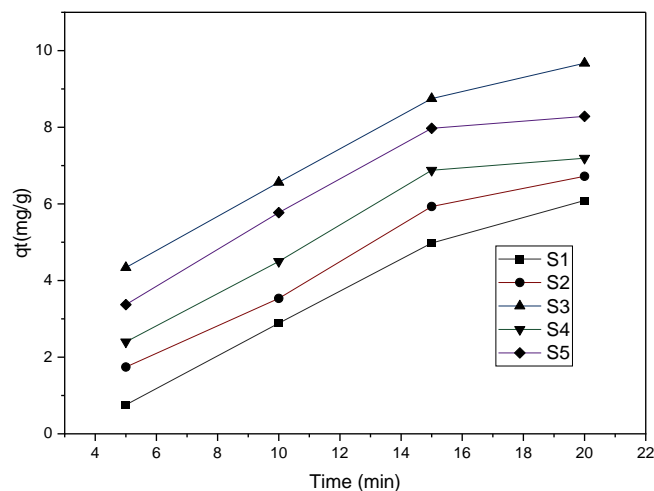


Figure 4. Effect of contact time on adsorption of phenol at concentration of 75mg/L, and 100mg

Figure 4 displays the results obtained, and for each sample, phenol adsorption increased with contact time. The magnetite solution displayed the least phenol adsorption. This can be attributed to the uneven distribution of the solid particles in the initial organic mixture. The sample of undissolved iron sponges yielded similar results to the previous sample for the same reasons. The three samples that made use of liquid iron nitrate yielded better results, as there was more even distribution in the organic mixture, resulting in a sample of constant composition. An increase in the amount of iron sponge added to the mixture increased phenol adsorption. A clarification for a decline in the adsorption rate after 15 minutes is that the solutions are approaching equilibrium. This can be attributed to the large number of vacant sites on the magnetic nanoparticle surface, which are gradually occupied over time as adsorption takes place.

Mechanism

Using kinetic models, the rate of the adsorption process and the rate-controlling step are explored to fully comprehend the phenomena involved in phenol adsorption on magnetic nanopowder. In addition, it is crucial to consider the fact that the adsorption mechanism is dependent on the physical and/or chemical properties of the adsorbent as well as the mass transport process. To investigate the mechanism of phenol adsorption onto magnetic nanopowder, pseudo-first-order, pseudo-second order, and intraparticle diffusion models are considered to fit the experimental data obtained from batch studies, and the correlation coefficient is regarded as a measure of the relationship between the experimental data and these proposed models.

The mechanism for phenol adsorption on carbon foam as adsorbent is based on their mainly sp²-dominated electronic structures. As a result, one could speculate that the adsorption mechanism for this system involves interactions between delocalized electrons on the carbon surface structure and electrons from the aromatic ring (Luz-Asunción, 2015).

Kinetic modelling

Lagergren pseudo-first order and pseudo-second order models were used for the investigation of modelling of adsorption kinetics. The nonlinear form of pseudo-first order is given by the following equation:

$$q_t = q_e(1 - e^{-K_1 t}) \quad (2)$$

The nonlinear form of pseudo-second order is given by the following equation:

$$q_t = \frac{q_e^2 K_2 t}{1 + K_2 q_e t} \quad (3)$$

where q_t (mg/g) is the amount absorbed at time t , q_e (mg/g) is the amount remaining after equilibrium of adsorption, and K_1 and K_2 are the pseudo-first and pseudo-second order model rate constants, expressed in min^{-1} and g/mg/min , respectively. Table 1 and Table 2 illustrate the calculated values of q_e , K_1 , K_2 , and the regression coefficient R^2 values. Figure 5 shows the plot of the pseudo-first order and pseudo-second order. The validity of model is judged by evaluating the correlation coefficients R^2 , and the comparability of the

experimental and calculated values of q_e . Considering these findings, it is possible to conclude that the pseudo-first-order kinetic model gives a stronger correlation for phenol adsorption onto magnetic nanopowder immobilised on carbon foam than the other models. Results indicate that R^2 is closer to 1 for pseudo-first order compared to pseudo-second order model for all 5 samples.

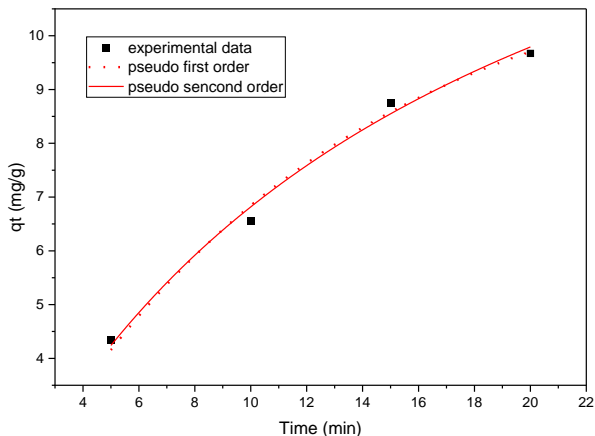


Figure 5. Nonlinear fit of pseudo-first order and pseudo-second order for phenol adsorption of sample 3 at a 75mg/L of concentration, and 100mg sorbent

Table 2. Pseudo-first order parameters

Pseudo-first order				
Sample	Exp. q_e (mg/g)	Calc. q_e (mg/g)	K1 (min^{-1})	R^2
Sample 1		39.99×10^2	7.64×10^{-8}	0.953
Sample 2	7.3	26.21	0.015	0.974
Sample 3	6.5	11.76	0.872	0.992
Sample 4	9.8	11.84	0.050	0.963
Sample 5	8.5	10.74	0.080	0.976

Table 3. Pseudo-second order parameters

Pseudo-second order				
	Exp. Q_e (mg/g)	Calc. q_e (mg/g)	K2 (g/mg/min)	R^2
Sample 1		46.54×10^2	1.42×10^{-8}	0.95
Sample 2	7.3	50.50	1.58×10^{-4}	0.97
Sample 3	6.5	17.22	3.79×10^{-3}	0.99
Sample 4	9.8	19.88	1.54×10^{-3}	0.96
Sample 5	8.5	16.34	3.41×10^{-3}	0.97

Intraparticle diffusion

The intraparticle diffusion resistance was evaluated utilising the intraparticle particle diffusion model by Weber and Morris (Weber, 1963b), given by the following equation:

$$q_t = k_{id}t^{1/2} + c \quad (4)$$

where q_t (mg/g) is the adsorption amount at time t (min), k_{id} (mg/g/min^{1/2}) is the adsorption rate constant of the intraparticle diffusion model, and c is a constant related to the thickness of the boundary layer. The plot illustrated in Figure 6 is linear, and the sorption process is solely regulated by intra-particle diffusion since the plot of q_t versus $t^{1/2}$ yields a straight line. The difference in mass transfer rates between the start and final stages of adsorption may be the cause of the plot's departure from the origin. If intraparticle diffusion is involved in the sorption process, a graph of adsorbate uptake vs the square root of time would have a linear connection, and intraparticle diffusion would be the rate-regulating step if this line passes through the origin (Banat, 2000).

Furthermore, such a departure from the origin of the straight line suggests that pore diffusion is not the only factor affecting rate (Y. El Maguana, 2019).

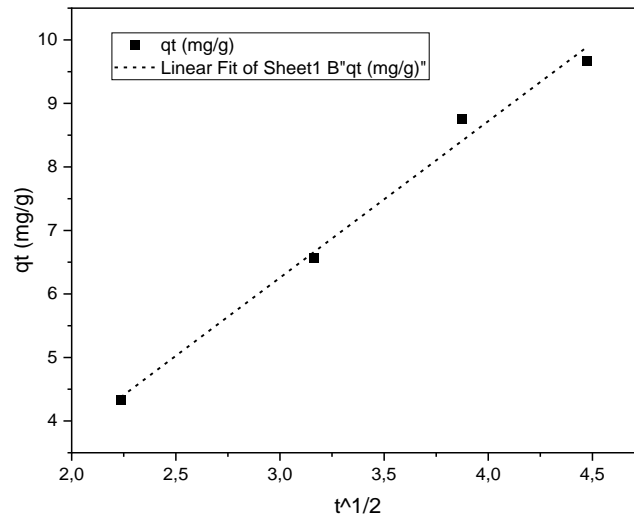


Figure 6. Plot of the intraparticle diffusion model for phenol onto iron supported by carbon foam (75mg/L of concentration, and 100mg sorbent)

Equilibrium adsorption

Adsorption equilibrium occurs between the adsorbed molecules and the adsorbent surface when an adsorbate is in contact with the adsorbent. The adsorption isotherm is the equilibrium relationship between the amount of adsorbed adsorbate (q_e) and the residual adsorbate concentration (C_e) at a constant temperature. In general, adsorption isotherms provide information on the affinity and the binding energy between the adsorbate and the adsorbent, on the adsorption capacity, and on the surface phase, which may be considered a monolayer or multilayer. The modelling of the adsorption isotherms consists of describing

the exponential data using theoretical or empirical mathematical equations and allowing the determination of isotherm parameters to compare the efficiency of different adsorbents.

Three adsorption equilibrium isotherm models were tested in the present research, namely the Freundlich, Langmuir, and Temkin isotherm models. The empirical Freundlich model, which is known to be satisfactory for low concentrations and is based on sorption on the heterogeneous surface, is expressed by the following equation:

$$q_e = K_F C_e^{1/n} \quad (5)$$

Where C_e (mg/L) is the equilibrium concentration of adsorbate, q_e (mg/g) is the amount of adsorption at the equilibrium. K_F and n are Freundlich constants related to the adsorption capacity and adsorption intensity, respectively. All the parameters of the isotherm models were calculated from nonlinear fitting of q_e versus C_e on Origin Lab software. The Temkin model reflects the properties of indirect adsorbate-adsorbent interactions on the adsorption isotherm. It assumes that the heat of adsorption of all molecules in the layer decreases linearly with coverage due to adsorbate-adsorbent interactions. The Temkin model is expressed by the following equation.

$$q_e = \frac{RT}{b} \ln(AC_e) \quad (6)$$

Where q_e (mg/g) is the amount of adsorption at the equilibrium, C_e (mg/L) is the equilibrium concentration of adsorbate, T (K) is the temperature in Kelvin, R (J/mol/K) is the universal gas constant, b (J/mol) is related to the heat of adsorption and K_T is the equilibrium binding constant corresponding to the maximum binding energy.

The Langmuir isotherm equation is expressed as follows:

$$q_e = \frac{q_m K_L C_e}{1 + K_L C_e} \quad (7)$$

Where q_e (mg/m) is the monolayer adsorption capacity, C_e (mg/L) is the equilibrium concentration of adsorbate, q_m (mg/g) is the monolayer adsorption capacity, and K_L is the Langmuir constants.

Figure 7 illustrates the curves of the Freundlich, Temkin and Langmuir models using equations 5, 6, and 7, respectively. Table 3 depicts the calculated parameters of the Freundlich and Temkin isotherms, the R^2 values obtained by the nonlinear fitting method. Based on the R^2 value comparisons, the Freundlich model represents a better fit of the experimental data at equilibrium compared to both the Langmuir and Temkin models. Thus, the Temkin isotherm best describes the phenol adsorption process, which indicates multilayer adsorption on a heterogeneous surface with different energy distribution. The Freundlich constant, n , is a measure of adsorption intensity. A value of $1/n$ was found to be between 0 and 1, indicating that Freundlich was also favourable for the adsorption of phenol (Medjor, 2015).

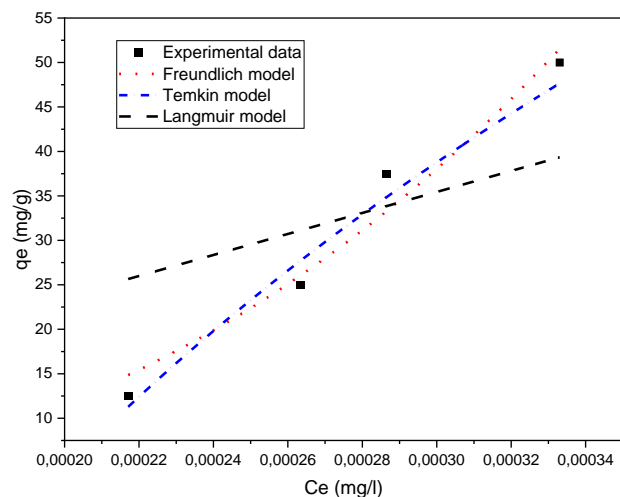


Figure 7. Fitting of adsorption isotherms into experimental data for sample 3

Table 4. Temkin, Freundlich, and Langmuir model parameters

Sample	Temkin Model			Freundlich			Langmuir		
	b	A	R ²	N	K _F	R ²	q _m	K _L	R ²
Sample 1	38.76	7920.14	0.98	1.97	16564.28	0.91	82750.91	1.96	0.78
Sample 2	30.89	5480.35	0.94	2.348	60792.25	0.87	88020.63	1.19	0.66
Sample 3	29.16	5260.43	0.98	2.908	401434.6	0.97	105489	1.12	0.61
Sample 4	24.53	4494.55	0.97	2.991	577825	0.93	159254.5	0.67	0.52
Sample 5	23.10	4075.37	0.94	2.916	252312.6	0.87	83231.45	1.27	0.55

Conclusion

The amount of phenol adsorbed for these tests all increased with the increase in initial concentration. Adsorption also increased with the increase in iron content in the carbon form, and the magnetite sample had lower adsorption capabilities compared to other samples. The adsorption values increased rapidly with time on the q_t (mg/g) versus time (min) graph, and then they started to level out as the solutions got closer to equilibrium. This was attributed to the fact that there were a lot of open sites on the magnetic nanoparticle surface, which over time, as adsorption occurred, gradually filled up. This study demonstrates that magnetic nanopowder immobilised on carbon foam significantly reduces phenol concentrations. The correlation between the adsorption data and the pseudo-first-order equation is the highest. The Temkin adsorption model is more suitable for describing the phenol adsorption equilibrium data.

References

ADELEYE, A. S., CONWAY, J.R., GARNER, K., HUANG, Y., SU, Y., KELLER, A.A. 2016. Engineered nanomaterials for water treatment and remediation: costs, benefits, and applicability. *Journal of Chemical Engineering*, 286, 640-662.

- AGRAWAL, V. R., VAIRAGADE, V. S., & KEDAR, A.P. 2017. Activated Carbon as Adsorbent in Advance Treatment. *Journal of Mechanical and Civil Engineering (IOSR-JMCE)*, 14, 36-40.
- AHMED, R. E. A. 2022. Biodegradable acid based nanocomposite-cuo-zno-ni(oh)₂/PA: A novel material for water cleansing. *Journal of Cleaner Production*, 341, 130860.
- AL-KADHI, N., S. 2019. The kinetic and thermodynamic study of the adsorption Lissamine Green B dye by micro-particle of wild plants from aqueous solutions. *The Egyptian Journal of Aquatic Research*, 45, 231-238.
- ALKHOUZAAM, A. Q., H. 2021. Functional Go-based membranes for water treatment and desalination: Fabrication Methods, performance, and advantages. A Review. *Chemosphere*, 274, 129853.
- ANTAL, M. J. A. M. G. G. 2003. The Art, Science, and Technology of Charcoal Production. *Industrial & Engineering Chemistry Research* 42, 1619-1640.
- ANTONIO TURCO , A. G. M., ELISABETTA MAZZOTTA, GIUSEPPE MARUCCIO, COSIMINO MALITESTA 2018. An Innovative Porous Nanocomposite Material for the Removal of Phenolic Compounds from Aqueous Solutions. *Nanomaterials*, 8, 334.
- ARORA, A. K., JASWAL, V. S., SINGH, K., & SINGH, R. 2016. Metal/Mixed Metal Oxides and their Applications as Adsorbents. *international Journal of Chemical Science*, 3215-3227.
- ASENCIOS, Y. J. O., LOURENÇO, V. S. & CARVALHO, W. A. 2022. Removal of phenol in seawater by heterogeneous photocatalysis using activated carbon materials modified with TiO₂. *Catalysis Today*, 388-389, 247-258.
- ASHRAF, I., SINGH, N.B. & AGARWAL, A. 2022. Green synthesis of iron oxide nanoparticles using Amla seed for methylene blue dye removal from water. *Materials Today: Proceedings*.
- ASOKAN, K. 2011. *Mass Transfer Concepts*, University press.
- BABU, S. G. A. B. 2010. Experimental, kinetic, equilibrium and regeneration studies for adsorption of Cr(VI) from aqueous solutions using low cost adsorbent (activated flyash). *Desalination and Water Treatment*, 20, 168-178.
- BAHRAM BAGHERI, S. A. H., HABIB MEHRIZADEH 2020. A Comparison of the Catalytic Activity of Cu-X₂ (X=Mn, Co) Nano Mixed Oxides toward Phenol Remediation from Wastewater by Catalytic Wet Peroxide Oxidation. *J. Water Environ Nanotechnol.*, 5, 139-146.
- BANAT, F., AL-BASHIR, B., AL-ASHEH, S. AND HAYAJNEH, O. 2000. Adsorption of Phenol by Bentonite. *Environmental Pollution*, 107, 391-398.
- BASKAR, P. P. S. A. R. B. P. P. S. A. R. 2019. Mass Transfer Enhancement for CO₂ Absorption in Structured Packed Absorption Column. *Journal of the chemical society of pakistan*, 41, 820-820.
- BEECHEM T., L. K., & ELGAFY A 2005. Bubble growth mechanism in carbon foams. *Carbon*, 43, 1055-1064.
- BENGUELLA, B., & YACOUTA-NOUR, A. 2009. *Comptes Rendus Chimie* 12, 62-771.
- BRUNO LELLIS, C. Z. F.-P., JOÃO ALENCAR PAMPHILE, JULIO CESAR POLONIO 2019. Effects of textile dyes on health and the environment and bioremediation potential of living organisms. *Biotechnology Research and Innovation*, 3, 275-290.
- CHEN, C., KENNEL, E. B., STILLER, A. H., STANSBERRY, P. G., & ZONDLO, J. W. 2006. Carbon foam derived from various precursors. *Carbon*, 44, 1535-1543.
- CHONG, M. N., JIN, B., CHOW, C.W.K. & SAINT, C. 2010. Recent developments in Photocatalytic Water Treatment Technology: A Review. *Water Research*, 44, 2997-3027.
- CRINI, G., ROBERT, C., GIMBERT, F., MARTEL, B., ADAM, O., & DE GIORGI, F. 2008. The removal of Basic Blue dye from aqueous solutions by chitosan-based adsorbent: batch studies. *Journal of Hazardous Materials*, 153, 96-106.
- DIAZ, J., ALVIM-FERRAZ, M., ALMEIDA, M., RIVERA-UTRILLA, J. & SÁNCHEZ-POLO, M 2007. Waste materials for activated carbon preparation and its use in aqueous-phase treatment: A review. *Journal of Environmental Management*, 85, 833-846.
- DUTTA, M. B., J.K. 2013. Fixed-bed column study for the adsorptive removal of acid fuchsin using carbon-alumina composite pellet. *International Journal of Environmental Science and Technology*, 11, 87-96.

- E. O. OYELUDE, U. R. O. 2011. ADSORPTION OF METHYLENE BLUE FROM AQUEOUS SOLUTION USING ACID MODIFIED CALOTROPIS PROCERA LEAF POWDER. *Journal of Applied Sciences in Environmental Sanitation*, 6, 477-484.
- EKSILIOGLU A., G. N., YARDIM M.F, & EKINCI E. 2006. Mesophase AR pitch derived carbon foam: effect of temperature, pressure, and pressure release time. *Journal of Materials Science*, 41, 2743-2748.
- EL MAGUANA, Y., ELHADIRI, N., BOUCHDOUG, M., & BENCHANAA, M. 2019. Activated carbon from prickly pear seed cake: optimization of preparation conditions using experimental design and its application in dye removal. *International Journal of Chemical Engineering*, 12.
- FARAG, R. T. A. M. E. O. A. M. S. M. A. H. A. 2015. Metal Oxide Nano-particles as an Adsorbent for Removal of Heavy Metals. *Journal of Advanced Chemical Engineering* 5(3), 5.
- FATHY MUBARAK, M., MAHER AHMED, A. AND SAAD GABR, S. 2021. Nanoporous carbon materials toward phenolic compounds adsorption. *Nanopores*.
- FATIMA, B., SIDDIQUI, S. I., AHMED, R. & CHAUDHRY, S. A. 2019. Green synthesis of F-CdWO₄ for photocatalytic degradation and adsorptive removal of Bismarck Brown R dye from water. *Water Resources and Industry* 22, 100119.
- GE M, S. Z., CHI WD, AND LIU H. 2007. Anisotropy of mesophase pitch-derived carbon foams. *Carbon*, 45, 141-145.
- GIRI, S. K., DAS, N.N., AND PRADHAN, G.C. 2011. Synthesis and characterization of magnetite nanoparticles using iron ore tailings for adsorptive removal of dyes from aqueous solutions. *Colloids and Surfaces A: Engineering, Materials Science*, 389, 43-49.
- GURSES, A., DOGAR, C., YALCIN, M., ACIKYILDIZ, M., BAYRAK, R. & KARACA, S. 2006a. The adsorption kinetics of the cationic dye, methylene blue, onto Clay. *Journal of Hazardous Materials*, 131, 217-228.
- GURSES, A., DOGAR, M., YALCIN, M., BAYAQRAK, R., & KARACA, S 2006b. The adsorption of kinetics of the cationic dye, methylene blue, onto clay. *Journal of Hazardous Materials*, 131, 217-228.
- HELLEUR, R. E. A. 2001. Characterization and potential applications of pyrolytic char from ablative pyrolysis of used tires. *Journal of Analytical and Applied Pyrolysis*, 58-59, 813-824.
- IDAN, I., J., JAMIL, S., N., ABDULLAH, L.C., & CHOONG, T., S., Y. 2017. Removal of Reactive Anionic Dyes from Binary Solutions by Adsorption onto Quaternized Kenaf Core Fiber. *International Journal of Chemical Engineering*.
- INAGAKI, M. 2009. Pores in carbon materials-importance of their control. *New Carbon Materials*, 24, 193-232.
- INAGAKI, M., QIU, J. AND GUO, Q. 2015. Carbon foam: Preparation and application. *Carbon*, 87, 128-152.
- JAIN, N., DWIVEDI, M. K., AGARWAL, R., & SHARMA, P. 2015. Removal of Malachite Green from Aqueous Solution by Zeolite- Iron Oxide Magnetic Nanocomposite. *Journal of Environmental Science, Toxicology and Food Technology*, 9, 42.
- K.V., R. V. K. A. N. S. 2016. Dye Removal by Adsorption: A Review. *Journal of Bioremediation & Biodegradation*, 7.
- KANDISA, R. V., SAIBABA, N. K., SHAIK, K., B., & GOPINATH, R. 2016. Dye Removal by Adsorption: A Review. *Journal of Bioremediation & Biodegradation*, 7.
- KANG, M. I. A. F. 2015. Pore development in carbon materials. *Carbon Materials Science and Engineering*, 87, 123-152.
- KLETT J., H. R., ROMINE E., WALLS C., AND BURCHELL T 2000. High-thermal conductivity, mesophase-pitch-derived carbon foams: effect of precursor on structure and properties. *Carbon*, 38, 953-973.
- LAURA G. CORDOVA VILLEGAS, N. M., MIAO CHEN, DEBJANI MUKHERJEE, KEITH E. TAYLOR & NIHAR BISWAS 2016. A Short Review of Techniques for Phenol Removal from Wastewater. *Current Pollution Reports*, 2, 157-167.

- LI J., W. C., ZHAN L., QIAO W.M., LIANG X.Y., & LING L.C. 2009. Carbon foams prepared by supercritical foaming method. *Carbon*, 47, 1204-6.
- LI, N., ZHAO, P., & ASTRUC, D. 2014. Anisotropic gold nanoparticles: Synthesis, properties, applications, and toxicity. *Angewandte Chemie International Edition*, 53, 1756-1789.
- LOPEZ, F. J. A. A. F. A. 2020. Adsorption Processes in the Removal of Organic Dyes from Wastewaters: Very Recent Developments. In: SUMMERS, I. A. M. A. J. K. (ed.) *Promising Techniques for Wastewater Treatment and Water Quality Assessment*.
- LUZ-ASUNCIÓN, M. D., SÁNCHEZ-MENDIETA, V., MARTÍNEZ-HERNÁNDEZ, A.L., CASTAÑO, V.M., & VELASCO-SANTOS, C. 2015. Adsorption of phenol from aqueous solutions by carbon nanomaterials of one and two dimensions: kinetic and equilibrium studies. *Journal of Nanomaterials*, 16, 422.
- MAHMOODI, N., M., ARAMI, M 2010. Immobilized titania nanophotocatalysis: Degradation, modeling and toxicity reduction of agricultural pollutants. *Journal Alloys Compd*, 506, 155-156.
- MAHMOODI, N. M., NAJAFI, F. & NESHAT, A. 2013. Poly (amidoamine-co-acrylic acid) copolymer: Synthesis, characterization and dye removal ability. *Industrial Crops and Products*, 42, 119-125.
- MAHMOODI, N. M., SADEGHI, U., MALEKI, A., HAYATI, B. & NAJAFI, F 2014. Synthesis of cationic polymeric adsorbent and dye removal isotherm, kinetic and thermodynamic. *Journal of Industrial and Engineering Chemistry* 20, 2745-2753.
- MAHMOODIA, N., M., NAJAFIB, F., & NESHATC, A. 2013. Poly (amidoamine-co-acrylic acid) copolymer: Synthesis, characterization and dye removal ability. *Industrial Crops and Products*, 42, 119-125.
- MARCZENKA, Z. 2000. Separation, Preconcentration and Spectrophotometry in Inorganic Analysis. *Elsevier*.
- MARTÍNEZ, J. D. E. A. 2013. Waste tyre pyrolysis – A Review. *Renewable and Sustainable Energy Reviews*, 23, 179-213.
- MAVROS, P., DANILIDOU, A., C. 2008. Colour removal from aqueous solutions. Part I. Part I. Flotation. *Environmental Technology*, 15, 601-616.
- MCKAY, Y. S. H. A. G. 1998. Kinetic models for the sorption of dye from aqueous solution by wood. *Process Safety and Environmental Protection*, 76, 183-191.
- MEDJOR, W., WEPUAKA, C. AND GODWILL, S. 2015. Spectrophotometric Determination of Phenol in Natural Waters by Trichloromethane Extraction Method after Steam Distillation. *International Research Journal of Pure and Applied Chemistry*, 7, 150-156.
- MOHAJERSHOJAEI, K., MAHMOODI, N.M. AND KHOSRAVI, A. 2015. Immobilization of Laccase enzyme onto Titania nanoparticle and decolorization of dyes from single and Binary Systems. *Biotechnology and Bioprocess Engineering*, 20, 109-116.
- MOHAMMED M. RAHMAN, S. B. K., ASLAM JAMAL, AND ABDULLAH M. AISIRI 2011. Iron Oxide Nanoparticles. *Nanomaterials*.
- MP, S. 2016. Industrial Wastewater Treatment: A Challenging Task in the Industrial Waste Management. *Advances in Recycling & Waste Management*, 2.
- MP, S. 2017. Industrial wastewater treatment: A challenging task in the Industrial Waste Management. . *Advances in Recycling & Waste Management*, 01.
- NARASIMHARAO, K. E. A. 2022. Fe₃O₄@date seeds powder: A sustainable nanocomposite material for wastewater treatment. *Journal of Materials Research and Technology*, 18, 3581-3597.
- NASERI, N., VALIZADEH, H., & ZAKERI-MILANI, P. 2015. Solid lipid nanoparticles and nanostructured lipid carriers: Structure, preparation and application. *Advance Pharmaceutical Bulletin*, 5, 305.
- NIZAMUDDIN, S., SIDDIQUI, M.T.H., MUBARAK, N.M., BALOCH, H.A., ABDULLAH, E.C., MAZARI, S.A., GRIFFIN, G.J., SRINIVASAN, M.P. 2019. Iron oxide nanomaterials for the removal of heavy metals and dyes from wastewater. *Nanoscale Materials in Water Purification*, 447-472.

- OLASEHINDE, E., F., & ABEGUNDE, S., M. 2020. Adsorption of methylene blue onto acid modified raphia taedigera seed activated carbon. *Advance Journal Chemical Analysis*, 3, 663-679.
- OYELUDE, E. O., & OWUSU, U. R. 2011. Adsorption of Methylene Blue from Aqueous Solution Using Acid Modified Calotropis Procera Leaf Powder. *Water Contimination*, 6, 477-484.
- PATEL, H. 2019. Fixed-bed column adsorption study: a comprehensive review. *Applied water science*
- PATHANIA, D., SHARMA, S. & SINGH, P. 2017. Removal of methylene blue by adsorption onto activated carbon developed from ficus carica bast. *Arabian Journal of Chemistry* 10.
- PIRILLO, S., PEDRONI, V., RUEDA, E. & LUJÁN FERREIRA, M. 2009a. Elimination of dyes from aqueous solutions using iron oxides and chitosan as adsorbents: A comparative study. *Química Nova*, 32, 1239–1244.
- PIRILLO, S., PEDRONI, V., RUEDA, E., & FERREIRA, M. L. 2009b. Elimination of dyes from aqueous solutions using iron oxides and chitosan as adsorbents: a comparative study. *Química Nova*, 35, 1239-1244.
- QIAO, N., CHANG, J., HU, M. & MA, H. 2015. Novel bentonite particle electrodes based on Fenton catalyst and its application in Orange II removal. *Desalination and Water Treatment* 1-9.
- RATHI, G., SIDDIQUI, S. I., PHAM, Q. & NAM, V. T. 2020. Nigella sativa seeds based antibacterial composites: A sustainable technology for water cleansing - A Review. *Sustainable Chemistry and Pharmacy*, 18, 100332.
- RENDO, D. 2021. Adsorption of Methylene Blue Dye using Fe₃O₄ Magnetized Natural Zeolite Adsorbent. *Jurnal Kimia Sains dan Aplikasi*, 24, 51-57.
- S. F. HASANY, I. A., RAJAN J, AND A. REHMAN 2012. Systematic Review of the Preparation Techniques of IronOxide Magnetic Nanoparticles. *Nanoscience and Nanotechnology*, 2, 148-158.
- SADEGHI-KIAKHANI, M., ARAMI, M., & GHARANJIG, K. 2013. *Journal of Applied Polymer Science* 127, 2607-2619.
- SAIF, S., TAHIR, A., & CHEN, Y. 2016. Green Synthesis of Iron Nanoparticles and Their Environmental Applications and Implications. *Nanomaterials*, 6, 209.
- SANGHI, R., & BHATTACHARYA, B. 2002. Review on decolorisation of aqueous dye solutions by low cost adsorbents. *Colour Technology*, 118, 256-269.
- SEGUN M., A., KAYODE S., I., OLORUNSOLA M., A, & TINUADE, A. 2020. A review on the influence of chemical modification on the performance of adsorbents. *Resources, Environment and Sustainability*, 1.
- SHAH, M. 2016. Industrial Wastewater Treatment. *A Challenging Task in the Industrial Waste Management*
- SHOHREH MOHAMMADI, A. K., HAMIDREZA SANAEEPUR, KHALIL ABBASSIAN, ATEFEH NAJAFI & ELHAM MOFARRAH 2015. Phenol removal from industrial wastewaters: a short review. *Desalination and Water Treatment*, 53, 2215-2234.
- SONG, W., GAO, B., XU, X., XING, L., HAN, S., DUAN, P., SONG, W. & JIA, R. 2016. Adsorption–desorption behavior of magnetic amine/Fe₃O₄ functionalized biopolymer resin towards anionic dyes from wastewater. *Bioresource Technology*, 210, 123–130.
- TAMAN, R., OSSMAN, M., MANSOUR, M., & FARAG, H. 2015. Metal Oxide Nano-particles as an Adsorbent for Removal of Heavy Metals. *Journal of Advanced Chemical Engineering* 5(3), 5.
- TAN, B. H., TENG, T. T., & MOHD, O. A. 2000. Removal of Dyes and Industrial Dye Wastes by Magnesium Chloride. *PII: S0043-1354*, 99, 597-601.
- TANKSALE, S. N. A. M. T. H. S. A. N. M. M. A. H. A. B. A. E. C. A. A. S. A. M. A. G. G. A. M. S. A. A. 2019. Iron Oxide Nanomaterials for the Removal of Heavy Metals and Dyes From Wastewater. *Nanoscale Materials in Water Purification*.
- TARA, N., SIDDIQUI, S. I., BACH, Q.-V. & CHAUDHRY, S. A. 2020. Reduce graphene oxide-manganese oxide-black cumin based hybrid composite (RGO-MNO₂/BC): A novel material for water remediation. *Materials Today Communications*, 25.

- TAROMI, A. A., & KALIAGUINE, S. 2018. Hydrodeoxygenation of triglycerides over reduced mesostructured Ni/ γ - alumina catalysts prepared via one-pot sol-gel route for green diesel production. *Applied Catalysis*, 140-149.
- UĞURLU, M. 2009. Adsorption of a textile dye onto activated sepiolite. *Microporous and Mesoporous Materials*, 119, 31-59.
- V. FIERRO, V. T.-F., D. MONTANÉ AND A. CELZARD 2007. Adsorption of phenol onto activated carbons having different textural and surface properties. *Microporous and Mesoporous Materials*, 111, 276-284.
- V.FIERRO, V. T.-F., D.MONTANÉ AND A.CELZARD 2008. Adsorption of phenol onto activated carbons having different textural and surface properties. *Microporous and Mesoporous Materials*, 111, 276-284.
- VANITHA KATHERESAN, J. K., AND SIE YON LAU 2018. Efficiency of various recent wastewater dye removal methods: A review. *Journal of Environmental Chemical Engineering*, 6, 4676-4697
- VASQUES, A., R., ULSON DE SOUZA, S. M., VALLE, J. E., & ULSON DE SOUZA, A. A 2009. Removal of Dyes from the Textile Industry by Adsorption in Fixed Bed Columns: A Sustainable Process. *Chemical Product and Process Modeling*, 4.
- VIKASH R AGRAWAL, V. S. V., AND AMOL P KEDAR 2017. Activated Carbon as Adsorbent In Advance Treatment of Wastewater. *Journal of Mechanical and Civil Engineering (IOSR-JMCE)*, 14, 36-40.
- WANG, S., BOYJOO, Y. CHOUJEIB, A. 2005. *Chemosphere*, 60, 1401-1407.
- WANG Y., M. Z., CAO M., & XU D. 2009. Effect of heating conditions on pore structure and performance of carbon foams. *New Carbon Mater*, 24, 321-6.
- WEBER, W., J., & M, J. C. 1963a. Kinetics of Adsorption on Carbon from Solutions. *Journal of the Sanitary Engineering Division, American Society of Civil Engineers*, 89, 31-60.
- WEBER, W. J., & MORRIS, J.C. (1963). KINETICS OF ADSORPTION ON CARBON FROM SOLUTION. *JOURNAL OF THE SANITARY ENGINEERING DIVISION*, 89, 31-59. 1963b. Kinetics of Adsorption on Carbon from Solution. *Journal of the Sanitary Engineering Division*, 89, 31-59.
- Y. EL MAGUANA, N. E., M. BOUCHDOUG, M. BENCHANAA, AND A. JAOUAD 2019. Activated Carbon from Prickly Pear Seed Cake: Optimization of Preparation Conditions Using Experimental Design and Its Application in Dye Removal. *International Journal of Chemical Engineering*, 12.
- Y. ELSAYED, A. T. B. 2001. A Study of Acetaldehyde Adsorption on Activated Carbons. *Journal of Colloid and Interface Science*.
- YAO, T., GUO, S., ZENG, C., WANG, C. & ZHANG, L. 2015. Investigation on efficient adsorption of cationic dyes on porous magnetic polyacrylamide microspheres. *Journal of Hazardous Materials*, 292, 90–97.
- YAQOUB, A., A., PARVEEN, T., UMAR, K., & MOHAMAD, I., M., N 2020. Role of nanomaterials in the treatment of wastewater: A review. *Water*, 12, 495.
- YUAN, Y., DING, Y., WANG, C., XU, F., LIN, Z., QIN, Y., LI, Y., YANG, M., HE, X., PENG, Q. & LI, Y. 2016. Multifunctional Stiff Carbon Foam Derived from Bread. *ACS Applied Materials & Interfaces*, 8, 16852-16861.
- YUNXIA, Y., KEN, C., & NICK, B. 2011. Porous carbon- supported catalysts for energy and environmental applications. *Catalysis Today*, 178, 197-205.
- ZYGMUNT MARCZENKO, M. B. 2000. *Separation, Preconcentration and Spectrophotometry in Inorganic Analysis*, Elsevier.

Chapter Six

PREPARATION AND USE OF IRON ON CARBON FOAM FOR REMOVAL OF ORGANIC DYE FROM WATER – BATCH STUDIES

Khumalo, S. P. *, Lokhat, D.,

School of Engineering, University of KwaZulu-Natal, Howard College Campus, Durban, South Africa

Correspondence should be addressed to Khumalo S.P.: spgkhumalo@gmail.com

(Submitted and under review)

Abstract

The dyes in textile effluents have a deleterious impact on water bodies and impede photosynthesis by decreasing sunlight penetration. This study examined the adsorption capacity of an iron oxide sorbent immobilised on carbon foam generated from natural sources to remove organic methylene blue dye from water. The carbon precursor and iron oxide precursor were combined in a single tank and then carbonised. Baking and carbonization of the natural grain mixture provide a porous structure that can effectively support the iron oxide particles. Transmission electron microscopy (TEM) techniques were used to examine the physical properties and surface morphology of the synthesised carbon foam. The generated carbon foam is a self-assembled structure that inherits the shape and original network structure of bread. The preparation process for iron-based nanoparticles significantly influences particle shape and size, size distribution, active sites, and, consequently, applications. Due to the increased number of active sites, dye adsorption increased as the number of nanoparticles increased. At high temperatures, the dye molecules interacted more effectively, allowing for simple dye removal. The Magnetite sample exhibited endothermic adsorption, and all other samples exhibited exothermic adsorption. Intraparticle diffusion was not the sole rate-limiting step for all samples in the adsorption of methylene blue onto iron supported by carbon foam. The adsorption rate was governed by a multistep elementary reaction mechanism in which multiple processes occurred simultaneously. This experiment is best described by the pseudo-second order kinetic model ($R^2 > 0.96$), whereas the Freundlich isotherm best describes the adsorption equilibrium ($R^2 > 0.999$). The results indicate that an iron oxide sorbent immobilised on natural carbon foam is a good sorbent for removing methylene dye.

Introduction

The release of hazardous wastes, poisonous gases, and smoke from industry has had a significant impact on the environment because of rapid industrialization and its products (MP, 2017). Numerous sectors, including textiles, paper, printing, plastic, food, and cosmetics, employ dyes to colour their products (Adeleye, 2016). This industry's waste typically contains several colours that are dumped untreated into the drain water (Ashraf, 2022). Due to the decrease in light transmission, dyes inhibit the photosynthetic movement of aquatic life (MP, 2016). In addition, some colours are toxic and carcinogenic to numerous aquatic organisms, such as fish and bacteria (Chong, 2010). These dyes are responsible for serious harm to the kidney, reproductive system, liver, brain, and central nervous system of humans (Bruno Lellis, 2019). Every year, people around the world use more than 10,000 different pigments and dyes that add colour to things (Tanksale, 2019). Due to the inherent non-biodegradability of most dyes, biological and chemical methods for dye removal have proven insufficient. Adsorption is currently being used for the removal of organic dyes due to its low cost, precision, viability, and easy design requirements (Lopez, 2020). Activated carbon is the preferred adsorbent for wastewater treatment, but its high cost restricts its industrial application (Vikash R Agrawal, 2017). So, the textile industry is always looking for cheaper ways to replace activated carbon.

The physicochemical properties of iron nanoparticles facilitate their use in environmental applications, such as decontaminating contaminated soil and groundwater (Mohammed M. Rahman, 2011). The functional groups serve to define an absorbent's efficiency, selectivity, capacity, and reusability (Nizamuddin, 2019). In addition, iron oxide nanoparticles have an effect since they decrease Gibbs' free energy demand. The majority of colours are nonbiodegradable and resistant to aerobic digestion (Song, 2016). The iron-based oxide nanomaterial exhibited a variety of sorption capabilities for concurrently removing colours, organic contaminants, and inorganic pollutants with great efficacy (Tanksale, 2019). In solutions, nanoparticles tend to agglomerate, reducing their reactivity. Therefore, the stability of nanoparticles is essential for their high reactivity and mobility, as the rate of aggregation and deposition decreases with increasing material stability (Nizamuddin, 2019). The preparation process of iron oxide nanoparticles is crucial in influencing particle shape and size, size distribution, surface chemistry, and therefore their applications (S. F. Hasany, 2012). The environmental uses of iron oxide nanoparticles are strongly dependent on their features, including their magnetic properties, specific surface area, and core-shell structure (Tanksale, 2019). Low toxicity, biocompatibility, and chemical inertness are three further benefits of iron oxide nanoparticles.

Due to their increased specific surface area, high porosity, and strong magnetic response, nanoparticles based on iron exhibit remarkable sorption capabilities, resulting in an outstanding sorption capacity. Various types of iron oxide exist in nature, including maghemite ($\gamma\text{Fe}_2\text{O}_3$), magnetite (Fe_3O_4), and hematite ($\alpha\text{Fe}_2\text{O}_3$) (Mohammed M. Rahman, 2011). It has been observed that nanoparticle sizes between 10 and 20 nm provide the best performance (Mohammed M. Rahman, 2011). It has been claimed that these particles exhibit superparamagnetic behaviour, a type of magnetism that has been observed in ferromagnetic particles (Nizamuddin, 2019). Due to the size of the particles, the decrease in demand for magnetic materials may result in instability, as micro- and nanometer-sized particles tend to form agglomerates, which reduce the energy-related ratio of surface-to-volume nanomaterials (Song, 2016). Thus, the active response of nanoparticles based on iron oxide to chemical processes causes them to lose their magnetism and become non-essential (Yao, 2015).

This work examines the fabrication and evaluation of carbon foam as a substrate for iron nanoparticles. The carbon-based foam was made by combining the produced iron nitrate with baking flour, yeast, and water

to produce a natural grain-based carbon foam that is economical. This mixture was subjected to an argon environment, which resulted in the carbonization of the foam. Four tests were conducted on each sample to establish whether this porous foam exhibited any thermal, mechanical, or sorption properties: the effect of the initial concentration, the effect of temperature, the effect of contact time, and the effect of the amount of carbon foam.

Materials and Methods

Equipment and materials used

The following materials were used: 1000 g of baking flour, 50 g of dry yeast, water (distilled), magnetite (iron sponge), nitric acid, iron (granules), argon gas, nickel grease, pressurised air, and ethylene blue dye (powder). All chemicals were used as supplied with no further purification.

Sample Preparation

Five samples were created to investigate if carbon foam possesses thermal, mechanical, or absorbent qualities. The first four samples included variable amounts of iron and nitric acid, but the fifth sample contained a particular amount of magnetite. In this experiment, the amount of iron and nitric acid injected were among the test variables. This is how the magnetite sample was prepared: 10 grammes of magnetite (iron sponge) were combined with 300 grammes of flour, 5 grammes of dry yeast, and 200 millilitres of water. Due to the somewhat larger size of the magnetite particles, a greater quantity of wheat and yeast was employed to accommodate them. The mixture was agitated at 500 rpm for 5-10 minutes. After preparing the five mixes, each was placed on an aluminium baking sheet to undergo the carbonization process. Table 1 shows the composition of other samples.

Table 1. Sample A, Sample B, Sample C, and Sample D sample

	Sample A	Sample B	Sample C	Sample D
Amount of Iron (g)	1.0	2.0	3.0	3.0
Amount of Nitric acid (ml)	3.34	6.68	10.01	3.34

Aqueous Solution Preparation

To test the effectiveness of the carbon foam support along with iron and magnetite nanoparticles, aqueous solutions, containing methylene blue dye powder, were prepared at different concentrations. 250 mL of distilled water was measured out in five glass beakers, to which varying amounts of methylene blue dye were added. Table 2 depicts the amount of methylene blue added to each beaker, along with the resulting concentrations.

Table 2. Aqueous solutions of known concentrations

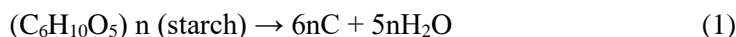
Solution number	Methylene blue dye (mg)	Concentration (mg/L)
1	10	40
2	20	80
3	30	120
4	40	160
5	50	200

Results and discussion

Sorbent preparation

Utilizing the natural grain composition, carbon foam was created. For 5–10 minutes, the mixture was stirred with an electrically driven stirrer to ensure an even distribution of ingredients and a consistent texture throughout. The mixture was left to ferment at 60 °C for 60 minutes, baked at 180°C for 40 minutes, and then 80°C was used for 18 hours to get rid of any extra water. The carbonization process took place in an Argon gas atmosphere with a flow rate of 0.4 cm³/min, and the flow rate was controlled to provide a continuous flow of Argon gas throughout the tube. On the tube furnace, the heating rate was set to 10 °C/min. Within the tube furnace, the carbonising foam attained a maximum temperature of 600 °C and this temperature was maintained for 90 minutes (also known as the holding time). After 90 minutes, the carbonised foam in an argon environment had naturally cooled to 25 °C, which is the same temperature as the air around it.

This procedure involves two chemical reactions: dehydration and carbonization. The following reaction occurs during carbonisation in an argon gas atmosphere:



The characteristics of porous carbon compounds are mostly determined by pore size and distribution. The density of carbon foam with bigger and irregular holes is low. By adjusting the quantities of yeast, water, iron, nitric acid, and magnetite in the mixture, the size of the foam's holes can be altered. A few hundred micrometres in diameter, nearly spherical pores are visible to the human eye.

Characterisation

The addition of iron nitrate particles to granular carbon foam produced a structure that was more amorphous and porous. The surface of the material featured geometrical properties such as an irregular form, large agglomerates, and a rough surface, which would provide extra sites for adsorbing heavy metal ions (Giri, 2011).

Effect of time

The effect of contact time on adsorption at constant dye concentrations (MB-40 mg/L and 10 mg adsorbent) at different time intervals (5–35 min) was investigated, and the results are shown in Figure 1. The percentage of dyes removed rose as contact time increased (Vanitha Katheresan, 2018). The rate of adsorption was initially very high for magnetite (sample B) and Sample D samples because the reactive site was still available on the surface of the adsorbent. Figure 1 indicates that the Sample D sample removes the most amount of dye (70%) while sample C removes the least (35%) after 35 minutes. The results show that adsorption increases with time. The adsorption of dye was rapid for the Sample D sample compared to other samples. This rapid adsorption is due to iron and nitric acid being well incorporated into the baking flour before the carbonization process (Vanitha Katheresan, 2018). For the first 10 minutes, the adsorption process was relatively low; thereafter, it increased steadily. In samples A, B, and C and in the magnetite sample, fluctuations in the percentage of dye removed can be seen. The magnetite sample demonstrates superior adsorption capabilities compared to all other samples.

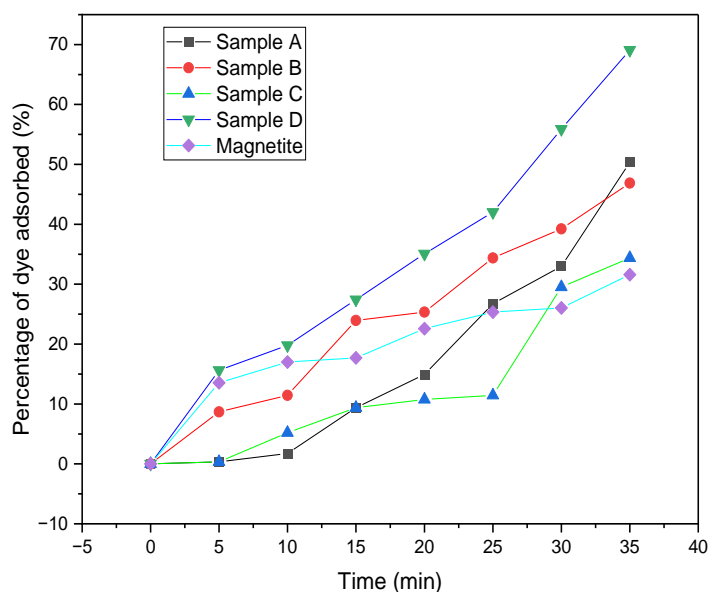


Figure 1. Dye removal using 40 mg/L solution under the effect of contact time

Effect of sorbent dosage nanoparticles

The number of nanoparticles containing iron added to each solution is exactly equal to the amount of dye removed. This merely indicates that as the quantity of nanoparticles increases, so does dye adsorption (Saif, 2016). Figure 2 demonstrates that sample B, as well as the undiluted and magnetite samples, have effective adsorption properties when introduced in large volumes. The highest percentage of dye adsorbed was roughly 27% for all three samples, whereas samples A and C had the lowest percentages of dye removed from the solutions, 11.5% and 17.7%, respectively. Sample A has the least adsorption, followed by Sample C; this indicates that Sample B has the optimal number of nanoparticles, which is greater than Sample A but less than Sample C. This demonstrates that the number of iron-based nanoparticles plays a crucial role in influencing the adsorption of the adsorbent. Sample B, as well as the undilute and magnetite samples, had greater concentrations of iron, nitric acid, and magnetite; hence, these samples demonstrate a

significantly higher adsorption rate. As the number of adsorption sites grows, this can be attributed to the increased surface area of iron-based nanoparticles and the carbon foam support added to the solution.

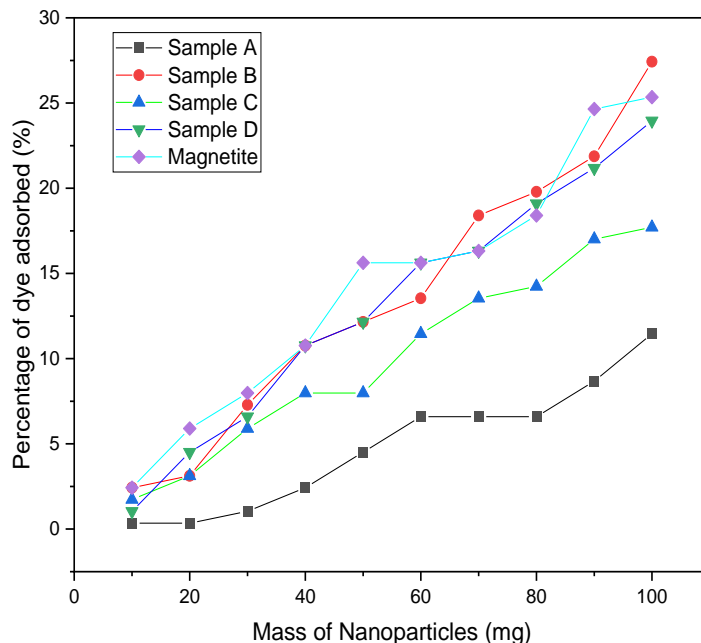


Figure 2. Dye removal using a varying number of nanoparticles in increments of 10 mg

Effect of initial concentration

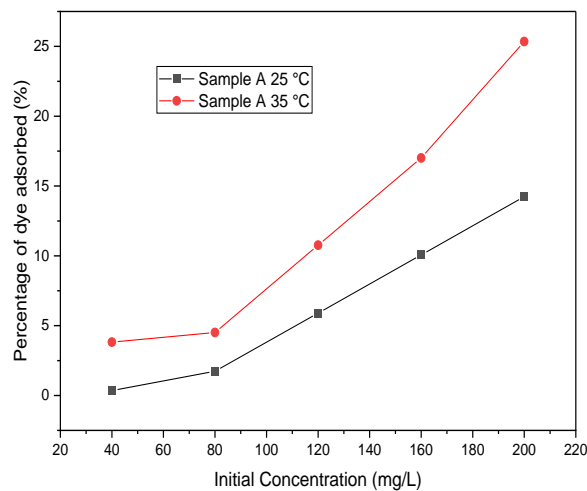
Various initial dye concentrations (20–100 mg/L for MB) during the adsorption process at a given dosage of 10 mg of carbon foam were weighed and then added to 20 mL of solution, which was then agitated at 500 rpm for 10 minutes. Figure 3 (a–e) demonstrates that an increase in the initial dye concentration induces an acceleration of the dye adsorption process (Lopez, 2020). The particles were magnetically drawn to the bottom of the beaker, and the remaining solution was added to the photocell of the spectrophotometer to produce a concentration reading. The test was conducted on all samples using the variously prepared solutions at room temperature. Figure 5 demonstrates that sample B, together with the undiluted and magnetite samples, once again outperformed samples A and C, which exhibited significantly less effective adsorption properties (how). The maximum percentage of dye removed by samples B and magnetite was 24%, a substantially greater proportion than samples A and C, which removed 7.29% and 3.88% of the dye, respectively. In Table 3, all samples exhibited a modest percentage of dye removal for the first 3 solutions. However, for the last 2 solutions, samples B and magnetite exhibit a substantial increase. This indicates that these samples can remove dye from solutions of high concentration (Yao, 2015).

Table 3. Initial concentration test

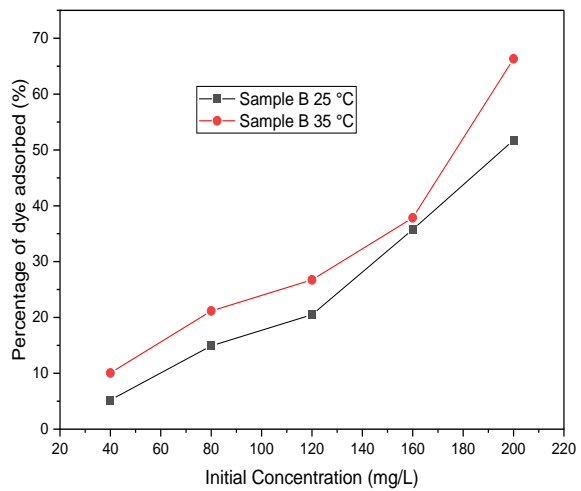
Initial concentration (mg/L)	Sample A	Sample B	Sample C	Sample D	Magnetite
	% Dye removed				
40	0.35	1.74	0.35	0.35	5.21
80	2.43	3.82	0.35	4.51	5.90
120	4.51	8.68	1.04	8.68	8.68
160	4.51	14.24	3.13	10.07	18.40
200	7.29	23.96	3.82	12.15	23.96

Effect of temperature

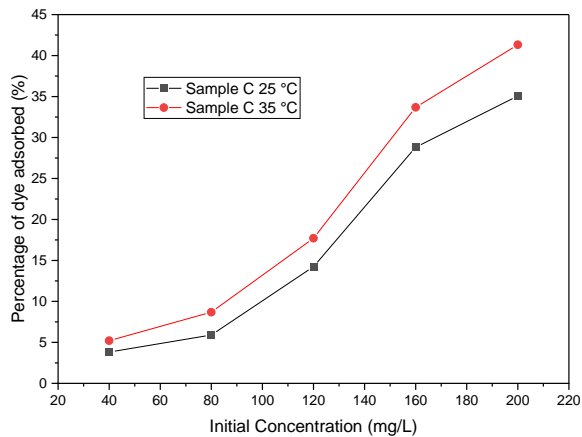
Figure 3 depicts the effect of temperature on the adsorption rate, and it was discovered that as the temperature increased, so did the proportion of methylene blue that was removed. Temperature increases the availability of active sites on the surface and the rate of pore volume opening of the adsorbent (Nizamuddin, 2019). When the temperature rises, the viscosity of the dye suspension reduces, allowing more adsorbate to permeate through the outer boundary layer and through the internal pores of the adsorbent. In addition, as the temperature rises, the dye molecules exert kinetic energy, which increases the adsorption rate.



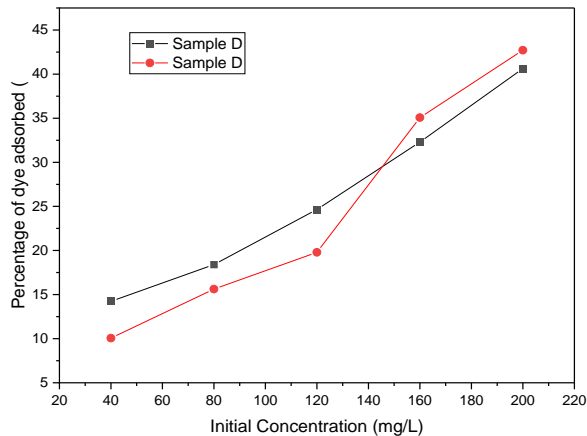
a.



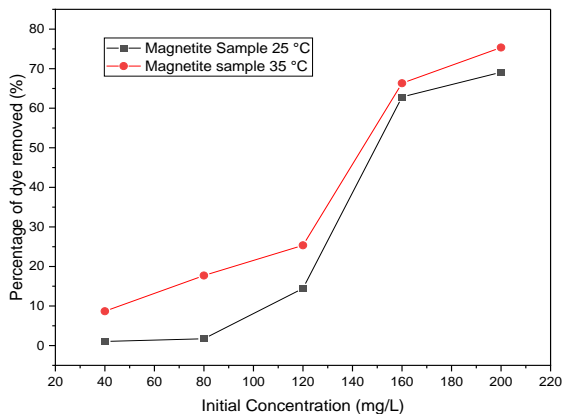
b.



c.



d.



e.

Figure 3. Magnetite sample temperature effects

The interaction between the dye molecules and the adsorbent should improve as the temperature rises, leading to an increase in the diffusion rate of methylene blue dye molecules across the external boundary layer and internal pores of the iron-based nanoparticles (MP, 2017). To test this notion, a simple temperature test was conducted at 25°C and 35°C to discover if temperature has any effect on the amount of dye eliminated. Figure 3 demonstrates that every sample was tested at both temperatures. All samples had more than 35% of the dye removed, with sample B, the Sample D sample, and the magnetite sample showing the most. These three samples had the highest percentage of dye elimination at both 25°C and 35°C. Figures 3a, 3d, and 3e demonstrate that performance is enhanced at both temperatures, demonstrating a straight proportional relationship. This proves the above-mentioned idea that a higher temperature promotes more absorption. All samples exhibit a rapid increase in adsorption at 35 °C when compared to the samples at 25 °C. The correlation between adsorption capacity and temperature indicates that the adsorption process requires heat to function efficiently. The results show that there might be a way to make a cheap and safe iron-based nanomaterial with a carbon foam support for use in industry, protecting the environment, and making energy use more efficient.

Equilibrium Adsorption

Adsorbate molecules and an adsorbent surface reach equilibrium when in contact. Adsorption isotherms represent the equilibrium of adsorbed amount (q_e) and residual adsorbate concentration (C_e) at a constant temperature. Adsorption isotherms provide information on affinity, binding energy, adsorption capacity, and surface phase, which may be monolayer or multilayer. Modelling adsorption isotherms involves summarising exponential data using theoretical or empirical equations and estimating isotherm parameters to compare adsorbent performance. The adsorption isotherm examines the relationship between dye adsorption and dye concentration (Ugurlu, 2009). The empirical Freundlich model, which is good for low concentrations and is based on sorption on the uneven surface, is shown by the following equation:

$$q_e = K_F C_e^{1/n} \quad (2)$$

C_e (mg/L) represents equilibrium adsorbate concentration, and q_e (mg/g) represents equilibrium adsorption quantity. K_F and n are proportional to adsorption capacity and intensity. Freundlich's model is an empirical equation based on solid-liquid solute equilibrium. The Freundlich model can describe heterogeneous surfaces but not adsorption data (Mahmoodi, 2013). Origin Lab was used to determine isotherm parameters by nonlinearly fitting q_e versus C_e . The Temkin model depicts indirect adsorbate-adsorbent interactions on an adsorption isotherm. Due to adsorbate-adsorbent interactions, it's anticipated that adsorption heat decreases linearly with coverage. Adsorption is characterised by a constant range of binding energies (Mahmoodi, 2013). Temkin model equation:

$$q_e = \frac{RT}{b} \ln(AC_e) \quad (3)$$

q_e (mg/g) represents the amount of adsorption at equilibrium, C_e (mg/L) is the equilibrium adsorbate concentration, T (K) is the Kelvin temperature, R (J/mol/K) is the universal gas constant, b (J/mol) is the

Table 4 displays Freundlich and Temkin R^2 values determined by nonlinear fitting. Based on R^2 values, the Freundlich model fits equilibrium data better than the Temkin model R^2 values, the Freundlich model fits equilibrium data better than the Temkin model. Thus, the Freundlich isotherm best represents the adsorption of methylene blue, which indicates multilayer adsorption on a heterogeneous surface with variable energy distribution. n measures adsorption intensity. $1/n$ between 0 and 1 suggests methylene blue adsorption (Gurses, 2006a).

Table 4. Isothermal equilibrium parameters

sample	Freundlich		
	N	K_F	R^2
Sample A	-10.97×10^{-3}	78.410	0.999
Sample B	-10.95×10^{-3}	78.412	0.999
Sample C	-11.03×10^{-3}	78.407	0.999
Sample D	-11.65×10^{-3}	78.368	0.999
Magnetite	-11.45×10^{-3}	78.380	0.999

Thermodynamic Analysis

The thermodynamic parameters Gibbs energy (ΔG), enthalpy (ΔH), and entropy (ΔS) are the actual indicators for the practical use of the adsorption process. Based on the values of these parameters, the spontaneously occurring process can be predicted. The thermodynamic parameters were computed using the following equations (Pirillo, 2009):

$$\Delta G = \Delta H - T\Delta S \quad (4)$$

$$K_c = \frac{q_e}{C_e} \quad (5)$$

$$\ln K_c = \frac{\Delta S}{R} - \frac{\Delta H}{RT} \quad (6)$$

$$\Delta G = -RT\ln K_c \quad (7)$$

where K_c , R , and T denote the equilibrium constant, the equilibrium concentration of dye in the solution, the equilibrium concentration of dye on the adsorbent, the gas constant (8.314 J/mol K), and the absolute temperature, respectively (K). H and S values can be estimated using the slopes and intercepts of a graph depicting $\ln K_c$ vs. $1/T$. As shown in Table 5, thermodynamic parameters can be determined using various equations and graphs. Temperature-dependent adsorption data are required for this purpose. R^2 values ($R^2 = 1$) indicate which plot is more appropriate for estimating the thermodynamic properties of the adsorption process. Thermodynamic investigations can reveal the spontaneity ($G^0 < 0$), endothermic nature ($H^0 > 0$), or exothermic nature ($H^0 < 0$) of the adsorption process. The Gibbs free energy of change indicates the spontaneity and practicability of adsorption processes for all the samples. All the samples had an exothermic adsorption except the magnetite sample, which had an endothermic adsorption. The graphs of $\ln K_c$ vs. $1/T$ are provided in appendix D from Figure D.14 to D.18. Table D.1 in appendix D depicts the intercepts and slopes of $\ln K_c$ vs. $1/T$ graphs.

Table 5. Thermodynamic parameters

Parameters	Sample A	Sample B	Sample C	Sample D	Magnetite sample
ΔH	-334.80	-625.61	-334.80	-240.32	531.99
ΔS	41.93	13.12	41.93	42.28	44.88
ΔG	-12829.59	-4534.47	-12829.59	-12840.51	-12843.63

Adsorption Kinetics

Pseudo first and pseudo second order

For the research of adsorption kinetics modelling, Lager Gren pseudo-first order and pseudo-second order models were utilised. The following equation represents the pseudo-first order nonlinear form:

$$q_t = q_e(1 - e^{-K_1 t}) \quad (8)$$

The following equation represents pseudo-second order in its nonlinear version.

$$q_t = \frac{q_e^2 K_2 t}{1 + K_2 q_e t} \quad (9)$$

Where q_t (mg/g) is the quantity adsorbed at time t , q_e (mg/g) is the amount remaining after equilibrium of adsorption, and K_1 and K_2 are the pseudo-first and pseudo-second order model rate constants, respectively, represented in min^{-1} and g/mg/min . Shown in Table 5 are the calculated q_e , K_1 , and K_2 values and the corresponding linear regression coefficient R^2 values. Figure 4 shows the fitting of pseudo-first order and pseudo-second order models. The correlation coefficient R^2 , and the agreement between the calculated and experimental q_e values, indicate the applicability of the model. Therefore, the pseudo-first-order model is predominant compared to the pseudo-second order.

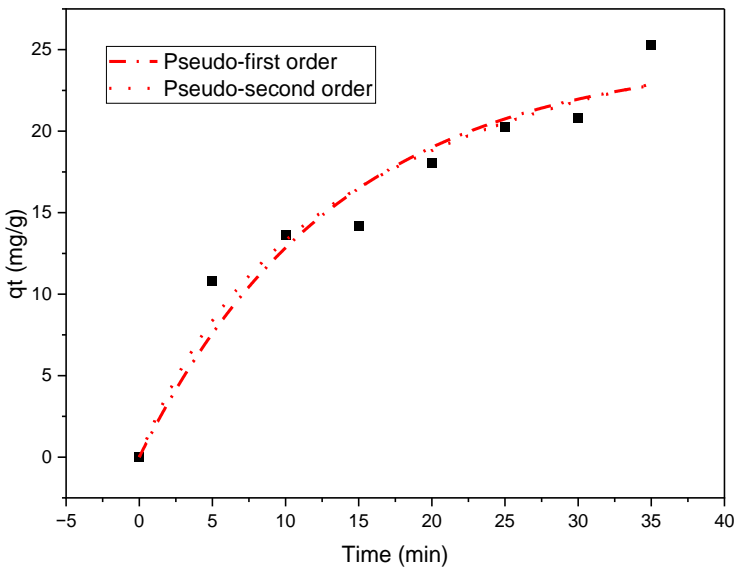


Figure 4. Fitting of pseudo-first order and pseudo-second order for magnetite sample

Table 6. Pseudo-first order and pseudo second order parameters

Sample	Pseudo-first order		Pseudo-second order	
	K_1 (min^{-1})	R^2	K_2 (g/mg/min)	R^2
Sample A	6.70×10^{-2}	0.985	1.15×10^{-9}	0.848
Sample B	4.50×10^{-3}	0.986	4.89×10^{-6}	0.986
Sample C	6.28×10^{-2}	0.945	2.00×10^{-9}	0.825
Non diluted	1.04×10^{-4}	0.977	3.32×10^{-8}	0.976
Magnetite	7.34×10^{-2}	0.940	2.19×10^{-3}	0.955

Intraparticle diffusion

The intraparticle diffusion resistance was calculated using Weber and Morris's (Mahmoodi, 2013) intraparticle particle diffusion model, denoted by the following equation:

$$q_t = k_{id}t^{1/2} + c \quad (10)$$

Where q_t (mg/g) is the adsorption quantity at time t (min), k_{id} (mg/g/min^{1/2}) is the adsorption rate constant of the intraparticle diffusion model, and c is a parameter relating to the boundary layer thickness. If the plot of q_t vs $t^{1/2}$ is linear and passes through the origin, then it is the only rate-limiting stage in the adsorption process. When the lines of uptake pass through the origin, intraparticle diffusion controls the rate. When the plots do not pass through the origin, it suggests that intraparticle diffusion is not the only rate-limiting process, and that other kinetic models may also govern the adsorption rate (Mahmoodi et al., 2013). Figure 5 depicts linear plot of intraparticle diffusion that pass through the origin. This suggests that intraparticle diffusion was not the only rate-limiting phase in the adsorption of methylene blue onto all samples, therefore other mechanisms may potentially regulate the rate of adsorption for other four samples (Dutta, 2013).

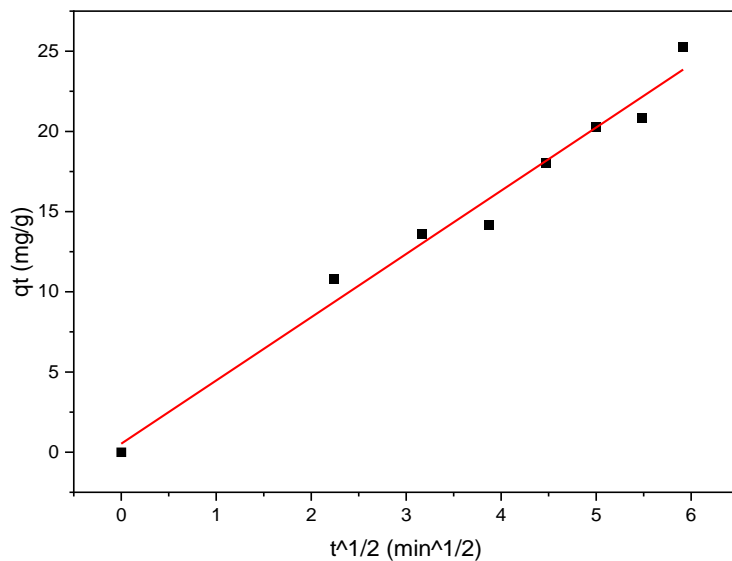


Figure 5. Intraparticle diffusion for magnetite sample

Conclusion

A systematic approach was utilised, with a combination of literature research and experimentation methods were employed to investigate iron-based nanoparticles, in conjunction with a natural grain mixture procedure, to determine any thermal, mechanical, and sorption properties that the particles may possess. Four tests were performed, namely the initial concentration and temperature tests, the effect of contact time, and varying the number of nanoparticles. The role of pore structure on temperature distributions has been examined and how pore structure affects the heat transferred throughout the material. Pore sizes can be varied by controlling the iron, nitric acid, magnetite, yeast, and water content. This allows the nanomaterials to be used for a variety of applications. The method of preparing the iron-based nanoparticles plays a key role in determining the particle shape and size, size distribution, active sites, and subsequently, the

applications. Sample B and the Sample D and magnetite samples showed good adsorption properties, as compared to samples A and C, in all the tests performed. The Gibbs free energy of change indicates spontaneity and practicability of adsorption processes for all the samples. All the samples had and exothermic adsorption except the magnetite sample which had an endothermic adsorption. when the temperature rises, the viscosity of the dye suspension reduces, allowing more adsorbate to permeate through the outer boundary layer and through the internal pores of the adsorbent. Intraparticle diffusion was not the only rate-limiting step in the adsorption process of methylene blue onto iron supported by carbon foam, the adsorption rate was controlled by a multistep elementary reaction mechanism, with many processes functioning simultaneously. The pseudo-second order kinetic model best describes this investigation ($R^2 > 0.96$), while the Freundlich isotherm best describes the adsorption equilibrium ($R^2 > 0.999$). According to the results, an iron oxide sorbent immobilised on natural carbon foam is an excellent sorbent for eliminating methylene dye.

Chapter Seven
Concluding Remarks and Future Research Scope

Conclusion

Natural grains and various pyrolytic char compositions were used to create carbon foam, which was then characterised by TEM analysis, an open flame test, and an ethanol-soaked burn test. The distribution of pores within porous materials impedes temperature transfer. Due to the unequal distribution of pores, the temperature within the porous material is no longer uniform, and the temperature distribution along the direction of heat flow is irregular. Heat conductivity decreases as porosity increases. Carbon foam may be mass-produced like bread and is a viable alternative to foams generated from other substances. Carbon foam is relatively inflammable and stable. The pore size can be altered by adjusting the temperature, pressure, precursor, water, and pyrolytic tyre char content. This permits the carbon foam to be utilised for a variety.

Iron oxide immobilised on carbon foam obtained from natural sources possesses adequate adsorption properties removing organic dyes from aqueous solutions. According to adsorption experiments, increasing the iron dosage produced the maximised removal effectiveness. Studies of adsorption isotherms and kinetic models found that the, Temkin, Langmuir isotherm and pseudo-first-order kinetic models offered the best fit to the data. The percentage of dye removal for the sample containing 15 wt.% iron was 9.21% higher than that of the sample containing 6 wt.% iron, indicating that sorbent efficiency increased with increasing iron content. Due to increased concentration gradients, contact time and sorbent dose experiments revealed that higher concentrations of dye solution result in greater adsorption. Due to the increased availability of adsorption sites, increasing the sorbent dosage boosted the adsorptive characteristics of the sorbent. Increased contact duration allowed for sorbent saturation, maximising sorbent adsorption capacity.

A greater bed height extends the contact time between the dye and the sorbent, thereby extending the breakthrough time. Higher flow rates decreased the sorbent's efficiency and shortened the breakthrough time since the contact time between dye molecules and the sorbent's surface decreased. Using flow-through equipment is economical and eliminates the need for sorbent recovery. It is appropriate for enormous amounts of water, making it suitable for industrial application on a large scale. The data indicated that the adsorption process may be enhanced by decreasing flow rates and increasing contact duration, dye solution concentration, sample iron content, and sorbent dosage. The physical properties and surface morphology of synthesized carbon foam were evaluated using TEM and BET techniques. As intraparticle diffusion was not the only rate-limiting step in the adsorption process of methylene blue onto iron supported by carbon foam, the adsorption rate was controlled by a multistep elementary reaction mechanism with many processes functioning simultaneously. The pseudo-first-order kinetic model best describes this investigation ($R^2 > 0.96$), while the Freundlich isotherm best describes the adsorption equilibrium ($R^2 > 0.99$). According to the results, an iron oxide sorbent immobilised on natural carbon foam is an excellent sorbent for eliminating methylene dye.

Adsorption of phenol by nanoparticles on natural grain carbon foam increased as the original concentration rose. In addition, adsorption increased with an increase in iron concentration in the carbon form, but the magnetite sample possessed diminished adsorption capacities relative to other samples. On the qt (mg/g) versus time (min) graph, the adsorption values grew fast between 5 and 15 min and began to level out as the solutions approached equilibrium. This was attributed to many open sites on the magnetic nanoparticle surface, which gradually filled over time as adsorption occurred. This study reveals that magnetic

nanopowder immobilised on carbon foam reduces the concentration of phenol substantially. The correlation between the data on adsorption and the pseudo-first-order equation is the strongest. The Temkin adsorption model is more appropriate for representing the equilibrium phenol adsorption data.

Significance and Impact of the Research

Higher dye concentrations result in more adsorption due to increasing concentration gradients in contact time and sorbent dose trials. Increasing sorbent dosage increases adsorptive properties due to more adsorption sites. Increased contact time saturates the sorbent, maximising adsorption capacity. A higher bed height extends dye-sorbent contact time, lengthening breakthrough time. Higher flow rates reduce sorbent efficiency and breakthrough time because dye molecules spend less time on the sorbent's surface. Using flow-through equipment eliminates sorbent recovery. It is ideal for large amounts of water, making it industrially applicable. Reduce flow rates and increase contact duration, dye solution concentration, sample iron content, and sorbent dosage to improve adsorption. Pore structure influences temperature distributions and heat transport across materials. Iron, nitric acid, magnetite, yeast, and water can alter pore diameters. This makes nanoparticles versatile. Iron-based nanoparticle preparation determines particle form, size, size distribution, active sites, and applications.

Future Research Scope

The following proposals would provide an intriguing follow-up to these investigative studies for future research: Samples of sorbents can be analysed using SEM and TEM. Additional parameter research, including pH and temperature. Characterizing and utilising actual industrial waste, followed by evaluating the adsorbents used in the study. To guarantee that homogenous, effective particles are introduced to solutions, the created magnetic nanopowder must be evaluated and classed in terms of its size distribution.

Appendices

The content of these appendices can be summarised as follows:

Appendix A shows instrument calibration plots used during the experiments.

Appendix B shows the raw data.

Appendix C shows sample calculations.

Appendix D shows the graphs.

Appendix E shows the experimental pictures.

Appendix A

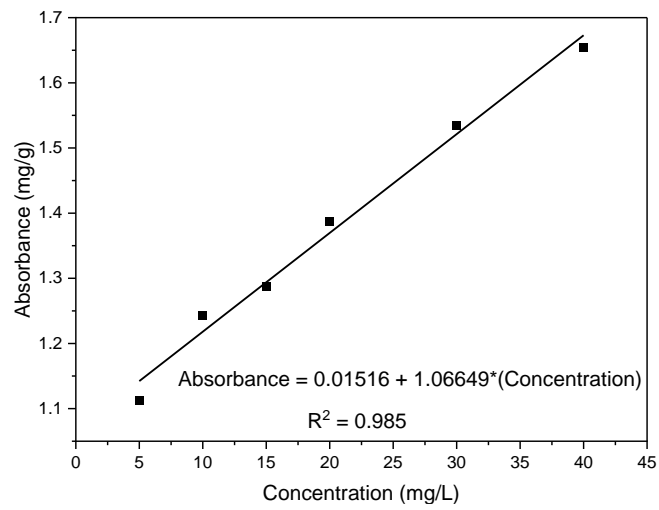


Figure A.1 Spectrometer calibration for the adsorption of methylene blue dye in chapter 2

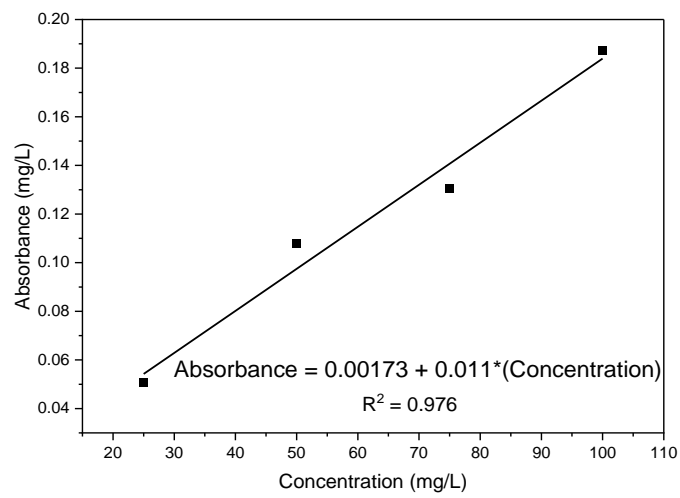


Figure A.2 Spectrometer calibration of adsorption of phenol in chapter 3

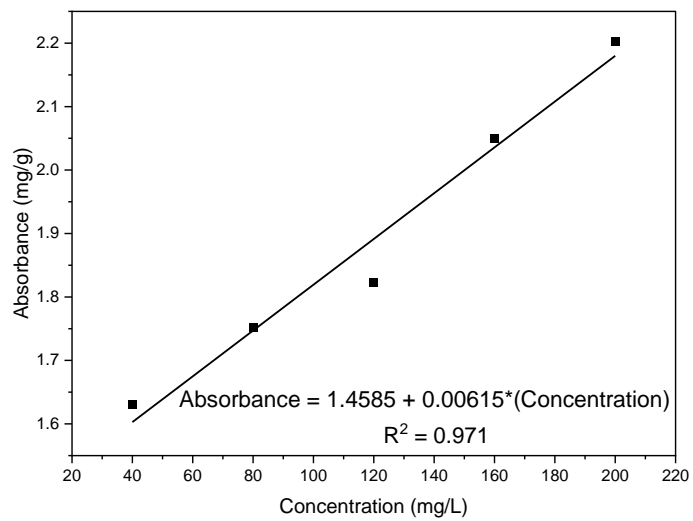


Figure A.3 Spectrometer calibration of adsorption of methylene blue dye in chapter 4

Appendix B

Chapter 4 Raw data

Table B.1 Data for iron content test using 10 mg/L dye solution

wt%	Average absorbance	Final Conc.(mg/L)	% MB Adsorbed	q_t (mg/g)
0	1.218	9.9473684	0.526	0.053
6	1.202	8.8947368	11.053	1.105
15	1.188	7.9736842	20.263	2.026

Table B.2 Sorbent dosage test for 6 wt% iron sample using 10 mg/L, 20 mL dye solution, and 180 minutes contact time

Amount(g)	Average absorbance	Final Conc. (mg/L)	% MB Adsorbed	q_t (mg/g)
0.02	1.211	9.487	5.132	0.513
0.04	1.193	8.281	17.193	0.860
0.06	1.175	7.096	29.035	0.968
0.08	1.164	6.373	36.272	0.907
0.1	1.157	5.956	40.439	0.809

Table B.3 Sorbent dosage test for 6 wt% iron sample using 20 mg/L, 20 mL dye solution, and 180 minutes contact time

Amount(g)	Average absorbance	Final Conc. (mg/L)	% MB Adsorbed	q_t (mg/g)
0.02	1.337	17.776	11.118	2.224
0.04	1.310	15.978	20.110	2.011
0.06	1.266	13.083	34.583	2.306
0.08	1.231	10.803	45.987	2.299
0.1	1.222	10.232	48.838	1.954

Table B.4 Contact time test for 6 wt% iron sample using 10 mg/L, 20 mL dye solution, and 50 mg of sorbent

Time (min)	Average absorbance	Final Conc. (mg/L)	% MB absorbed	q_t (mg/g)
30	1.214	9.706	2.939	0.118
60	1.182	7.579	24.211	0.968
90	1.153	5.671	43.289	1.732
120	1.137	4.640	53.596	2.144
150	1.137	4.618	53.816	2.153
180	1.137	4.640	53.596	2.144

Table B.5 Contact time test for 6 wt% iron sample using 20 mg/L, 20 mL dye solution, 100 mg of sorbent

Time (min)	Average absorbance	Final Conc. (mg/L)	% MB absorbed	q_t (mg/g)
30	1.333	17.491	12.544	1.004
60	1.299	15.298	23.509	1.881
90	1.292	14.816	25.921	2.074
120	1.289	14.596	27.018	2.161
150	1.289	14.596	27.018	2.161
180	1.288	14.575	27.127	2.170

Table B.6 Sorbent dosage test for 15 wt% iron sample using 10 mg/L, 20 mL dye solution, and 180 minutes of contact time

Amount(g)	Average absorbance	Final Conc. (mg/L)	% MB Adsorbed	Absorbance (mg/g)
0.02	1.205	9.070	9.298	0.930
0.04	1.186	7.842	21.579	1.079
0.06	1.163	6.329	36.711	1.224
0.08	1.146	5.189	48.114	1.203
0.1	1.136	4.531	54.693	1.094

Table B.7 Sorbent dosage test for 15 wt% iron sample using 20 mg/L, 20 mL dye solution, and 180 minutes of contact time

Amount(g)	Average absorbance	Final Conc. (mg/L)	% MB Adsorbed	q_t (mg/g)
0.02	1.331	17.404	12.982	2.596
0.04	1.298	15.211	23.947	2.395
0.06	1.248	11.943	40.285	2.686
0.08	1.209	9.355	53.224	2.661
0.1	1.193	8.325	58.377	2.335

Table B.8 Contact time test for 15 wt% iron sample using 10 mg/L, 40 mL dye solution and 50 mg of sorbent

Time (min)	Average absorbance	Final Conc. (mg/L)	% MB absorbed	q_t (mg/g)
30	1.189	8.018	19.825	0.793
60	1.169	6.724	32.763	1.311
90	1.139	4.728	52.719	2.109
120	1.130	4.180	58.202	2.328
150	1.122	3.610	63.904	2.556
180	1.122	3.632	63.684	2.547

Table B.9 Contact time test for 15 wt% iron sample using 10 mg/L, 40 mL dye solution and 50 mg of sorbent

Time (min)	Average absorbance	Final Conc. (mg/L)	% MB absorbed	q_t (mg/g)
30	1.333	17.535	12.325	0.986
60	1.296	15.079	24.605	1.968
90	1.281	14.092	29.539	2.363
120	1.276	13.763	31.184	2.495
150	1.275	13.697	31.513	2.521
180	1.274	13.610	31.952	2.556

Table B.10 Sorbent dosage test for 0 wt% iron sample using 10 mg/L, 20 mL dye solution, and contact time of 180 minutes

Amount(g)	Average absorbance	Final Conc. (mg/L)	% MB Adsorbed	q_t (mg/g)
0.02	1.218	9.947	0.526	0.053
0.04	1.218	9.947	0.526	0.026
0.06	1.217	9.882	1.184	0.039
0.08	1.216	9.816	1.842	0.046
0.1	1.215	9.750	2.500	0.050

Table B.11 Sorbent dosage test for 0 wt% iron sample using 10 mg/L, 20 mL dye solution, and contact time of 180 minutes

Amount(g)	Average absorbance	Final Conc. (mg/L)	% MB Adsorbed	q_t (mg/g)
0.02	1.368	19.838	0.811	0.162
0.04	1.368	19.794	1.031	0.103
0.06	1.367	19.728	1.360	0.091
0.08	1.364	19.553	2.237	0.112
0.1	1.362	19.421	2.895	0.116

Table B.12 Contact time test for 0 wt% using 10 mg/L, 40 mL dye solution, and 50 mg of sorbent

Time (min)	Average absorbance	Final Conc. (mg/L)	% MB absorbed	q_t (mg/g)
30	1.218	9.947	0.526	0.021
60	1.217	9.882	1.184	0.047
90	1.216	9.816	1.842	0.074
120	1.216	9.816	1.842	0.074
150	1.215	9.750	2.500	0.100
180	1.214	9.684	3.158	0.126

Table B.13 Contact time test for 0 wt% iron using 20 mg/L, 40 mL dye solution, and 100 mg of sorbent

Time (min)	Average absorbance	Final Conc. (mg/L)	% MB absorbed	q_t (mg/g)
30	1.369	19.882	0.592	0.047
60	1.365	19.596	2.018	0.161
90	1.362	19.421	2.895	0.232
120	1.362	19.443	2.785	0.223
150	1.360	19.311	3.443	0.275
180	1.359	19.224	3.882	0.311

Table B.14 Bed height data for 6 wt% sample

Bed height			
Time	1 cm	2 cm	3 cm
	Average absorbance	Average absorbance	Average absorbance
10	1.193	1.175	1.167
20	1.197	1.174	1.167
30	1.204	1.179	1.168
40	1.211	1.185	1.175
50	1.216	1.193	1.179
60	1.218	1.209	1.186
70	1.218	1.218	1.204
80	1.218	1.218	1.218
90	1.218	1.218	1.219
100	1.218	1.219	1.219

Table B.15 Flowrate test for 6 wt% sample

Flowrate			
Time	5 ml/min	10 ml/min	15 ml/min
	Average absorbance	Average absorbance	Average absorbance
10	1.166	1.188	1.193
20	1.165	1.188	1.202
30	1.165	1.189	1.209
40	1.175	1.193	1.216
50	1.185	1.201	1.216
60	1.194	1.209	1.218
70	1.202	1.218	1.218
80	1.215	1.219	1.217
90	1.219	1.219	1.218
100	1.218	1.219	1.218

Table B.15 Bed height test data for 15 wt% sample

BED HEIGHT			
Time	1 cm	2 cm	3 cm
	Average absorbance	Average absorbance	Average absorbance
10	1.18	1.172	1.167
20	1.181	1.172	1.167
30	1.189	1.172	1.168
40	1.196	1.179	1.169
50	1.207	1.193	1.17
60	1.209	1.197	1.185
70	1.214	1.209	1.191
80	1.218	1.215	1.197
90	1.218	1.218	1.219
100	1.218	1.219	1.218

Table B.16 Flowrate test for 15 wt% sample

FLOWRATE			
Time	5 ml/min	10 ml/min	15 ml/min
	Average absorbance	Average absorbance	Average absorbance
10	1.159	1.188	1.193
20	1.159	1.188	1.202
30	1.159	1.189	1.209
40	1.162	1.193	1.216
50	1.17	1.201	1.216
60	1.178	1.209	1.218
70	1.184	1.218	1.218
80	1.195	1.219	1.217
90	1.206	1.219	1.218
100	1.213	1.219	1.218

Chapter 5 Raw data

Table B.17 Concentration Test Results for Sample 1

Initial Conc. (mg/L)	Absorbance	Final Conc. (mg/L)	q_t (mg/g)
25	0.0052	0.4683	12.2658
50	0.0056	0.7126	24.6436
75	0.0070	1.4471	36.7764
100	0.0087	2.4299	48.7850

Table B.18 Concentration Test Results for Sample 2

Initial Conc. (mg/L)	Absorbance	Final Conc. (mg/g)	q _t (mg/g)
25	0.0061	0.9572	0.4007
50	0.0065	1.2020	0.8132
75	0.0074	1.6924	1.2217
100	0.0092	2.6762	1.6220

Table B.19 Concentration Test Results for Sample 3

Initial Conc. (mg/L)	Absorbance	Final Conc. (mg/L)	q _t (mg/g)
25	0.008330993	2.183884789	11.4080576
50	0.010105436	3.169686823	23.4151566
75	0.010995384	3.66410239	35.6679488
100	0.01278077	4.655983384	47.6720083

Table 7 Table B.20 Concentration Test Results for Sample 4

Initial Conc. (mg/L)	Absorbance	Final Conc. (mg/L)	q _t (mg/g)
25	0.007446482	1.69249	11.65375
50	0.007888512	1.938062	24.03097
75	0.009217308	2.676282	36.16186
100	0.010550182	3.416768	48.29162

Table B.21 Concentration Test Results for Sample 5

Initial Conc. (mg/L)	Absorbance	Final Conc. (mg/L)	q _t (mg/g)
25	0.007888512	1.938062	11.53097
50	0.008330993	2.183885	23.90806
75	0.009217308	2.676282	36.16186
100	0.010995384	3.664102	48.16795

Table B.22 Time Test Results for Sample 1

Time (min)	Absorbance	Final Conc	q _t (mg/g)
5	0.1366	73.4872	0.7563
10	0.1290	69.2284	2.8857
15	0.1214	65.0434	4.9782
20	0.1174	62.8197	6.0901

Table B.23 Time Test Results for Sample 2

Time (min)	Absorbance	Final Conc	q_t (mg/g)
5	0.1331	71.5123	1.7438
10	0.1266	67.9329	3.5335
15	0.1180	63.1361	5.9319
20	0.1152	61.5581	6.7209

Table B.24 Time Test Results for Sample 3

Time (min)	Absorbance	Final Conc	q_t (mg/g)
5	0.1237	66.3234	4.3382
10	0.1157	61.8729	6.5635
15	0.1079	57.5029	8.7485
20	0.1045	55.6541	9.6729

Table B.25 Time Test Results for Sample 4

Time (min)	Absorbance	Final Conc	q_t (mg/g)
5	0.1307	70.2046	2.3976
10	0.1232	66.0027	4.4986
15	0.1146	61.2437	6.8781
20	0.1135	60.6162	7.1918

Table B.26 Time Test Results for Sample 5

Time (min)	Absorbance	Final Conc	q_t (mg/g)
5	0.1272	68.2562	3.3718
10	0.1186	63.4529	5.7735
15	0.1106	59.0546	7.9726
20	0.1095	58.4327	8.2836

Chapter 6 Raw data

Table B.27 Data for the contact time test

Time (min)	Absorbance				
	Sample A: Sample D	Sample A: Diluted	Sample B: Diluted	Sample C: Diluted	Magnetite sample
5	1.625	1.602	1.590	1.602	1.622
10	1.631	1.600	1.586	1.595	1.627
15	1.642	1.589	1.568	1.589	1.628
20	1.653	1.581	1.566	1.587	1.635
25	1.663	1.564	1.553	1.586	1.639
30	1.683	1.555	1.546	1.560	1.640
35	1.702	1.530	1.353	1.553	1.648

Table B.28 Data for the varying amounts of adsorbent added to solution 1

Mass (mg)	Absorbance				
	Sample A: Sample D	Sample A: Diluted	Sample B: Diluted	Sample C: Diluted	Magnetite sample
10	1.604	1.603	1.599	1.605	1.599
20	1.609	1.603	1.607	1.607	1.611
30	1.612	1.604	1.613	1.611	1.614
40	1.618	1.606	1.618	1.614	1.618
50	1.620	1.609	1.620	1.614	1.625
60	1.625	1.612	1.622	1.619	1.625
70	1.626	1.612	1.629	1.622	1.626
80	1.630	1.612	1.631	1.623	1.629
90	1.633	1.615	1.634	1.627	1.639
100	1.637	1.619	1.642	1.628	1.639

Table B.29 Data for the effect of temperature on the nanoparticles

Conc. (mg/L)	Absorbance									
	Sample A		Sample B		Sample C		Sample D sample		Magnetite sample	
	25°C	35°C	25°C	35°C	25°C	35°C	25°C	35°C	25°C	35°C
40	1.603	1.608	1.610	1.617	1.597	1.610	1.582	1.588	1.601	1.590
80	1.600	1.609	1.624	1.633	1.611	1.615	1.576	1.580	1.605	1.628
120	1.611	1.618	1.632	1.641	1.623	1.628	1.638	1.631	1.624	1.639
160	1.617	1.627	1.654	1.657	1.644	1.651	1.649	1.653	1.693	1.698
200	1.623	1.639	1.677	1.698	1.653	1.662	1.611	1.664	1.702	1.711

Appendix C

To establish the ultimate metal loadings of the sorbent samples, a scaling technique of calculation was necessary. For this computation, the samples had to be weighed following the drying and carbonisation processes, and the amount of sample introduced into the U-tube furnace had to be recorded. This computation was performed on samples A and B. The calculations listed below are representative of sample A.

Weight percentage of sample after drying:

Iron nitrate added to bread mixture: 4 grams

Weight of sample after drying = 300 g

$$\frac{\text{Mass of iron nitrate}}{\text{Mass of sample after drying}} = \frac{4 \text{ g}}{281.6 \text{ g}} = 1.42 \text{ wt. \%}$$

Amount of iron in furnace tube sample:

Amount of sample inserted into furnace tube = 40.05 g

$$\begin{aligned} \text{amount in furnace tube} \times \text{weight percent after drying} &= 40.05 \text{ g} \times 1.42 \% \\ &= 0.57 \text{ g} \end{aligned}$$

Weight percentage of sample after carbonisation:

Weight after carbonisation = 9.5 g

$$\frac{\text{iron in furnace tube}}{\text{weight after carbonisation}} = \frac{0.57}{9.5} = 5.99 \%$$

Thus, the final weight percent of iron in sample A \approx 6 wt%

Similarly:

Sample B - 15 wt%

Final concentration calculation:

Calibration of the spectrophotometer produced the following linear equation:

$$y = 0.0152x + 1.0668$$

Where:

x - Concentration of dye solution

y – Absorbance reading from spectrophotometer

This equation was used to evaluate the final concentration of the samples. A sample calculation is shown below for sample A- sorbent dosage test using the 10 mg/L solution (Table 9):

$$\text{From the calibration curve equation: } x = \frac{1.211 - 1.0668}{0.0152} = 9.487 \frac{\text{mg}}{\text{L}}$$

To determine the percentage of dye removed from the initial solution.

From equation (E2):

$$\%R = \frac{C_o - C}{C_o} \times 100 = \frac{10 - 9.487}{10} \times 100 = 5.132 \%$$

To determine the amount of dye adsorbed (mg) per gram of sorbent.

From equation (E1):

$$Q_e = \frac{(C_o - C_e) \times V}{m} = \frac{(10 - 9.487) \times 0.02}{0.02} = 0.513 \frac{\text{mg}}{\text{g}}$$

Appendix D

Chapter 4 Graphs

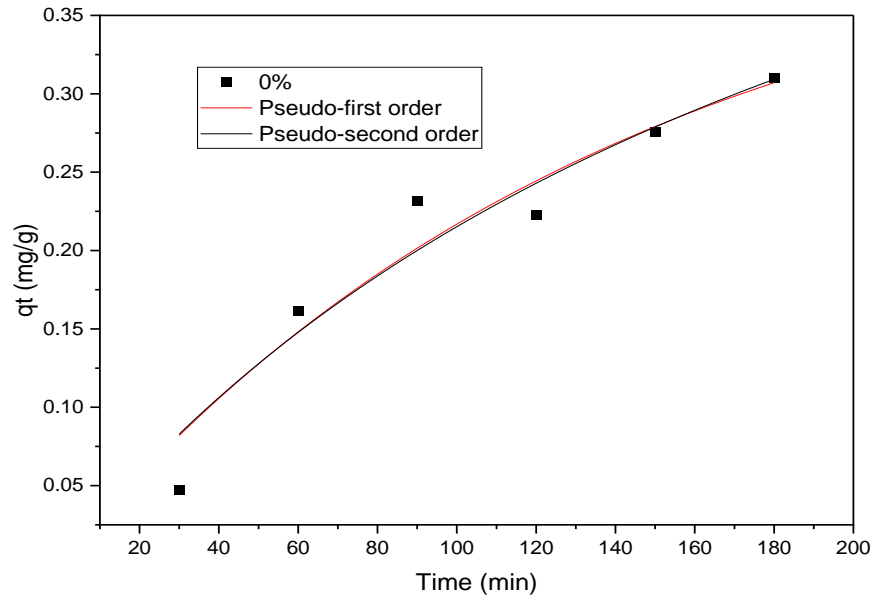


Figure D.1 Nonlinear fit of pseudo-first order and pseudo-second order for dye adsorption on carbon foam with 0 wt% iron, 20 mg/L solution, initial concentration of 10 mg/L

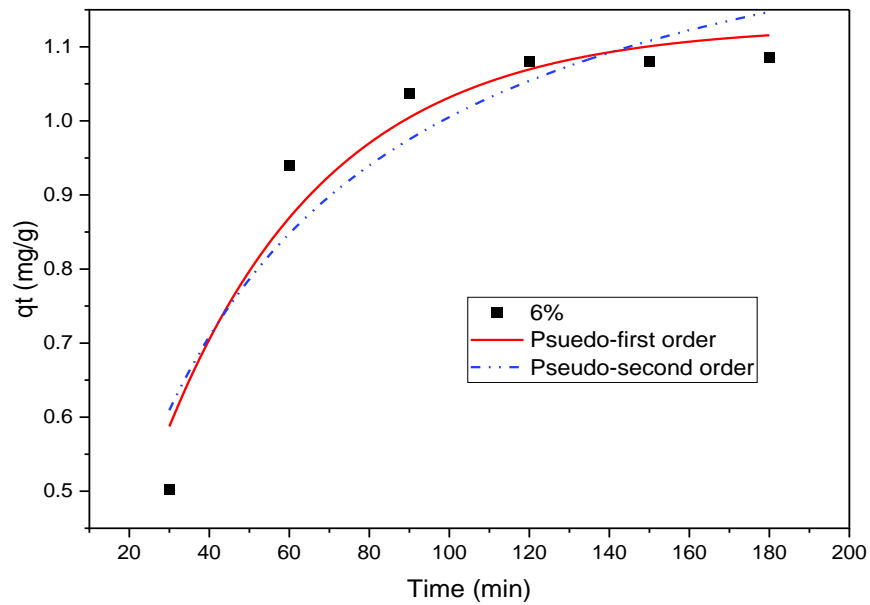


Figure D.2 Nonlinear fit of pseudo-first order and pseudo-second order for dye adsorption on carbon foam with 6 wt% iron, 20 mg/L solution, initial concentration of 10 mg/L

Chapter 5 Graphs

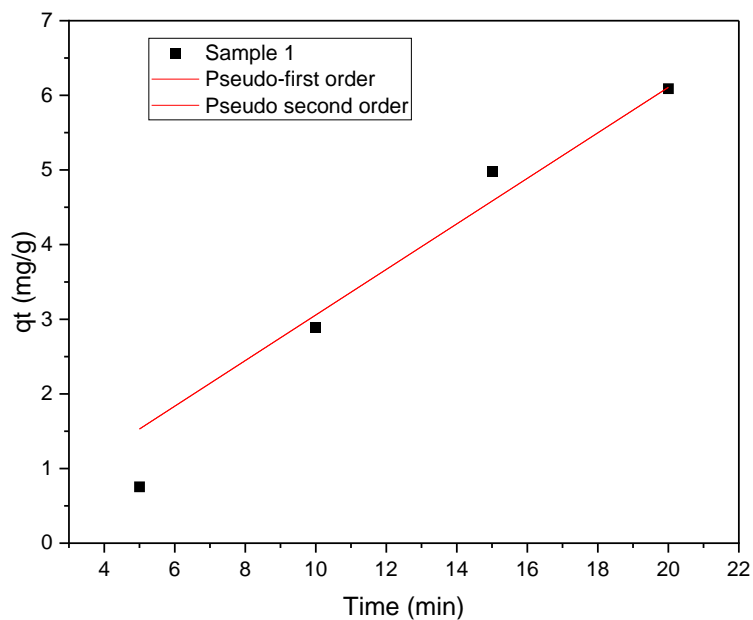


Figure D.3 Nonlinear fit of pseudo-first order and pseudo-second order for phenol adsorption of sample 1 at a 75mg/L of concentration, and 100mg sorbent

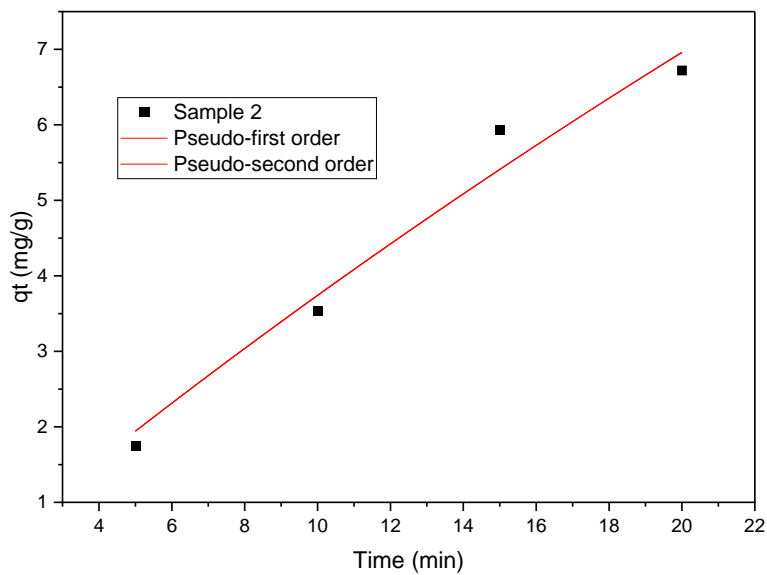


Figure D.4 Nonlinear fit of pseudo-first order and pseudo-second order for phenol adsorption of sample 2 at a 75mg/L of concentration, and 100mg sorbent

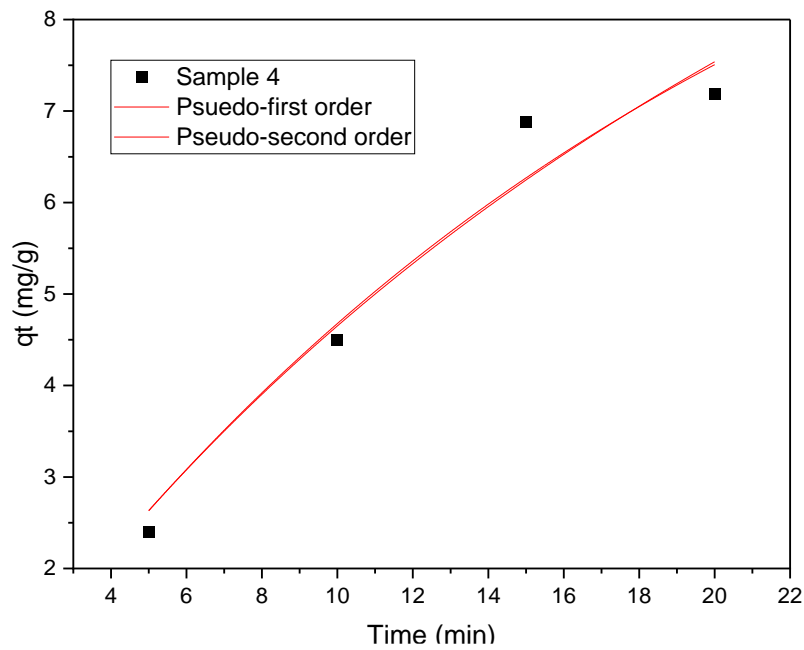


Figure D.6 Nonlinear fit of pseudo-first order and pseudo-second order for phenol adsorption of sample 4 at a 75mg/L of concentration, and 100mg sorbent

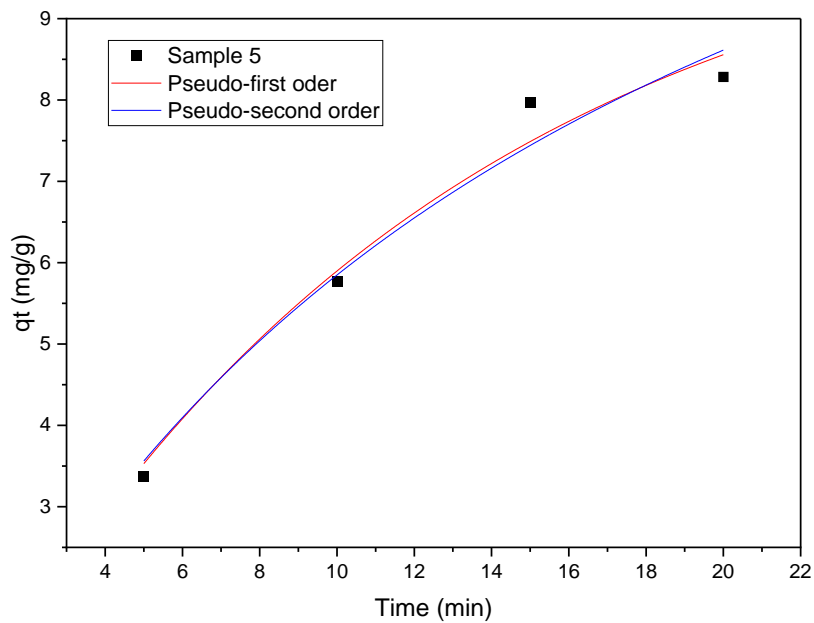


Figure D.7 Nonlinear fit of pseudo-first order and pseudo-second order for phenol adsorption of sample 5 at a 75mg/L of concentration, and 100mg sorbent

Chapter 6 Graph

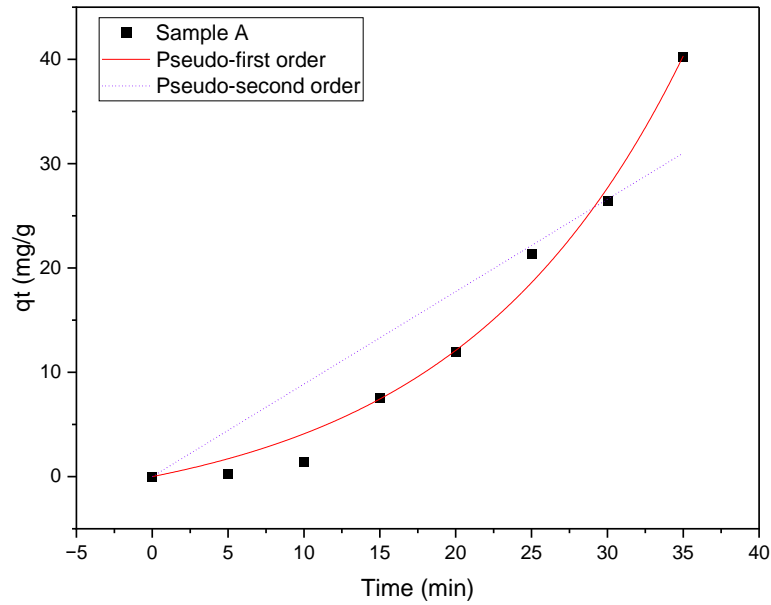


Figure D.8 Nonlinear fitting of pseudo-first order and pseudo-second order for sample A

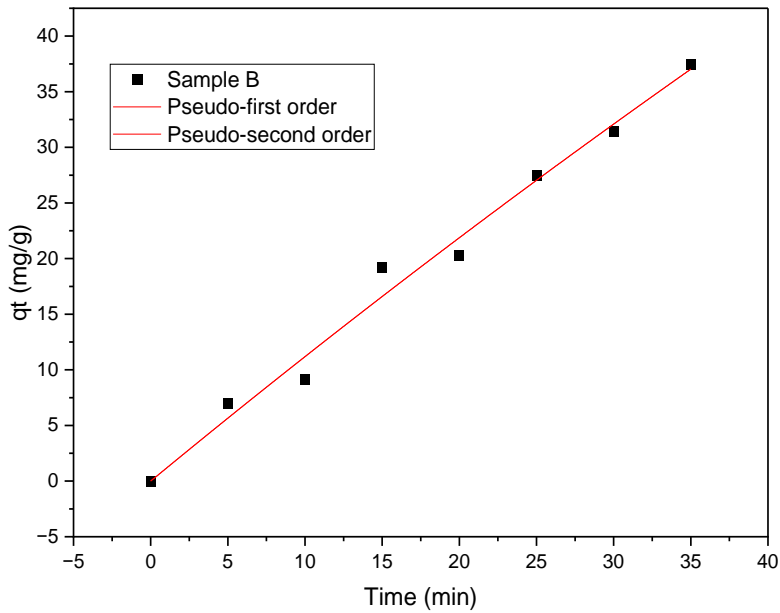


Figure D.9 Nonlinear fitting of pseudo-first order and pseudo-second order for sample B

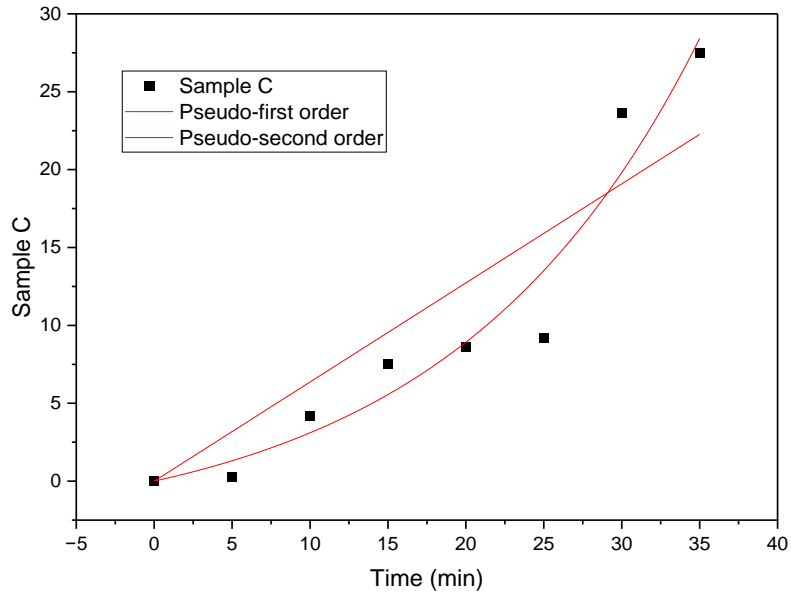


Figure D.10 Nonlinear fitting of pseudo-first order and pseudo-second order for sample C

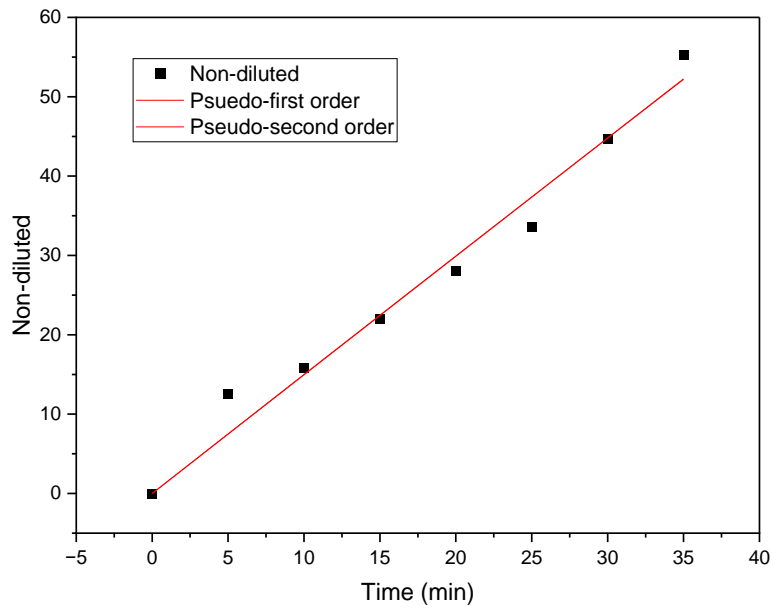


Figure D.11 Nonlinear fitting of pseudo-first order and pseudo-second order for Sample D sample

Chapter Thermodynamic Analysis Data

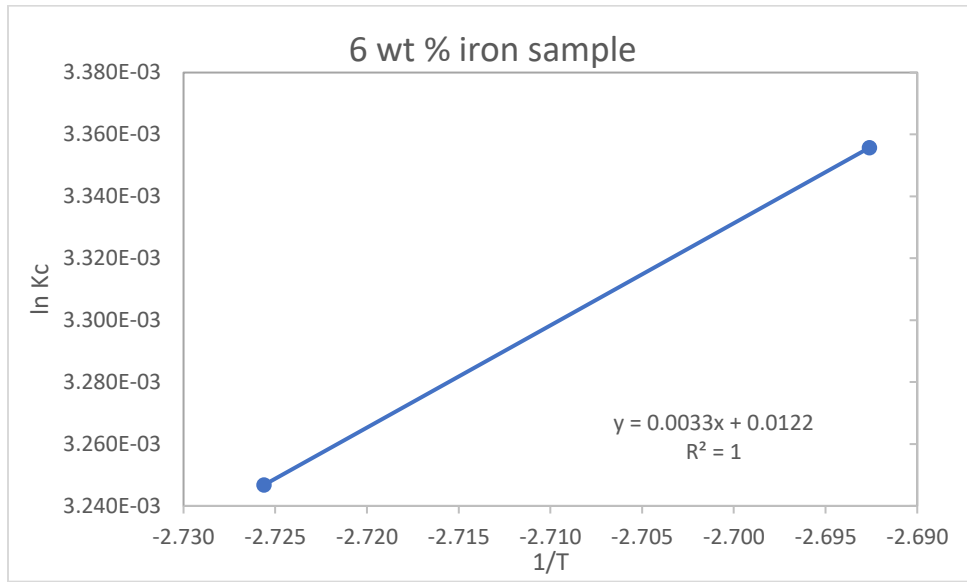


Figure D.12 6 wt % iron sample graph of ln Kc versus 1/T

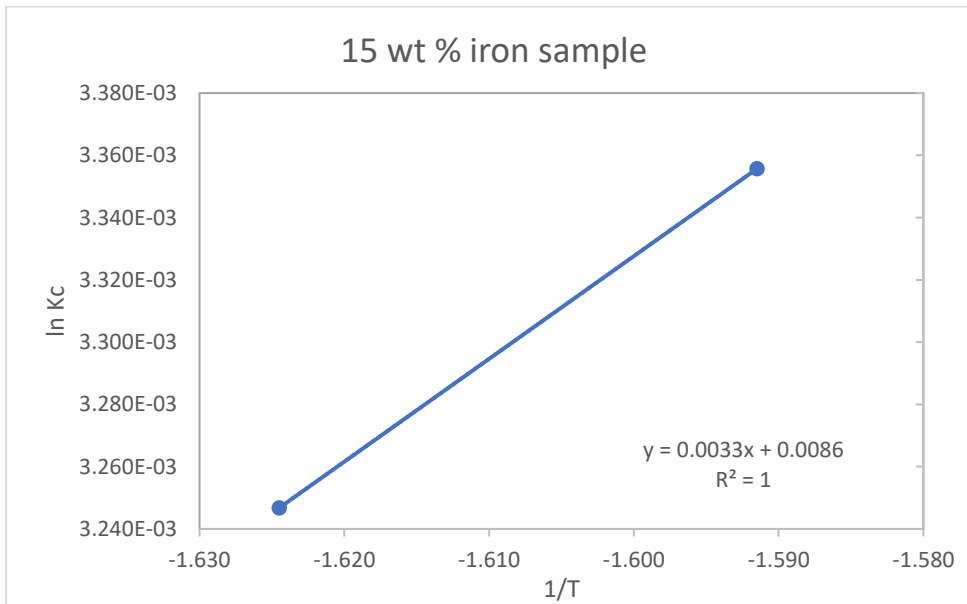


Figure D.13 6 wt % iron sample graph of ln Kc versus 1/T

Table D.1 Chapter 6 Thermodynamic analysis data

Ln Kc vs. 1/T	Sample A	Sample B	Sample C	Non-diluted	Magnetite sample
Slope	40.270	75.248	35.130	28.906	-63.987
Intercept	5.043	4.934	5.078	5.086	5.399

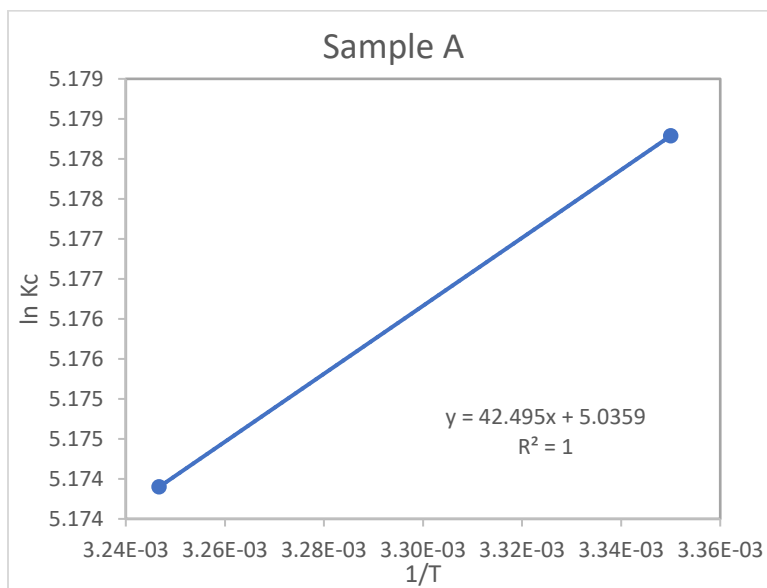


Figure D.14 Sample A graph of ln Kc versus 1/T

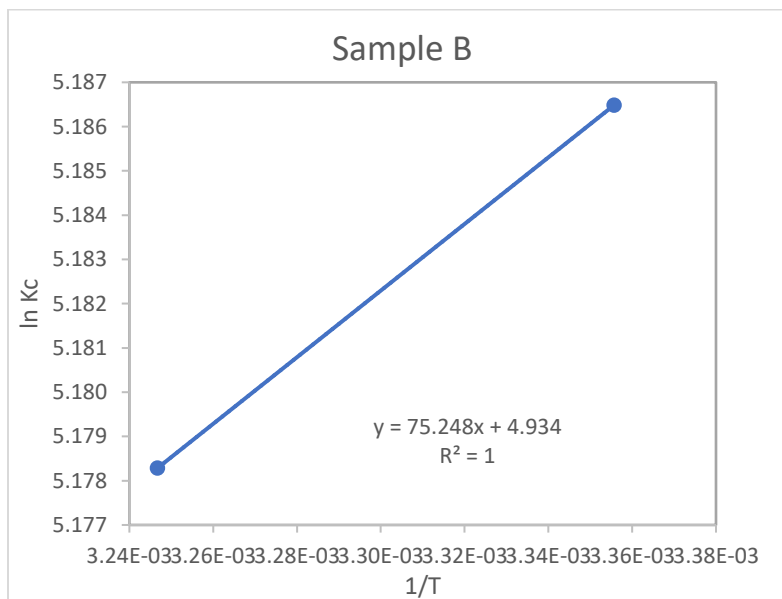


Figure D.15 Sample B graph of ln Kc versus 1/T

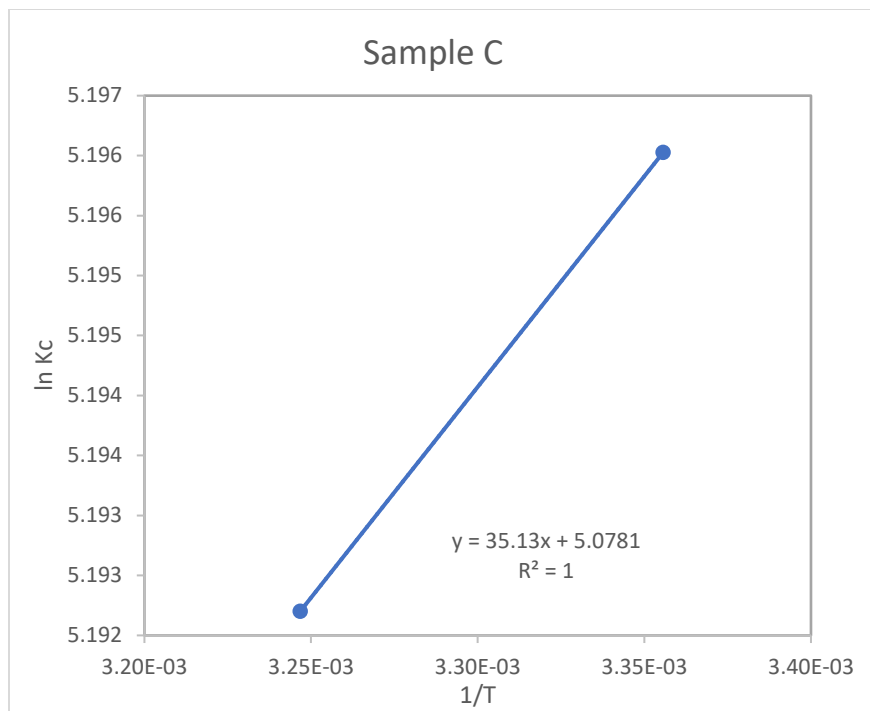


Figure D.16 Sample C graph of ln Kc versus 1/T

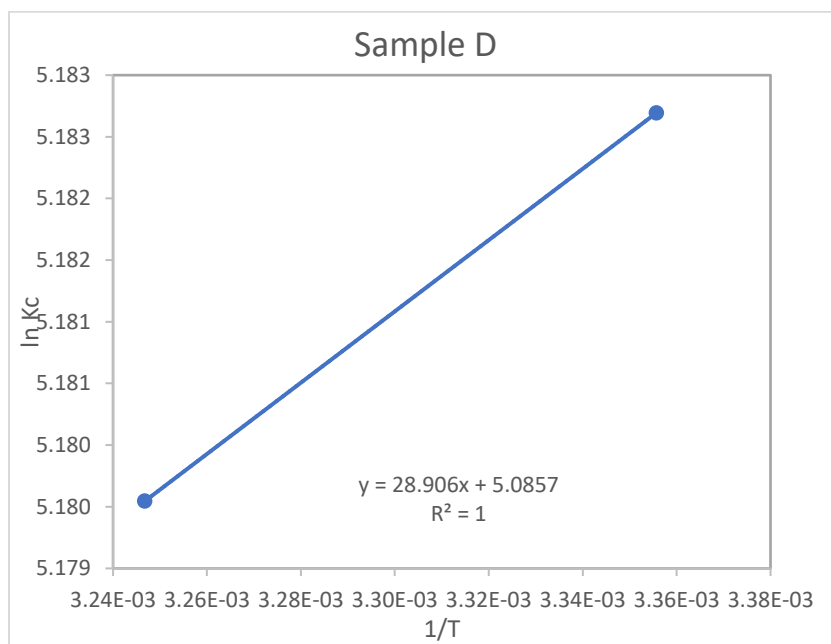


Figure D.17 Sample D graph of ln Kc versus 1/T

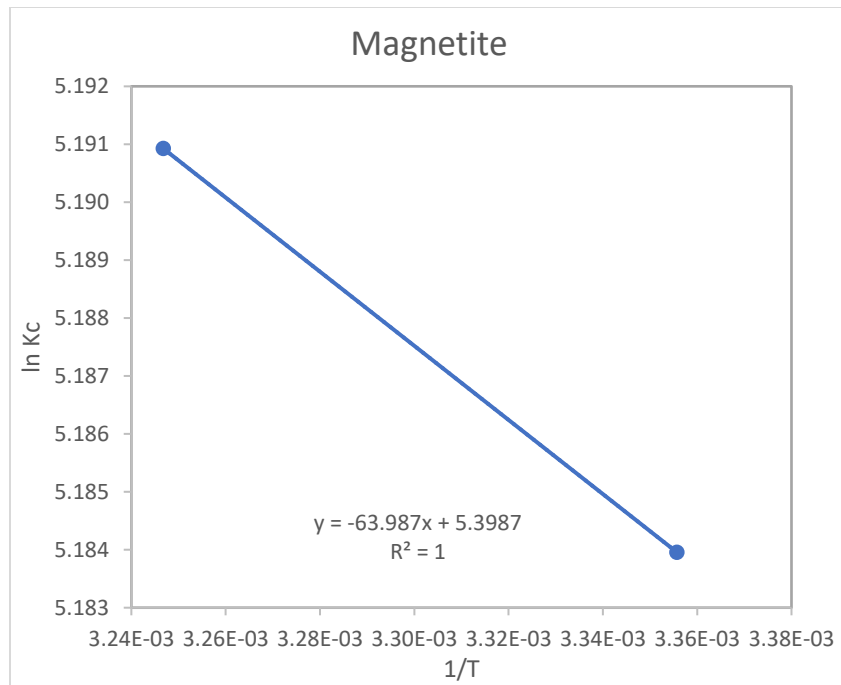


Figure D.18 Sample magnetite graph of ln Kc versus 1/T

Appendix E Pictures



Figure E.1 Sorbent after baking process

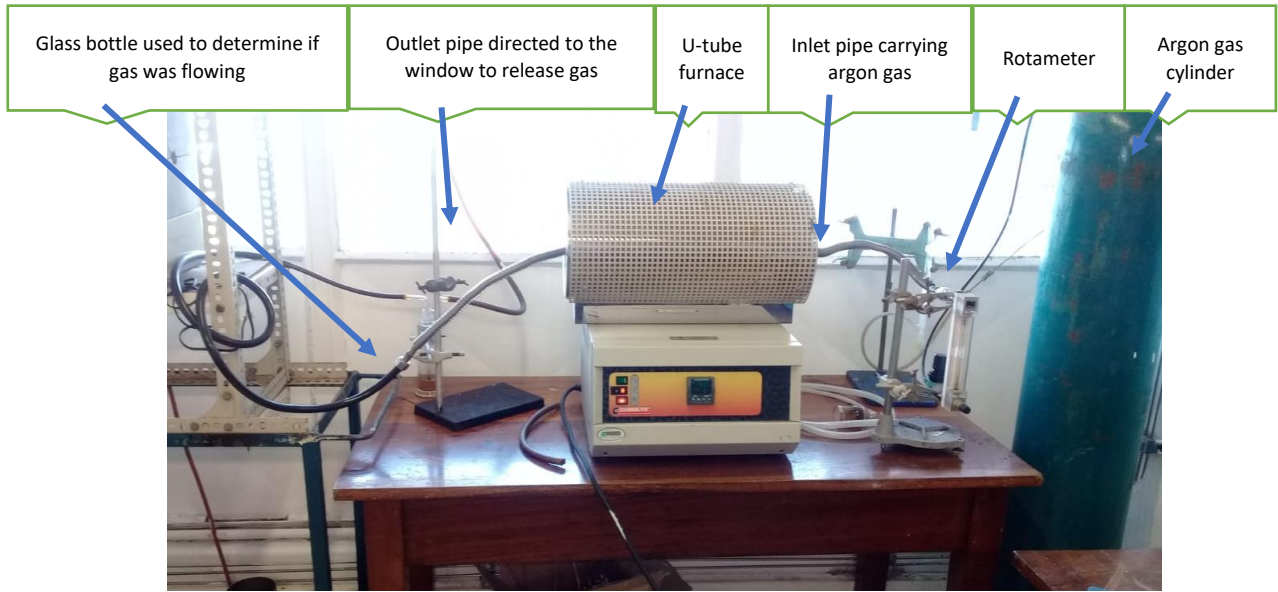


Figure E.2 Set up of U-tube furnace

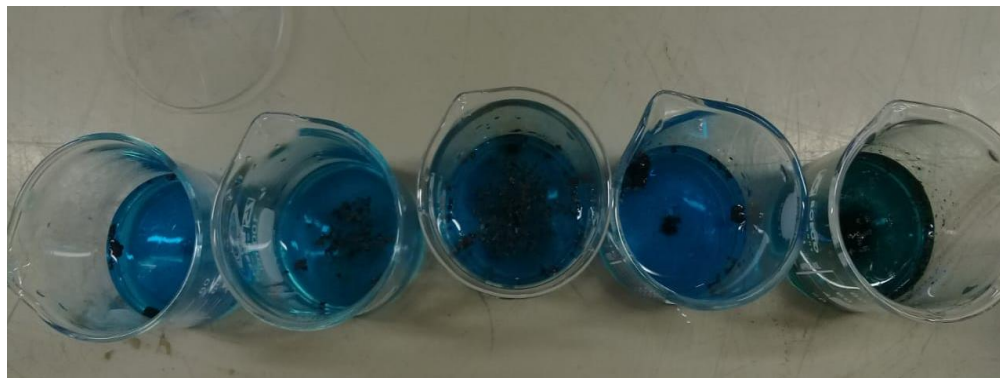


Figure E.3 Contact time test



Figure E.4 Peristaltic pump



Figure E.5 Sample prior to baking



Figure E.6 Spectrophotometer



Figure E.7 Packed sorbent bed

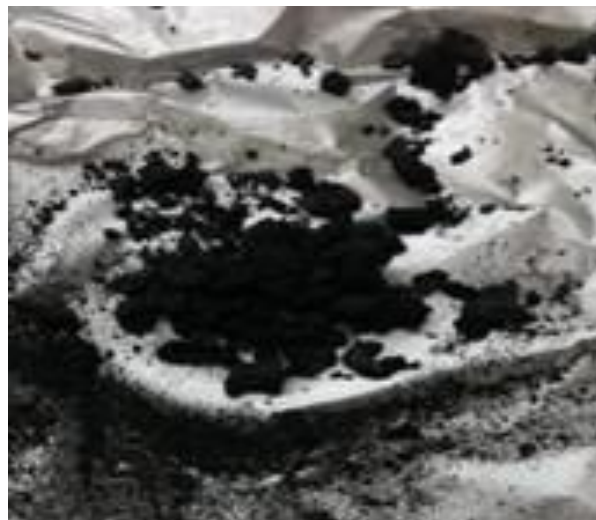


Figure E.8. Final sorbent



Figure E.9 Overhead stirrer